Uniwersytet im. Adama Mickiewicza w Poznaniu

Wydział Biologii

Agata Henschke

Rozprawa doktorska

“Wpływ liposomów załadowanych fisetyną na komórki senescentne indukowane terapią”

Promotorzy:

Prof. UAM dr hab. Luis Emerson Coy Romero

oraz

dr Sergio Moya

Rozprawa doktorska zrealizowana w Centrum NanoBioMedycznym w ramach grantu pt.:
„**Badania losu zaawansowanych nośników polimerowych *in vitro* i formowania się korony białkowej na ich powierzchni**”
UMO-2019/33/B/ST5/01495

Poznań 2024

Adam Mickiewicz University

Faculty of Biology

Agata Henschke

Doctoral dissertation

“The influence of fisetin-loaded liposomes on therapy-induced senescent cells”

Supervisors:

Prof. UAM dr hab. Luis Emerson Coy Romero

and

dr Sergio Moya

Doctoral dissertation completed at the NanoBioMedical Center under the grant entitled: " ***In-vitro* biological fate and protein corona studies of advanced polymeric nanocarriers**”
UMO-2019/33/B/ST5/01495

Poznań 2024

To my family and friends,

Thank you for believing in me more than I believed in myself.

List of abbreviations

AMPK - 5’ Adenosine Monophosphate-activated Protein Kinase

API - Active Pharmaceutical Ingredient

ATM - Ataxia-Telangiectasia Mutated

ATP - Adenosine Triphosphate

ATR - Ataxia Telangiectasia and Rad3-related protein

BrdU - 5-bromo-2'-deoxyuridine

BSA - Bovine Serum Albumin

CCF - Cytoplasmic Chromatin Fragments

CDK - Cyclin Dependent Kinase

cDNA - complementary DNA

CHK - Checkpoint protein Kinase

CLSM - confocal Laser Scanning Microscopy

Cryo-SEM - Cryogenic Scanning Electron Microscopy

DDR - DNA Damage Response

DDS - Drug Delivery System

DEPC - Diethylpyrocarbonate

DLS - Dynamin Light Scattering

DMSO - Dimethyl Sulfoxide

DNA - Deoxyribonucleic acid

DOPC - 1,2-dioleoyl-sn-glycero-3-phosphocholine

DOX - Doxorubicin

DPBS - Dulbecco’s Phosphate-Buffered Saline

DSPE - 1,2-distearoyl-sn-glycero-3-phosphoethanolamine

EdU - 5-Ethynyl-2’-deoxyuridine

ELISA - Enzyme-Linked Immunosorbent Assay

EMEM - Eagle’s Minimal Essential Medium

EMT - Epithelial-Mesenchymal Transition

EthD-2 - Ethidium Homodimer-2

FDA - Food and Drug Administration

HBSS - Hanks’ Balanced Salt Solution

HEPES - 4-(2-hydroxyethyl)-1-piperazineethanesulfonic acid

IL-6 - Interleukin 6

IL-8 - Interleukin 8

LMNA - Lamin A

LMNB1 - Lamin B1

LMNB2 - Lamin B2

MDSC - Myeloid-Derived Suppressor Cells

MOF - Metal-Organic Framework

mtDNA - mitochondrial DNA

mTOR - Mammalian Target of Rapamycin

NAD+ - Nicotinamide Adenine Dinucleotide

NF-κB - Nuclear Factor kappa-light-enhancer of activated B cells

PBS - Phosphate-Buffered Saline

PCR - Polymerase Chain Reaction

qPCR - quantitative Polymerase Chain Reaction

RNA - Ribonucleic Acid

ROS - Reactive Oxygen Species

RT - room temperature

SA-beta-gal - Senescence-Associated β-galactosidase

SAHF - Senescence-Associated Heterochromatin Foci

SASP - Senescence-Associated Secretory Phenotype

SCAP - Senescent Cell Anti-apoptotic Pathway

SIPS - Stress-induced Premature Senescence

TIS - Therapy Induced Senescence

X-gal - 5-bromo-4-chloro-3-indoyl-β-d-galactopyranoside

Table of Contents

Streszczenie

Starzenie komórkowe odnosi się do stanu zatrzymania wzrostu, w którym komórki tracą zdolność do podziału i wzrostu, mimo że wciąż pozostają żywe i aktywne metabolicznie. Proces ten może być wywołany przez różne czynniki stresogenne, w tym środki chemioterapeutyczne. Komórki nowotworowe, które weszły w stan starzenia komórkowego w wyniku chemioterapii, mogą później wrócić do cyklu komórkowego i wznowić podziały komórkowe, co zwiększa ryzyko nawrotu i progresji choroby. Opracowywane są innowacyjne strategie, takie jak zaawansowane systemy dostarczania leków na bazie naocząstek, mające na celu zwiększenie skuteczności terapii. Połączenie tych systemów dostarczania leków z senoterapią - podejściem selektywnie ukierunkowanym na komórki w stanie starzenia - może stanowić obiecujące rozwiązanie, zmniejszające ryzyko nawrotu nowotworu.

Niniejsza rozprawa koncentruje się na badaniach dotyczących indukcji starzenia komórkowego oraz ocenie żywotności komórek, szczególnie w kontekście terapii przeciwnowotworowych. Wpływ systemów dostarczania leków, opartych na liposomach z załadowaną fisetyną, analizowano na dwóch liniach komórkowych poddanych procesowi starzenia (senescencji): A549 (ludzki niedrobnokomórkowy rak płuc) i WI38 (ludzkie fibroblasty płucne). Celem niniejszej dysertacji było opracowanie protokołu indukcji starzenia komórkowego przy użyciu chemioterapeutyku (doksorubicyny), oceny żywotności komórek po indukcji starzenia, a także analiza różnych markerów związanych z procesem starzenia komórek. Badania podkreślają złożoność odpowiedzi komórkowych na środki chemioterapeutyczne, wskazując na konieczność dogłębnej analizy biomarkerów w celu precyzyjnej charakterystyki komórek, które przszły proces starzenia komórkowego. Ponadto, praca ta szczegółowo opisuje przygotowanie, charakterystykę oraz zastosowanie liposomów jako systemów dostarczania leków dla nierozpuszczalnego w wodzie związku - fisetyny. Liposomy zsyntetyzowano za pomocą metody hydratacji cienkowarstwowej, która pozwala na optymalizację ich rozmiarów oraz wydajną enkapsulację leku. Ostatnia część pracy skupiła się na ocenie cytotoksyczności fisetyny zarówno na komórki stare, jak i te, które nie zostały poddane procesowi starzenia. Wyniki pokazały, że fisetyna nie wykazuje selektywności w indukcji apoptozy i wpływa na oba typy komórek przy wyższych stężeniach. Chociaż fisetyna nie

wykazała właściwości senolitycznych w liniach komórkowych A549 i WI38, ujawniła działanie senomorficzne, modulując wydzielanie prozapalnych cytokin IL-6 i IL-8. Co więcej, enkapsulacja fisetyny w liposomy zwiększyła jej wydajność w porównaniu z formą wolną. Wyniki sugerują, że choć fisetyna nie eliminuje skutecznie komórek starych, może ograniczać ich szkodliwe skutki poprzez działania senomorficzne.

Abstract

Cellular senescence refers to a state of growth arrest in which cells remain metabolically active. Various stressors, including chemotherapeutic agents can trigger this condition. Senescent cancer cells may contribute to tumorigenesis through multiple pathways, including influencing the tumor microenvironment by secreting SASP (Senescent Associated Secretory Phenotype) or by escaping cell cycle arrest, which can ultimately lead to cancer relapse. Innovative strategies, such as advanced drug delivery systems based on nanoparticles, are being developed to improve the efficiency of therapeutic agents. Combining these drug delivery systems with senotherapy, an approach that selectively targets senescent cells, could offer a promising solution for reducing the risk of cancer recurrence.

This thesis is focused on examining the induction of cellular senescence and investigating cell viability, particularly in the context of cancer treatment. The research explored how drug delivery systems utilizing liposomes with encapsulated fisetin can influence two senescent cell lines: A549 (lung carcinoma) and WI38 (lung fibroblast). The study describes protocols for inducing cellular senescence using doxorubicin, assessing cell viability following doxorubicin treatment, and evaluating various senescence markers. The research emphasizes the complexity of cellular responses to chemotherapeutic agents and underscores the need for comprehensive biomarker analysis to characterize senescent cells accurately. This study comprehensively examines liposomes' preparation, characterization, and evaluation as drug delivery systems for the water-insoluble senotherapeutic drug fisetin. Utilizing established methodologies for liposome prepartion, particularly the thin-film hydration method, the study focuses on optimizing liposome size and encapsulation efficiency, which are critical factors for effective therapeutic applications. The study evaluated fisetin's cytotoxicity on senescent versus non-senescent cells, revealing that it lacks selective apoptosis properties and affects both cell types at higher concentrations. While fisetin did not demonstrate senolytic properties in the A549 and WI38 cell lines, it exhibited senomorphic effects by modulating the secretion of pro-inflammatory cytokines IL-6 and IL-8. Encapsulating fisetin in liposomes enhanced its efficiency compared to the free form of this

senotherapeutic drug. The findings suggest that although fisetin does not effectively eliminate senescent cells, it may reduce their harmful effects through senomorphic actions.

Chapter 1 Introduction

Approximately 50 years ago, Hayflick and his colleagues first introduced and described the concept of cellular senescence. They found a slowing in the proliferation of human fibroblasts after multiple passages, ultimately leading to a complete loss of their ability to divide, a phenomenon called Hayflick's limit [1]. This was the beginning of a new field of research that focused on the exploring of this biological process and its significance in the biology of ageing, and disease aspects. During these studies, it was discovered that senescence can also be induced by various stress stimuli such as DNA damage, ionizing radiation, chemotherapy and much more, causing premature senescence.

1.1 Cellular senescence

Cellular senescence is a state at which cells stop growing, and it is considered to be a key process that controls aging in both cells and organisms. For many years, it was believed that this state was stable and irreversible, but some discoveries showed the ability of senescent cells to return the cell cycle. Even with stopped division, those cells are still metabolically active and their morphology, in most cases, changes drastically. Changes depend on the cell line and the method of senescence induction [2], but some are very characteristic for all senescent cells. Cellular senescence is called "double-edge sword" because it can benefit and harm the organism. In the short term, it plays a crucial role in embryonic development [3], wound healing [4], and tumor suppression [5]. Preserving senescence can result in chronic inflammation [6], and tumor development [7]. During development, senescent cells regulate the cell population in embryonic tissues and play a role in tissue patterning within developing limb buds [8], [9]. This developmental senescence is a programmed mechanism that follows a specific time course, restricted to specific regions and structures of the embryo, favouring the growth and proliferation of one cell population over another. Senescent cells in embryos do not show DNA-damage markers, indicating that this programmed developmental senescence is a physiological process [8]. Senescence markers are also found in placental syncytiotrophoblasts, which shows their programmed, physiological role in the embryo and mature organisms [10]. Disruptions,

malfunctions, or dysregulation that are shown as cellular senescence markers are linked with complications in development and triggers pregnancy pathologies, including chorioamnionitis, preterm births and stillbirths [11], [12], [13]. In summary, three functions are assumed for the occurrence of senescent cells in embryonic development: serving in the signalling process to control tissue morphogenesis, assisting in damage control and tissue remodelling during implantation and maintaining the general cell population. Tissue regeneration is a complex process involving hemostasis, inflammation, proliferation, and remodelling. Effective communication among cells is crucial for these repair mechanisms and depends on various factors in the microenvironment such as growth factors, cytokines, chemokines, and more [14]. It is worth noting that these elements are closely linked to cellular senescence. Thus, it seems valid that cellular senescence could play an important role in tissue repair and wound healing. Studies provide evidence supporting the influence of senescence on tissue repair [4]; however, the specific mechanism behind needs to be investigated. The role of programmed cellular senescence in promoting tissue repair and wound healing has been recently recognized in studies on limb regeneration in salamanders and zebrafish [4], [9], [15]. It is found to be essential for development, regenerative processes, and acute wound repair, but the long-term presence of senescence can lead to tissue pathology. Another way of the positive impact of cellular senescence is found as it can limit tissue fibrosis [16], which is a form of pathological wound healing, leading to the formation of permanent scar tissue. Inflammation is a crucial response to harmful stimuli involving immune cells, blood vessels, and molecular mediators. Its main role is eliminating damaged cells, clearing damaged tissues, and initiating the repair process [14]. Cytokines and chemokines secreted by senescence-associated ecretory phenotype (SASP) help neutrophils and macrophages move to the site of inflammation as part of this protective mechanism [9], [17]. While acute inflammation benefits processes like wound healing and embryo development, excessive or prolonged inflammatory responses can have negative effects by increasing morbidity and mortality while also impacting on quality of life. In elders, chronic low-level inflammation known as “inflammaging” poses significant health risks, including osteoporosis, atherosclerosis, and neurodegenerative disorders such as Alzheimer's or

Parkinson's disease [6], [18], [19] although its direct cause or consequence in progressive neurodegeneration remains uncertain despite its established role in these disorders.

1.1.1 Cell cycle arrest

The cell cycle consists of two main phases: the interphase and the mitotic phase. During interphase, the cell goes through three stages where it grows, accumulates necessary proteins and mRNA (G_1), undergoes DNA synthesis (S), and after DNA replication, the cell rapidly grows (G_2) in order to prepare for the next phase called mitotic phase. In the mitotic phase, the cell divides into two daughter cells through mitosis (M). Another stage to note is the resting phase (G_0), where cells become quiescent if not preparing for division. Checkpoints in the cell cycle during G_1, G_2, and M phases ensure proper DNA integrity and chromosome duplication, preventing mutations in daughter cells [20].

Cellular senescence begins towards the end of the G_1 and, through slippage, in G_2 stage, when a cell with unrepaired DNA is halted at a checkpoint [21]. DNA damage, oncogene activity, and telomere shortening can all lead to cell cycle arrest at this point. These factors can trigger the activation of tumor suppression pathways such as p53/$p21^{CIP1}$ and pRB/$p16^{INK4a}$. While p53/$p21^{CIP1}$ primarily focuses on DNA damage repair, pRB/$p16^{INK4a}$ plays a crucial role in preventing tumor formation and halting the cell cycle in the G_1 phase [22], [23]. Research studies have demonstrated that p21 is involved in causing cells to stop dividing permanently when they experience DNA damage in the G_2 phase [24], [25], [26]. This is achieved by preventing the activation of certain cell cycle proteins and the phosphorylation of pRB. Cells with damaged DNA are programmed to halt DNA replication to prevent further division and multiplication of DNA damage. The protein p53 plays a crucial role in promoting senescence when DNA damage is irreparable and is essential for maintaining cellular and genomic integrity [23]. Stressful stimuli trigger phosphorylation of p53 and leads to the activation of the cyclin-dependent kinase (CDK) inhibitor $p21^{CIP1}$, which helps stabilize cell cycle arrest. Additionally, the activation of the protein $p16^{INK4a}$ blocks the activity of CDK4 and CDK6 [21]. The CDKs usually stop the phosphorylation of pRB, but when $p16^{INK4a}$ inhibits them, pRB becomes hypophosphorylated [23]. This prevents cells from entering the S-phase of the cell cycle, causing them to stop dividing. This halt in cell division cannot be undone by deactivating p53 or other proteins related to the RB family. The cell cycle

also includes E2F genes, which code for a set of transcription factors that are essential in controlling the progression of the cell cycle by running as either stimulators or inhibitors of gene expression in phases [21]. When these pathways and components are disrupted, it results in cell cycle arrest.

1.1.2 Morphology

One of the hallmarks of cellular senescence is the cell enlargement both *in vitro* and *in vivo*. The exact mechanism behind senescent cells enlargement is still not fully understood, but the cell cycle arrest plays an important role in this process. Blocking cell division in the cell cycle checkpoint and prolonging the cell's growth in size continues [27]. Changes in size can be very visible, as presented in Figure 1 with other examples of senescence hallmarks, or very subtle, all those varieties depend on the cell line and the way senescence is induced [2]. With cell size the ratio of DNA:cytoplasm is also changing, making the cell more “diluted”, and causing the functional decline of the cell [28]. This is due to a shortage of DNA in larger cells, which then causes an overall decrease in gene expression across all genes. The DNA copy number indicates the optimal size range for supporting cell function, surpassing the upper limit results in pathologies and aging. It is crucial to note that cells in a two-dimensional (2D) culture experience a distinct microenvironment compared to the three-dimensional (3D) tissue context found *in vivo* [29], [30]. The microenvironment plays a role in influencing cell size, and, consequently, cellular function as well. In normal physiological conditions, cells have the ability to regulate their size fluctuations by adjusting the speed of cellular growth and division, allowing them to return to their original size [31].

Mitochondria’s morphology varies from proliferating cells to senescent cells. In senescent cells, mitochondria mass and ROS production elevate, while the mitochondrial membrane potential lowers [32]. Regarding morphology, mitochondria appear to be larger at the G_1/S phase, mitochondria become elongated in preparation for further but uneventful division. Additionally, mitophagy is reduced in senescent cells, leading to a higher number of dysfunctional mitochondria. The higher mitochondrial mass might partially counteract the decline in mitochondrial function. Mitochondrial dynamics, referred to as fission and fusion, play a critical role in regulating the quantity, dimensions, structure, and distribution of mitochondria within a

cell. Fusion facilitates the exchange of damaged mitochondrial DNA (mtDNA) with intact mtDNA. Fission generates fresh mitochondria by assigning the Drp1 protein onto the surface of mitochondria through receptors such as FIS1. Decreased levels of FIS1 lead to the development of oversized mitochondria [32], [33]. The low mitochondrial membrane potential is linked to reduced adenosine triphosphate (ATP) synthesis and higher generation of reactive oxygen speciec (ROS). In such circumstances, ROS cause the disruption of homeostasis regulation due to a disorder in the balance between oxidants and antioxidants [32]. Another important metabolism aspect is that the senescent cells show elevated levels of NAD+, which is linked to p53 activation and reduced 5' adenosine monophosphate-activated protein kinase (AMPK), which, according to new studies, is also connected to cellular senescence induction [34].

Lysosomes contain enzymes that break down macromolecules. The acidity within these vesicles, with a pH of 4.5-5, is optimal for enzymatic hydrolysis and essential for identifying cellular senescence, which will be discussed later. Lysosomes play a role in functions like secretion, signalling and degradation. Dysfunction of lysosomes is strongly associated with pathways leading to apoptosis or cellular senescence, age-related diseases, and overall aging [35]. β-galactosidase is an enzyme located in the lysosomes and aids in decomposing carbohydrates containing galactose. Its function involves splitting the bond between sugar molecules to break down larger macromolecules, such as lactose. Although this protein is present in non-senescent cells, there is a notable accumulation in senescent cells due to various factors, including gene expression and cellular metabolism changes [36].

A characteristic feature of chromatin alterations that can be observed during cellular senescence is the senescence-associated heterochromatin foci (SAHF), which are formed through the compaction of chromatin resistant to nucleases. Reorganized facultative heterochromatin conceals extensive DNA damage and protects the cell from apoptosis while also contributing to promoting cell cycle arrest by suppressing genes that facilitate proliferation [37]; for instance, Cyclin A serves as an example, being essential for progression through the S-phase of the cell cycle [38]. The formation of SAHF is a highly intricate process involving multiple protein complexes. The enlargement of the nucleus in senescent cells has been associated with reduced quantities of nuclear envelope proteins, notably Lamin B1 [39]. Consequently, these cells may demonstrate

impaired genomic stability. Lamin B1, a fibrous protein responsible for both structural support and transcriptional regulation in cell nuclei, also plays a significant role in this process [40]. Chromatin modifications most likely contribute to differential genome expression and the preservation of cellular senescence. It is important to remember that the effects of SAHF vary depending on the cell line. Notably, the presence of SAHF is not consistently associated with senescence but appears to be linked to the activation of the p16/pRB pathway. Variations in SAHF presence may be due to different levels of the p16 CDK inhibitor and subsequent activation of the pRb pathway, which has been well-documented in its contribution to SAHF formation [38].

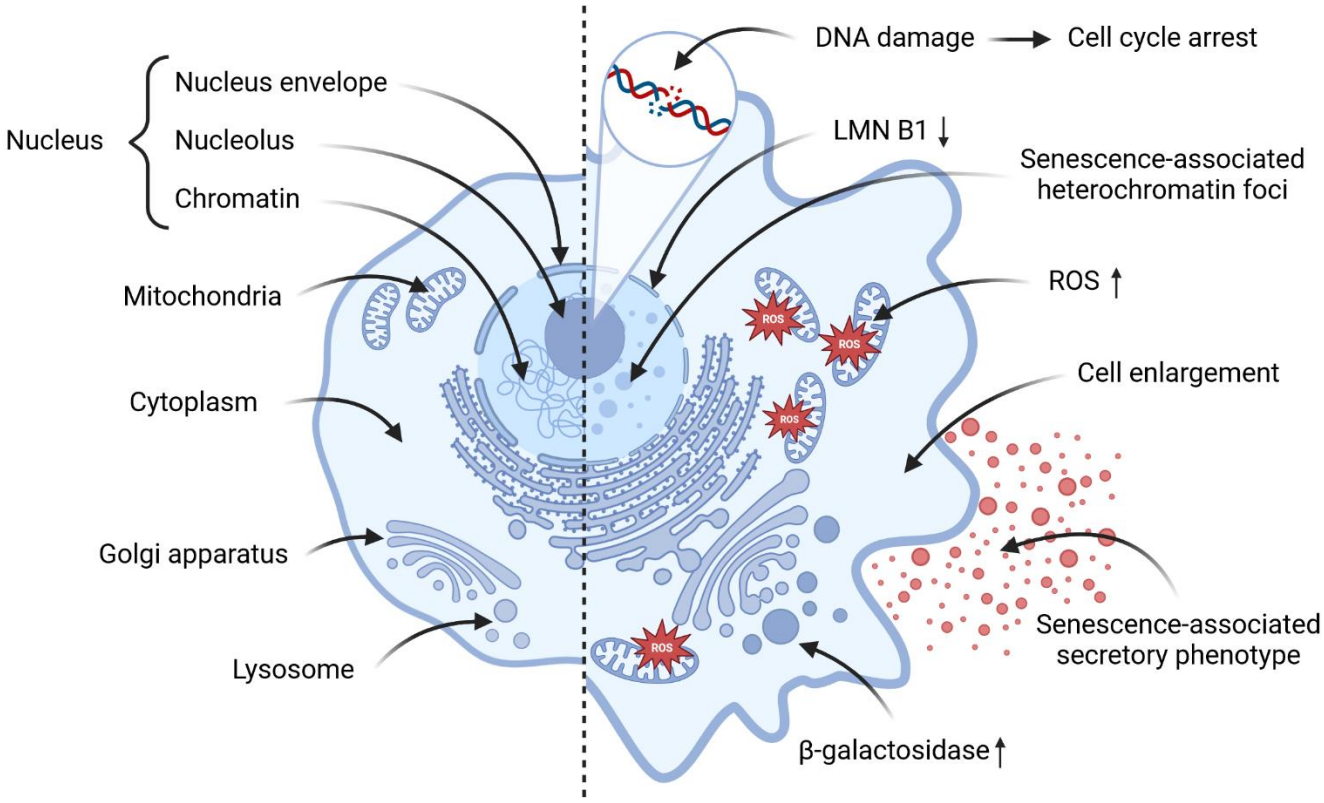

Figure 1. Graphical comparison of senescent and non-senescent cells.

1.1.3 SASP

Senescent cells exhibit changes in gene expression and secretion of various inflammatory factors, collectively known as the Senescence-Associated Secretory Phenotype, or SASP, first established by Coppé et al. in 2008 [41]. This heterogeneous complex includes numerous molecules such as chemokines, cytokines, proteases, and growth factors. The composition of SASP is not always the same, as it can vary between cell lines and induction techniques, depending on

the type of activated pathway in the process. Some of the most commonly occurring SASP components are IL-6, IL-8, MMP-1, -2, -3, GRO-α [42], [43], [44], [45], [46]. Known SASP components are included in Table 1, along with their classification. Secretion of SASP is a complex process regulated by the activation of various transcription factors, including NF-κB [47], mTOR [48], [49], and p38 MAPK [50] signalling pathways. The specific signalling mechanisms that trigger SASP activation are diverse and depend on the particular senescence-inducing stimuli, such as DNA damage, oncogene activation, or oxidative stress.

The SASP reinforces and propagates the senescent state through autocrine and paracrine signalling, where secreted factors can induce a senescent state in neighbouring cells [51]. Additionally, the SASP can activate immune responses that facilitate the clearance of senescent cells, which is considered a beneficial mechanism for removing these dysfunctional cells. However, the SASP also contributes to persistent chronic inflammation (inflammaging) within the tissue microenvironment, which can have detrimental effects on surrounding healthy cells and tissues. Moreover, it plays an important role in tumor support [51], [52], which will be discussed later in this chapter.

Table 1. Known components of SASP and their classification [52], [53], [54].

Class	Component
Chemokines	GRO-α, -β, -γ; MCP-1 (CCL2); MCP-2 (CCL8); MCP-4(CCL13); MIP-1a; MIP-3a; HCC-4; IL-8 (CXCL8); I-309; Eotaxin;
Interleukins	IL-6; IL-7; IL-1α, -1β; IL-13; IL-15;
Growth factors	Amphiregulin; Epiregulin; Heregulin; EGF; bFGF; HGF; KGF (FGF7); VEGF; PIGF; IGFBP-2, -3, -4, -6, -7;
Proteases	MMP-1, -3, -10, -12, -13, -14; TIMP-1; TIMP-2; tPA; uPA;
Receptors	ICAM-1; ICAM-3; sTNFRI; sTNFRII; uPAR;
Others	TGFβ; MIF; INF-γ; GM-SCE; PGE2; Fibronectin; SERPINB2; SERPINB4

1.2 Senescence induction

Although cellular senescence is a natural phenomenon caused by telomere erosion, it can also be rapidly induced by various potential stressors, such as DNA damage and oxidative stress. This process is referred to as stress-induced premature senescence (SIPS). Numerous mechanisms and inducers were extensively researched, such as ROS induction with H_2O_2 or CDK inhibition with Palbociclib [51], [55]. Therapy-induced senescence (TIS) is one of the types of SIPS observed in response to certain cancer therapies.

1.2.1 Therapy-induced cellular senescence

Various stressful stimuli can induce cellular senescence. Cancer treatment creates such a stressful environment that many cells, instead of going through apoptosis - programmed cell death - can lead to cellular senescence. In fact, cellular senescence was described as “permanent growth arrest”, but the notion of permanent senescence has been questioned because it has been observed that cells treated with chemotherapy can proliferate after being arrested in the cell cycle, without any genetic alternations [56]. Many chemotherapeutics can be responsible for cellular senescence induction, but this thesis will focus only on one, doxorubicin (DOX).

DOX is a well-known anthracycline chemotherapeutic isolated in 1969 from a microorganism called Streptomyces pencetius var. caesius [57] and due to its anticancer properties on a wide variety of cancers was approved by Food and Drug Administration (FDA) in 1974. Its chemical structure is showed in Figure 2b. The mechanism of action of DOX involves intercalation within the anthraquinone ring, which stabilizes the complex through hydrogen bonding with DNA bases. The resulting complex disrupts topoisomerase II activity by inhibiting the resealing of topoisomerase-mediated DNA breaks, thereby hindering replications and transcriptions, and promoting apoptosis. Intercalation also hampers essential enzyme activities such as those of topoisomerase II, DNA polymerase, and RNA polymerase, leading to cell arrest. In summary, DOX's intercalation destabilizes the structure of DNA and causes strand breakage and general damage [58], [59]. Due to various factors, DOX affects normal cells differently from cancer cells. Cancer cells have higher rates of DNA replication than healthy ones, which makes them more vulnerable to the DNA-damaging impact of DOX, leading to cell death. Moreover, cancer cells often possess disrupted antioxidant systems and elevated levels of reactive oxygen species. Consequently, exposure to DOX further increases the already high levels of reactive oxygen species in cancer cells, resulting in oxidative stress and, ultimately, apoptosis or senescence [60].

The DNA damage response (DDR) is a swift reaction to genetic material damage and its simplified pathway is presented in Figure 2a. When the damage becomes too extensive and cannot be fixed, the cell typically undergoes apoptosis to avoid spreading corrupted genomic material. DDR is naturally activated during the cell cycle and also plays a role in stress-induced premature senescence. Upon DNA damage, cells initiate a series of events to coordinate DNA repair and temporarily halt cell cycle progression until the DNA damage has been entirely resolved [61], [62]. DDR is a signalling cascade that has been conserved throughout evolution and is activated by DNA damage. It determines the fate of the cell towards either DNA repair, senescence, or apoptosis. Factors influencing whether apoptosis or senescence occurs may include characteristics like cell type, intensity, duration, and nature of the inflicted damage [62]. Sensors detect damaged DNA, such as double or single breaks, and transmit a signal to transducers, amplifying it and relaying it to effectors. The effectors carry out various cellular responses, including activating cell cycle checkpoints and mobilizing corresponding pathways to

repair the damage. ATM and ATR, the kinases involved in DDR signalling, become activated in response to DNA damage and are essential for initiating the pathway of DNA damage response and promoting cell cycle arrest [21], [62]. The phosphorylation of histone H2AX (γH2AX) by ATM and ATR represents a key step in DDR [62], [63]. Finally, DDR activates checkpoint protein kinases CHK1 and CHK2, leading to ATM-dependent phosphorylation of p53 and subsequent induction of senescence [21].

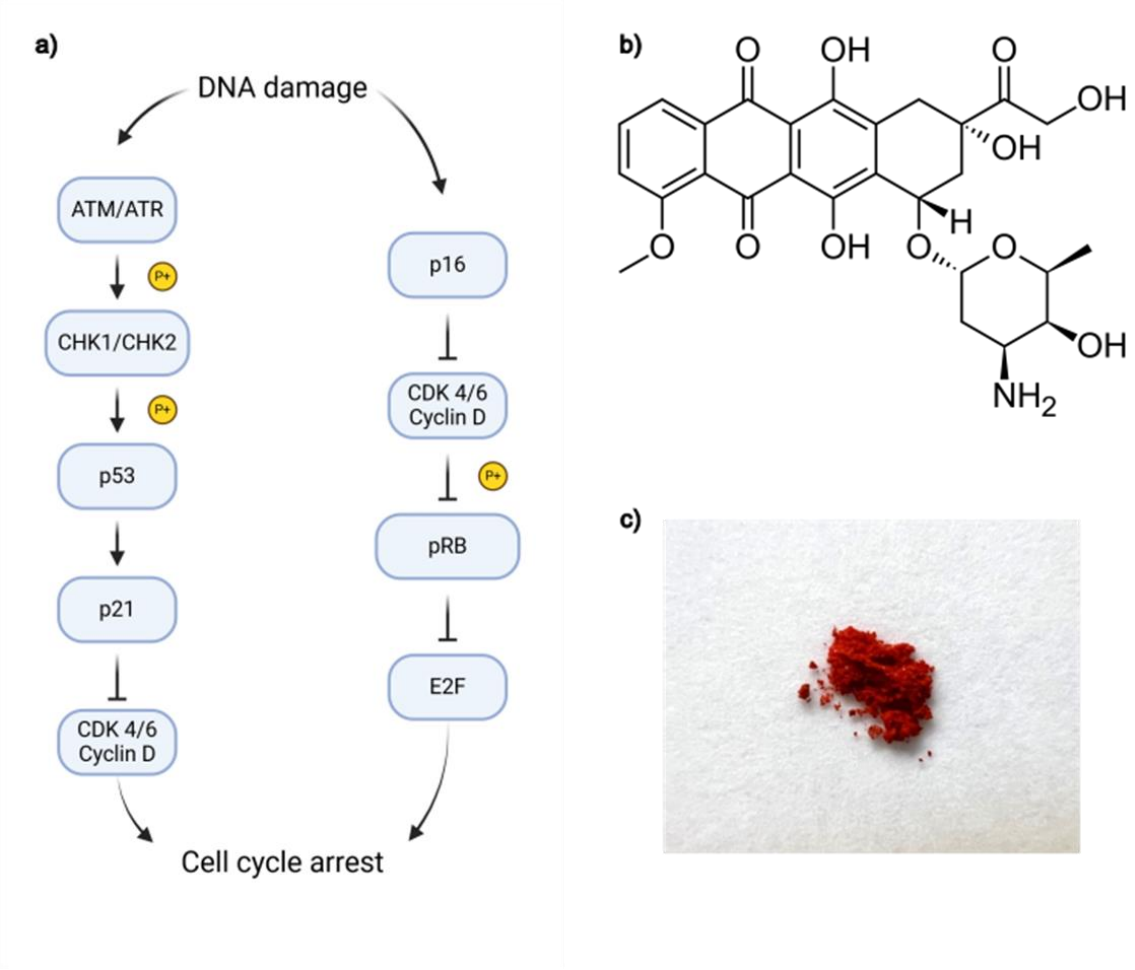

Figure 2. a) Simplified diagram of DNA damage response pathways leading to the cell cycle arrest, which can be caused by doxorubicin. Based on kegg.jp database [64]. b) Chemical structure of doxorubicin and c) picture of doxorubicin powder.

1.3 Senescence identification

As mentioned earlier, senescent cells undergo many changes at morphological and epigenetic levels. Many of these changes can be used as markers to identify senescent cells. It is

important to remember that no single method alone is sufficient to identify cellular senescence; rather, a combination of methods may be necessary.

Larger lysosomal content can be measured as it relates to increased activity of the enzyme β-galactosidase (β-gal), which is a very common senescent marker. It is because while normal cells' most optimal pH for β-gal activity is 4, for senescent cells, expression of its activity is also shown at pH 6 [36]. β-galactosidase reacts with X-gal (5-bromo-4-chloro-3-indoyl-β-d-galactopyranoside) at pH 6 due to hydrolysis, showing visible blue stains of accumulation of active enzyme, while normal cells are not able to develop such results. This is why incubating cells in place without additional CO_2 sources is so important [36].

Simple fluorescent labelling can also yield important data about the condition of a cell. For instance, marking the membrane or cytoskeleton can provide clues about the cell's expansion and expose abnormalities in its dimensions. Employing widely utilized nuclear fluorescent stains like DAPI or Hoechst can expose formations such as SAHF, manifesting as DNA punctuations within the nucleus composition [2], [37]. This method provides significant insights into cellular function, arrangement, and potential senescence-related changes.

Examining changes in the expression of crucial cell cycle genes using qPCR is essential; examples include p16, p21, and p53, which encode significant proteins that regulate the cell cycle, as mentioned earlier. The expression of these genes is augmented in senescent cells [3], [43], [56], [65]. To detect them, polymerase chain reaction (PCR) and its variant, real-time PCR, also referred to as quantitative PCR (qPCR) can be utilized to search for indications that cells have attempted DNA repair following exposure to stress. qPCR, is a modified version of PCR that enables the real-time detection and quantification of DNA amplification. This method offers instantaneous insights into the quantity of specific target DNA within a given sample. Various other markers can be identified using the same method, such as the reduction of Lamin B1 in the nuclear envelope [43], [56]. Western blot is another widely used technique employed in the field of molecular biology to identify distinct proteins, including senescent markers mentioned earlier. This method includes preparing samples containing a combination of proteins, utilizing electrophoresis for separation,

transferring the isolated proteins from the gel to a membrane, incubating them with suitable antibodies, and identifying the target protein [44], [45].

Cell proliferation tests that employ thymidine analogues like BrdU (5-bromo-2'-deoxyuridine) and EdU (5-ethynyl-2'-deoxyuridine) are an alternative method to illustrate growth arrest [44], [56]. This altered nucleotide replaces thymidine and is integrated into freshly produced DNA. The DNA needs to undergo denaturation for BrdU so that a fluorescent dye-labelled anti-BrdU antibody can attach to the BrdU-integrated DNA to be detected. Another technique to identify recently produced DNA is the application of EdU. In contrast to other methods, this strategy eliminates the need for DNA denaturation and relies on a "click" chemistry reaction to detect the new thymidine analogue. Following uptake by cells, EdU is integrated into newly synthesized DNA, where a fluorescent azide dye becomes covalently linked to each EdU alkyne group in the developing DNA. This method is recognized for its high sensitivity and offers benefits such as rapidity and reliability compared to BrdU [66].

All SASP factors can be identified with molecular assays such as Enzyme-Linked Immunosorbent Assay (ELISA). ELISA is a specific type of enzyme immunoassay that operates in the solid phase to detect the presence of a ligand in a liquid sample using specific antibodies designed for the protein being analyzed. This test shows colorimetric results and can be analyzed by spectrophotometer [42], [43], [44].

1.4 Cellular senescence and cancer

Cellular senescence is often described as “double-edge sword” due to its beneficial and harmful effects on the body. Many crucial biological functions rely on cells entering a state of cell cycle arrest and transitioning to final stages, such as embryogenesis, wound healing, and tumor suppression, but chronic senescence can lead to many pathologies, which are depicted in Figure 3.

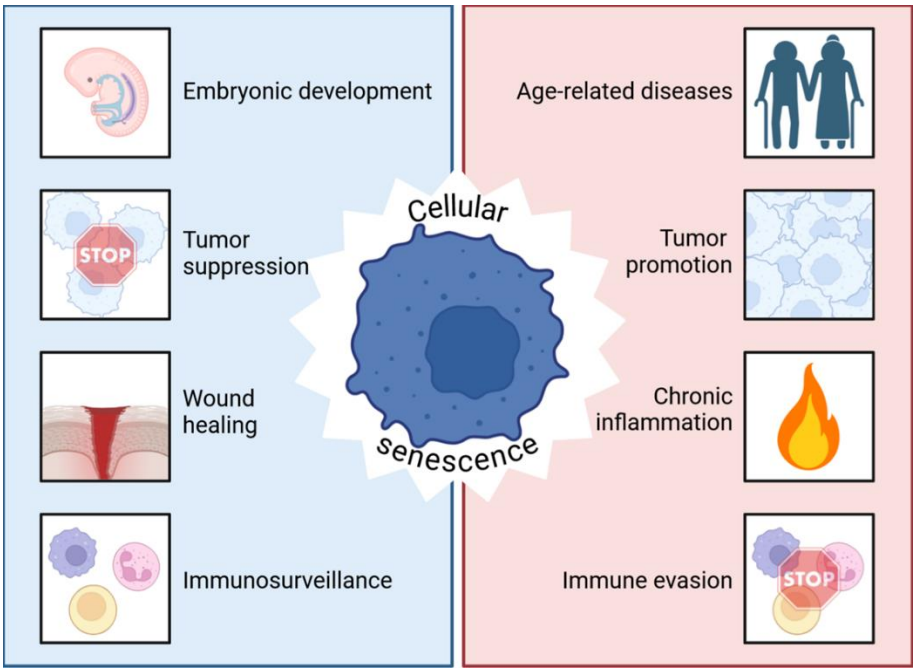

Figure 3. Representation of good and bad sides of cellular senescence

1.4.1 As a mechanism against cancer

Cancer is primarily characterized by its abnormal cell divisions, which can be blocked by a mechanism that inhibits its growth. Cellular senescence was described as irreversible cell growth arrest, and due to this paradigm, it was included as tumor suppressor mechanism [67]. Additionally, its ability to activate immune surveillance supports the clearance of cancer cells. SASP serves as a medium for senescent cells to communicate with neighbouring cells, playing an important antitumor role by generating various factors such as cytokines, chemokines, growth factors, and proteases. Additionally, it can activate the immune system to facilitate the clearance of cancer cells by recruiting natural killer (NK) cells and M1 macrophages following its formation to eliminate senescent or cancerous cells through immunosurveillance mechanisms [5], [68]. Considering all this a whole, cellular senescence serves as a mechanism for suppressing the development of various malignancies.

It is important to note that only short-term induction of cellular senescence plays a role in the beneficial mechanisms mentioned above: tumor suppression, wound healing, and embryogenesis [3], [4]. Moreover, it was noticed that the beneficial effect of senescence is more

visible at the early stages of cancer, while in the late stages, it leans more toward tumorigenesis, which overshadows its beneficial properties [69].

1.4.2. As a support of tumorigenesis

Although there is evidence supporting the tumour-suppressing properties of senescence, an indication that the existence of senescent cancer cells may lead to harmful consequences is growing among scientists. Senescent cells can engage in tumorigenesis process in many ways, though enhancing the invasiveness of the tumour, evading the immune surveillance, or escaping from cell cycle arrest.

Epithelial-mesenchymal transition (EMT) is a process in which a cell loses its adhesion, can migrate, and plays a crucial role in cancer metastasis. Cancer cells can detach from their original locations and spread to distant places within a body. It is suggested that SASP is the main source of activating EMT and strengthening invasive features [42], [70]. SASP can also hamper the immune system, which has a unique ability to identify and eliminate cancer cells, through the detection of their unique antigens or molecules. Some molecules secreted by SASP, such as IL-6 and CCL2, help in the generation of myeloid-derived suppressor cells (MDSCs), which are known for their immunosuppressive activities and may contribute to the depletion of anti-tumor immune surveillance [71]. Cancer cells that undergo TIS showed increased expression of some genes that are correlated with stemness, such as NANOG or CD34 and activation of Wnt signalling pathway, characteristic of stem cells. Stemness can occur independently in cell due to transcriptional reprogramming associated with senescence, but it is also believed that SASP can be highly involved [72]. Reversible senescence is commonly observed in therapy-induced senescence. Such a situation that occurs after chemotherapy can be potentially a risk of cancer recurrence. Escape from the senescence process may happen when the absence of essential upkeep genes allows cells to re-enter the cell cycle, even if they are held in a state of cellular senescence due to epigenetic changes. Such transformation can lead to aggressive cancer phenotype, often seen in cancer relapses. To the changes in cancer cells after escaping the TIS, named hallmarks, we can include the display of increased levels of transformation compared to parental cancer cells, higher aggressiveness, and resistance to anti-cancer treatments, which was shown in certain studies [56], [73], [74]. The mechanisms behind the escape from cell cycle arrest were not fully studied, but

there are epigenetic alternations that can be highlighted. One of them is the downregulation of p21, which leads to a lower generation of CD47 protein [46]. There's also overexpression of cyclin-dependent kinase Cdc2/CDK1, which level is low in the senescent population of cells [75]. Both of them play an important role in the cell cycle, and the changes promote TIS escape.

In summary, senescent cancer cells can resume proliferation and generate tumors, displaying more invasive and migratory properties. These cells show features similar to cancer stem cells, capable of self-renewal and cell type differentiation, which may suggest a potential for aggressive behaviour and cancer relapse. When senescent cells exhibiting stemness and invasiveness will evade immune surveillance and begin proliferation, there's a high risk of cancer recurrence.

1.5 Senotherapies

Senescent cells resist apoptosis by increasing the activity of pathways that prevent it, which may hamper their elimination through a protective mechanism known as the senescent cell anti-apoptotic pathway (SCAP). The higher expression of BCL-2 family members and PI3K/AKT pathway are well-known anti-apoptotic biomarkers [76], [77]. Out of senotherapies, two main strategies can be identified: senolysis, which involves clearing out senescent cells; and senomorphics, which aim is to reduce the production of SASP. It is important to remember that cellular senescence is a heterogenous process determined by various factors, including the type of stress stimuli, response pathways, cell type and line, and tissue source. Each variable can influence the effect of senotherapy, and deciding which one should be chosen is important.

Senolytics are a class of drugs that selectively eliminate senescent cells that are naturally apoptosis-resistant. Targeted treatments are often more precise and more effective compared to traditional methods, as they result in fewer off-target effects. Senolytics promote senescent cell apoptosis by specifically targeting components associated with anti-apoptotic mechanisms such as BCL-2, PI3K/ATK, and other relevant factors. During senescence, the high level of BCL-2 plays an important role, as their downregulation or inhibition in senescent cells leads to apoptotic cell death [76]. The PI3K/AKT pathway regulates crucial pro-survival functions, including protein synthesis, metabolism, and cell proliferation. Its role is to promote cell growth and inhibit

programmed cell death. AKT promotes cellular survival by blocking the activities of proteins and mechanisms that trigger programmed cell death. The inhibition of this pathway leads to apoptosis of senescent cells [77].

Senomorphics aim to reduce the harmful effects of SASP, leading to senostasis by preventing senescence through suppression of SASP expression and targeting mTOR, NF-κB and more. SASP is a key feature of senescent cells and contributes to their negative effects. It can promote cancer progression, speed up aging, and cause genetic mutations in the neighboring area. Many senomorphic compounds target one or a group of SASP factors, with possible effects on other aspects of cellular senescence, like cell cycle arrest. The functions of the mTOR pathway are wide-ranging, from the coordination of cell growth and proliferation to the regulation of aging and lifespan, as well as various other cellular processes [78]. mTOR serves as an important regulator of SASP, and its inhibition has the potential to be used in treatments targeting senescence.

Taking into consideration the heterogenous nature of senescent cells, it is unlikely that a single senolytic agent will be highly effective against all types of these cells. Some drugs are able to act as senomorphics and/or senolytics. The effect seems to vary based on the type of cell or/and the drug's concentration [76]. The exact mechanism of why the effects differ is still not explained.

1.5.1 Fisetin

Fisetin (3,3’,4’,7-tetrahydroxyflavone), is a bioactive yellow flavonoid polyphenol that occurs naturally in many fruits, vegetables, flowers, and tea. Its molecular formula is $C_{15}H_{10}O_{6,}$ with a molecular mass of 286.239 g/mol and Chemical structure showed in Figure 4b. Due to its crystalline nature, it exhibits low solubility in water but is soluble in organic solvents such as ethanol or DMSO. Fisetin and its chemical formula was first described in 1891 by Josef Herzig [79]. It is widely effective due to its neuroprotective, anti-inflammatory, tumor-suppressive and antioxidant properties. Fisetin's hydrophobic properties allow it to enter and build up in the cell membrane, exerting antioxidant and anti-inflammatory effects [80]. Surprisingly, the senotherapeutic effects of Fisetin differ based on the cell line it interacts with, which means its activity is cell-specific [76], [81]. For example, studies reported that HUVEC cells exhibit apoptosis,

while MEF cells demonstrate reduced senescent markers without signs of apoptosis [76]. Fisetin causes inhibition of various molecular targets and pathways in senescent cells. For example, it is capable of inhibiting the PI3K/AKT/mTOR pathway and of inhibiting BCL-2 family members or p53 binding [76], [77], [78], [82]. In addition to these effects, Fisetin may also impact other cellular processes related to senescence.

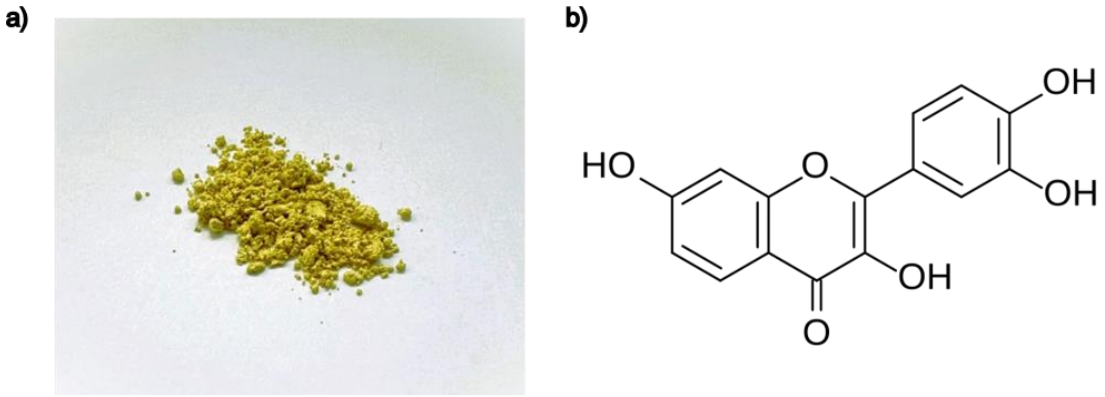

Figure 4. a) Picture of fisetin powder and b) chemical structure

1.6 Drug delivery system

Drug delivery system (DDS) enables delivery and distribution of a drug within the body, controlling the rate and place of release in the body without early degradation. Such approach help improve its efficiency and safety to achieve therapeutic outcomes [83]. One of the most well-known forms of DDS is through tablets or ointments. Such conventional DDS are widely available but have many limitations, including high dose dumping, repeated dosing, or fluctuations in plasma drug level, which in results can lead to overdosing or underdosing. For instance, tablets designed for immediate release disintegrate quickly and release the active pharmaceutical ingredient (API), but typically do not extend the duration of drug release or absorption. Consequently, a specific frequency of drug administration is necessary to sustain the required therapeutic level over an extended period [83].

There has been growing interest in developing new drug delivery systems that can regulate and enhance pharmacokinetics and pharmacodynamics, as well as the efficacy and toxicity of APIs. Nanotechnology has introduced drug-loaded nanocarriers and nanoparticles that can

improve the efficiency of drugs while decreasing the risk of side effects. The perfect nanoscale drug delivery system should target specific sites to increase the concentration of the drug, enhance solubility for easier administration, maintain a consistent rate of drug release, prolong the half-life of the drug by reducing clearance and improve the stability to minimize degradation of the drug [84].

Surface modification can be involved in the process of creating nanoparticles to enhance their biocompatibility and stability, reduce toxicity, and improve uptake. These modifications may involve the use of proteins, peptides, antibodies, polysaccharides or oligosaccharides, depending on the desired effect [85]. Certain nanoparticles exhibit natural toxicity to cells, but coating their surface with polysaccharides like dextran or chitosan has reduced this toxicity for iron-oxide nanoparticles [86], [87]. Modifications can be used to enhance nanoparticle uptake, with PEG being one of the most well-known uptake enhancers. PEGylation of nanoparticles also reduces their tendency to aggregate and increases their stability in biological fluids [88].

API is connected with nanoparticles by surface attachment, entrapment (built in the structure of nanoparticle), or encapsulation (the drug is confined within the nanoparticles). Nanoparticles range between 1 and 1000 nm and can be classified as organic, inorganic or carbon-based, where examples of nanoparticles from each class is showed in Figure 5. Organic nanoparticles include such structures as polymeric nanoparticles and lipid-based nanoparticles. Across inorganic nanoparticles, the most known are quantum dot, mesoporous, and gold nanoparticles. We can synthesize hybrid nanoparticles such as metal-organic frameworks (MOFs) by combining inorganic and organic compounds. Carbon-based nanoparticles, which are built out of graphene, can take various forms, including nanotubes, a cylindrical construction and fullerenes, a spherical structure [89].

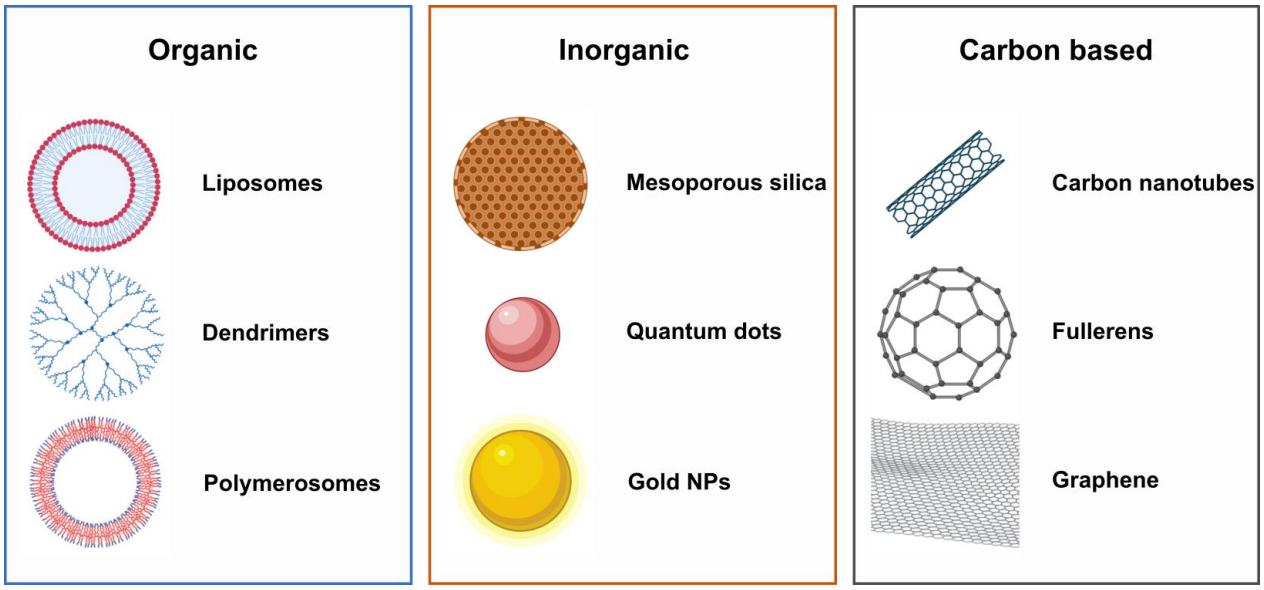

Figure 5. Classification of nanoparticles with examples.

One of the examples of a drug delivery system using nanoparticles to target senescent cells is based on SA-β-gal activity. When internalized by endocytosis, drugs encapsulated within galactosidase coating are transported to lysosomes for digestion and release the cargo. Senescent cells with high levels of lysosomal β-galactosidase can break down the galactosidase coat, while non-senescent cells keep the cargo encapsulated [90]. Another way to selectively eliminate senescent cells with minimal impact on other cell types is the creation of nanoparticles loaded with senolytics designed to recognize a marker on the surface of senescent cells [91]. A different approach involves using nanoparticles to target the tumor microenvironment and enhance the immune response against tumor cells. The researchers discovered that inducing cellular senescence and targeting the tumor microenvironment with certain agonists can increase INF-β production and activate natural killer and T cells within the tumor area by regulating the SASP [92].

1.6.1 Liposomes

Liposomes are one of the most explored nanocarriers used in nanomedicine and due to their biocompatibility, high bioavailability, and stability, some of the lipid-based drug delivery systems were FDA and EMA-approved in various therapeutic areas, which are listed in Table 2.

Their synthesis is simple, based on the process of emulsifying lipids in aqueous medium, creating self-assembled spherical lipid vesicles.[93] Naturally, liposome's size is in the nanoscale, but to use them in drug delivery, their size range should be around 50-150 nm, so their preparation also includes a thin-film extrusion technique that can help achieve the desired size range of liposomes [88]. Liposomes can be created with natural or synthetic lipids, usually with the addition of cholesterol, as it modulates membrane permeability and improves the stability of bilayer membranes in the presence of biological fluids [93]. Encapsulation of drugs is possible thanks to the hydrophobic and hydrophilic properties of liposomes' bilayer; in effect, liposomes can be used as carriers for drugs, independently of their solubility in water. The ability to incorporate both hydrophobic and hydrophilic drugs within a single liposome formulation extends the potential applications of liposomes in drug delivery, enabling more extensive and suitable therapeutic approaches [94]. Drug loading into liposomes can be achieved through two main methods: passive encapsulation or active remote loading. Passive loading is a straightforward approach where the lipids and drug are dissolved together during preparation. This results in the formation of liposomes with the drug entrapped within their aqueous core or integrated into the phospholipid membrane. In contrast, the active loading process involves filling pre-formed liposomes that already contain specific salt solutions in their core. As drug molecules diffuse through the phospholipid membrane, they become trapped within the liposome and are unable to escape. Active loading technique results in minimal drug loss and a high drug-to-lipid ratio compared to passive loading [95].

Table 2. Representative list of available EMA and/or FDA-approved liposomes used in medical treatments based on FDA and EMA data bases and available literature [84], [96].

Product name	Active ingredient	Application	Approval
Doxil®	Doxorubicin	Ovarian cancer; AIDS-related Kaposi's Syndrome; Multiple Myeloma	FDA 1995
DaunoXome®	Daunorubicin citrate	Advanced AIDS-related Kaposi's Syndrome	FDA 1996
Caelyx®	Doxorubicin	Metastatic breast cancer; Ovarian cancer; AIDS-related Kaposi's Syndrome; Multiple Myeloma	EMA 1996
AmBisome®	Amphotericin B	Fungal infections including Histoplasmosis, Cryptococcosis, Coccidioidomycosis, Candidiasis, Leishmaniasis, Talaromycosis	FDA 1997 EMA 1998
Inflexal®	Inactivated influenza virus vaccine	Prevents influenza infection	EMA 2006
Myocet®	Doxorubicin hydrochloride	Metastatic breast cancer	EMA 2000
Visudyne®	Verteporfin	Age-related macular degeneration (AMD); Choroidal neovascularisation	EMA 2000
DepoDur®	Morphine sulfate	Post-Surgical Pain Relief	FDA 2004 EMA 2006
Mepact®	Mifamurtide	High-grade non-metastatic osteosarcoma	EMA 2009

Marqibo®	Vincristine sulfate	Philadelphia chromosome-negative acute lymphoblastic leukemia	FDA 2012
Epaxal®	Inactivated virosomes	Hepatitis A virus	EMA 2000
Vyxeos®	Daunorubicin and cytarabine	Acute myeloid leukaemia	EMA 2018
Onivyde®	Irinotecan	Metastatic adenocarcinoma of the pancreas	EMA 2016
Onpattro®	Patisiran	Hereditary transthyretin-mediated amyloidosis	EMA 2018 FDA 2018

Lipid-based nanoparticles have significant limitations that impact their effectiveness as drug delivery systems. These include low drug loading capacity and suboptimal biodistribution, leading to high accumulation in the liver and spleen, which can reduce the amount of drug that reaches the target site. Additionally, the phospholipids that makeup liposomes are prone to oxidation, causing reactions similar to hydrolysis that can degrade the nanoparticle structure and compromise the stability of the encapsulated drugs. Another major drawback is the potential for leakage and fusion of the encapsulated drugs, which can result in premature drug release and reduced therapeutic efficacy. Furthermore, the mass production of liposomes as drug carriers is associated with high costs, which can limit their accessibility for patients [97], [98].

Chapter 2 Objectives

2.1 General objectives

As chemotherapeutics can cause cellular senescence in small dosages, patients after chemotherapy are at risk of not eliminating all cancer cells in their bodies. Studies have shown that senescent cells can re-enter the cell cycle, causing cancer recurrence. One of the best known serotherapeutic drug is fisetin, however due to its low solubility in water, it is important prepare a drug delivery system. This thesis is mainly concerned with studying the delivery of fisetin encapsulated in nanoparticles to senescent cells to evaluate the efficacy of the carriers, aiming at developing fisetin formulations that could be used in senotherapy applied to cancer patients.

2.2 Specific objectives

Senescence induction

The first objective was to develop a protocol of senescence induction on a big scale to obtain a large amount of senescent cells for subsequent experiments with fisetin. Induction has been performed with DOX, a well-known chemotherapeutic agent. After preparations, cells were analyzed for various senescent markers such as: SA-β-gal, cell size, proliferation, level of LMNA and LMNB2, and level of IL-6 and IL-8.

Liposomes preparation

The next objective was the preparation of liposome formulations encapsulating fisetin. Due to its hydrophobic properties, fisetin was encapsulated within the hydrophobic regions of the lipid membranes in the liposomes. After preparations, liposomes were extensively characterized in terms of size and morphology using dynamic light scattering (DLS) and cryogenic scanning electron microscopy (Cryo-SEM). The loading of fisetin was determined by using spectrofluorometer based on its fluorescence properties.

Liposomes uptake and drug delivery

Lastly, liposomes were fluorescently stained, and their cellular internalization was followed by confocal laser scanning microscopy (CLSM). The impact of fisetin on cells was studied in terms

of proliferation, secretion of previously analyzed interleukins and viability of A549 and WI38 cell lines.

Chapter 3 Materials and methods

3.1 Cell culture, passaging, cell counting and long-term storage

Human lung fibroblasts WI38 and small lung cancer cells A549 were purchased from ATCC. Both cell lines were cultured on T75 bottles maintained in EMEM enriched with 10% FBS, 1% sodium pyruvate and 1% antibiotics (penicillin 100 µg/mL, streptomycin 100 µg/mL), incubated at 37 °C in 5% CO_2. Cells were passaged each time they achieved about 80% of confluence to prevent overgrowth. The medium was discarded, and cells were washed with HBSS to remove residual serum. Then, 1.5 mL of Trypsin-EDTA was added to the flask and placed in an incubator for a 5 min until the cells detached. The trypsin was neutralized by adding 8.5 mL of media. To maintain cell culture for further experiments, 1 mL of A549 and 2.5 mL of WI38 were placed in new bottle with fresh medium at final volume 10 mL.

The remaining cells were centrifuged for 5 min at 1200 rpm for the experiments. After removing the supernatant, the cells were resuspended in 1 mL of fresh medium and thoroughly mixed. To count the cells, 10 µL of the cell suspension was loaded onto counting slides, and the cell concentration was determined using an automated cell counter.

Long-term storage was utilized to ensure a low passage stock of cells. Upon reaching approximately 80% confluency, cells were trypsinized and centrifuged as described above. Following supernatant removal, cells were resuspended in a medium with 10% DMSO and, immediately moved to cryovials and transferred to -80 °C in a freezing container containing isopropanol. After 24 h, the cells were moved from -80 °C to a liquid nitrogen storage tank. To refresh the cell culture, cells were thawed with a warm medium followed by centrifugation for 5 min at 1200 rpm and then seeded in a T75 bottle with fresh medium after removing the remaining supernatant.

Table 3. Reagents used for maintenance of cell cultures

Reagent	**Supplier**
Eagle's Minimum Essential Medium	Sigma Aldrich, Merck
Fetal Bovine Serum	Biowest
Dulbecco's Phosphate Buffered	Gibco, Thermo Fisher
Phosphate Buffered Saline	Sigma Aldrich, Merck
Hank's Balanced Salt Solution	Gibco, Thermo Fisher
Dimethyl Sulfoxide	Sigma Aldrich, Merck
Trypsin-EDTA	Gibco, Thermo Fisher
Antibiotics	Sigma Aldrich, Merck
Sodium pyruvate	Sigma Aldrich, Merck

3.2 Cell viability assay

Firstly, the concentration of the DOX that allows cells to go through cellular senescence instead of apoptosis was measured experimentally based on the available literature [99], [100], [101]. The doxorubicin concentration range tested in WI38 cells was between 0.75 µM and 3 µM, and in A549 between 0.05 µM and 800 µM. Cells were seeded in 96-well plates at a density of $2x10^3$ cells/well and incubated for 24 hours to allow cell attachment. Next, the cells were treated with chosen concentrations of DOX for 72 hours. Then, the cells were rinsed with HBSS, and the culture medium was replaced with fresh, drug-free EMEM for an additional 72 hours of incubation. Each concentration was studied in triplicates. After the induction procedure was finished, control cells were seeded at the same density and incubated for 24 hours to attach.

WST-1 assay was utilized to evaluate cell viability based on the metabolic activity of the cells. 10 µL of WST-1 reagent was added to each well containing cells in 200 µL of fresh medium. Wells without cells were used for background subtraction. Determined on color development, the A549 cell line was incubated with WST-1 reagent for 1 hour, and WI38 cell line for 3 hours. Absorbance was measured using an Anthos Zenyth 340rt microplate reader at 450 nm wavelength with a

reference wavelength at 620 nm. Calculations were conducted in MS Excel using Equation 1. The mean and standard deviation of the cell viability percentages were calculated.

$$\text{Cell viability } \% = \frac{(\text{Value X} - \text{Background})}{(\text{Control} - \text{Background})} * 100\%$$

Equation 1. Percentage of cell viability based on WST-1 assay.

Cell viability was measured using flow cytometry, technique that enables the analysis of thousands of individual cells in a continuous stream as they traverse laser beams. During this process, cells are evaluated based on their light scattering properties and fluorescence characteristics. This allows for precise determination of cell size and other morphological parameters.

To evaluate cell viability based on membrane integrity, a Live/Dead assay was performed following the manufacturer's instructions. Cells seeded in T25 flasks at density $1x10^5$ and treated in the same way as previously described. Next, cells were trypsinized and collected in 1.5 mL test tubes. The cell suspension was centrifuged at 1200 rpm for 5 min. The supernatant was discarded, and the cell pellet was resuspended in 1 mL of DPBS. To the resuspended cells, 1 µL of fluorescent reactive dye was added. The cell suspension was mixed thoroughly and incubated at RT for 30 min, protected from light. Following incubation, cells were fixed with 4% formaldehyde at RT for 15 min. Cells were washed with PBS buffer and centrifuged at 1200 rpm for 5 min after each step. For final resuspension, 50 µL of PBS was added to cell pellet and mixed, preparing the sample for further analysis. Samples were analyzed using Flowsight imaging flow cytometer (Amnis, Luminex) on the slowest flow rate to ensure good quality pictures for analysis. The fluorescent reactive dye was activated using 642 nm laser. Data and pictures of 1000 events in were collected in triplicate and analyzed in IDEAS® 6.3 software.

Table 4. Reagents used in WST-1, Live/Dead, SA-β-gal, ELISA and EdU assays.

Reagent	**Supplier**
WST-1 assay kit	Roche
LIVE/DEAD Fixable Far Red Dead Cell Stain Kit	Invitrogen, Thermo Fisher
Senescence cells histochemical staining kit	Sigma Aldrich, Merck
IL-6 ELISA kit	Bio-techne, R&D Systems
IL-8 ELISA kit	Bio-techne, R&D Systems
EdU Click-it kit	Baseclick
Hoechst 33342	Invitrogen, Thermo Fisher
Calcein	Invitrogen, Thermo Fisher
EthD-2	Invitrogen,Thermo Fisher

3.3 Cellular senescence induction with DOX

Cellular senescence was induced by treatment of cells with freshly prepared DOX solution. DOX was dissolved in PBS at a stock concentration of 0.5 mg/mL (920 µM). Next, final drug concentrations were prepared from the stock at values 1 µM and 0.2 µM for WI38 and A549 accordingly. $1x10^5$ cells were seeded in T25 bottles and left for 24 hours to attach before undergoing further treatment. Cells were treated with DOX for 72 hours, followed by washing with HBSS and changing the medium to fresh, drug-free EMEM, where they were left to incubate for an additional 72 hours. After that time, the cells were ready for further experiments. The cells were used within 7 days after treatment.

3.4 Senescence associated β-galactosidase staining

A histochemical kit measuring β-gal activity was used to identify senescent cells. WI38 and A549 cells were seeded on one-well LabTek chamber slides at a density of $5.6x10^4$ and $4.7x10^4$ cells/well, respectively, and left for 24 h to attach. The assay was performed according to the manufacturer's manual. The incubation time was established experimentally. All reagents were warmed beforehand at RT, while the X-gal reagent was heated to 37 °C to dissolve all crystals. Cells were washed three times with PBS provided in the kit and incubated for 6-7 min with a fixation buffer. In the meantime, the staining solution was prepared with manufacturer instructions and

then filtered using a 0.2 µm syringe filter. After removing the fixation buffer, cells were washed three times with PBS and then covered with a staining solution. Incubation was performed at 37 °C without the addition of CO_2, for 5 h for WI38 cells and overnight (approximately 15 h) for A549 cells. After incubation, cells were washed twice with PBS, and nuclei were stained with Hoechst 33342 dye, at final concentration of 16 µM. Such prepared cells were used to collect images for further analysis of the percentage of senescence induction success. Images were taken using FV1000 confocal laser scanning microscope (Olympus), quantification was performed using ImageJ Software, and all data was collected and presented using OriginLab Pro 2023.

3.5 Metabolic investigation

WST-1 assay was used to analyze the metabolic activity. Both cell lines were seeded in 96-well plated at density $2x10^3$ after the senescence induction and left for 24 hours to attach. After the incubation time, WST-1 assay was performed as described in Chapter 3.2. The optical density results were then calculated, comparing senescent to non-senescent metabolic percentages.

3.6 Identification of SASP components

The enzyme-linked immunosorbent assay (ELISA) was performed according to the manufacturer's protocol. Capture antibodies were freshly diluted with PBS to the working concentrations according to the attached datasheet for IL-6 and IL-8 antibodies. Plate layout afforded duplicate standards of each type of interleukins and 3 repetitions of each cell type. A 100 µL of prepared solution was added immediately to desired wells, sealed with an adhesive strip, and incubated overnight in RT. After each step, wells were washed thrice with wash buffer, and all remaining liquid was removed by blotting an inverted plate against paper towels. The next day, wells were blocked by adding a block buffer for an hour of incubation in RT. In the meantime, standards were prepared in 2-fold serial dilutions for 7-point standard curves for each interleukin. Reagent diluent was used as blank. Cells were seeded in approximately the same amount and were incubated in a fresh medium for 24 hours before the medium was taken for further analysis for the presence of the discussed interleukins. Samples, standards, and blanks were added in 100 µL to appropriated wells and incubated in RT for 2 hours. After that, the detection antibody was added to the wells and incubated for another 2 hours, which was followed by adding 100 µL of

the strepavidin-HRP to each well and incubated for 20 min in RT, in the dark, followed by incubation with a substrate solution in the same conditions. Adding substrate solution causes the production of a blue colour over time. The assay procedure was finished after adding 50 µL of stop solution to each well, which caused color change to yellow. Immediately, the optical density was determined using an Anthos Zenyth 340rt microplate reader set at 470 nm wavelength with 570 nm wavelength as a reference with the low shake option to ensure thorough mixing.

The ELISA protocol was repeated using cells that had been incubated for 48 hours with fisetin. All steps were repeated, and cells received fresh medium after treatment with the drug. The collected medium was used for further analysis after 24 hours.

3.7 RNA extraction, cDNA synthesis and qPCR for Lamins

Cells were trypsinized, collected in a 1.5 mL test tube, and stored at -80 °C until needed for further processing. To isolate RNA, 1 mL of Trizol reagent was added to each sample, and the mixture was incubated for 5 min at RT. The Trizol reagent effectively lyses the cells, releasing the RNA, and importantly, it also helps preserve the integrity and quality of the extracted RNA for analysis. Next, 200 µL of chloroform was added, and the solution was mixed. It was then incubated for an additional 2 min at RT. After incubation, the samples were centrifuged in Centrifuge 5415R (Eppendorf) at 4 °C for 15 min at 14,000 rpm. Chloroform helps purify the RNA, as it is extracted into the top, aqueous phase, while the protein and DNA remain in the lower phase of the solution. The water phase was transferred to a new test tube and mixed with 0.5 mL of isopropanol. The samples were incubated for 10 min at RT, then centrifuged at 4 °C for 10 min at 14,000 rpm. The samples were placed on ice, the supernatant was removed, and the pellet was washed with 1 mL of 75% ethanol in DEPC water. The samples were then centrifuged at 4 °C for 5 min at 8,000 rpm. The ethanol was removed, and the residual ethanol was allowed to evaporate before adding 20 µL of DEPC water. In order to remove any residual DNA, 1 µL of DNase was added to each sample and incubated at 37 °C for 25 min. Next, 4 µL of inactivator was added and thoroughly mixed, followed by a 5 min incubation at RT. The samples were then centrifuged at 10,000 rpm for 1.5 min, and the supernatant was transferred to a new test tube, taking care not to aspirate any residue. The RNA was then eluted with 10 µL of DEPC water, and its concentration was measured using a Nanodrop 2000 spectrophotometer (Thermo Fisher Scientific). The measured RNA

concentrations were calculated, and the samples were diluted in DEPC water to obtain consistent concentrations, which is crucial for further analysis.

Table 5. Reagents used for RNA's isolation and electrophoresis

Reagent	**Supplier**
TRIzol Reagent	Invitrogen, Thermo Fisher
Chloroform	Stanlab
Isopropanol	Stanlab
DNase	Bio-Rad
SYBR™ Safe	Invitrogen, Thermo Fisher

Electrophoresis was performed on a 1.5% agarose gel containing SYBR Safe, a nucleic acid stain, to analyze the quality of the isolated RNA. The gel was prepared by suspending 1.5 g of agarose powder in 100 mL of 1xTAE buffer in a flat-bottom flask. The flask was then heated in the microwave to allow the agarose to dissolve fully, and 5 µL of SYBR Safe was added. All obtained samples were then diluted to yield 750 ng of nucleic acid in a 10 µL mixture of sample and DEPC water. 2 µL of loading buffer was added to each diluted sample, and the resulting mixture was then loaded into the gel pockets. Electrophoresis was set to 70 V for 1.5 hours.

Total RNA was extracted from the sample and reverse transcribed into complementary DNA (cDNA) in C1000 Touch Thermal Cycler (Bio-Rad). To prepare the reaction cocktail, 4 µL of the reaction mix, 1 µL of reverse transcriptase, RNA template at the desired concentration and DEPC water were added to obtain a total volume of 20 µL. The process of RNA transcription into cDNA involved three steps described in Table 4.

Table 6. Reverse transcription conditions.

Step	**Temperature**	**Time**
Priming	20 °C	5 min
Reverse transcription	37 °C	20 min
Enzyme deactivation	70 °C	1 min

Table 7. Reagents used for cDNA transcription

Reagents	**Supplier**
iScript™ Reverse Transcription Supermix	Bio-Rad

The resulting cDNA was then used as the template for the qPCR analyses. The qPCR analysis was performed on the cDNA generated from reverse transcription using thermocycles CFX96 Real-Time System (Bio-Rad). The reaction mixture had a total volume of 12 µL, containing forward (1 µL) and reverse (1 µL) primer sequences, which are listed in Table 8, iTaq™ SYBR® Green Supermix (1 µL), DEPC water (5 µL), and the cDNA (2 µL). SYBR® Green is a fluorescent dye that binds specifically to DNA, and the fluorescent signal is proportional to the amount of DNA present in the sample. A negative control sample without cDNA was also included. The temperature and duration settings used for the qPCR analysis are shown in Table 6.

Table 8. Thermal cycling conditions for qPCR

Step	**Temperature**	**Time**	**Cycle**
Predenaturation	95 °C	5 min	1
Denaturation	95 °C	45 sec	
Starters connection	60 °C	45 sec	45
Elongation	72 °C	1 min	
Final elongation	72 °C	10 min	1
Cooling	15 °C	∞	

Table 9. Reagents used for qPCR.

Reagents	**Supplier**
Primers	Genomed
iTaq™ Universal SYBR® Green Supermix	Bio-Rad

Table 10. Sequences of primers used for qPCR

Gene symbol	Orientation	Primers Sequence (5' – 3')	Base pair (bp)
LMNA	Forward	AATGATCGCTTGGCGGTCTAC	21
	Reverse	CACCTCTTCAGACTCGGTGAT	21
LMNB2	Forward	GTCCTGGATGAGACGGCTC	19
	Reverse	GCGCTCTTGTTGACCTCGT	19
Actin	Forward	GCTCTTTTCCAGCCTTCCTT	20
	Reverse	CATACAGGTCTTTGCGGATGT	21

3.8 Cell proliferation analysis

The cell proliferation ability was analyzed by using ClickTech EdU cell proliferation assay. Cells were seeded in a 96-well plate at a density of $2x10^3$ cells/well and incubated for 24 hours to allow attachment. Next, a 200 µL of EdU working solution at 20 µM concentration was prepared following the manufacturer's instructions, and cells were then incubated for their doubling time. The doubling time for both cell lines is about 24 hours, according to ATCC information. Following this incubation period, the media was removed and replaced with 4% formaldehyde in DPBS for 15 min at RT. After removing the fixation solution, the cells were washed twice with 3% BSA in DPBS before being treated with 0.1 % Triton X-100 in DPBS as permeabilization solutions, and they were then left to incubate for another 20 min at RT. The reaction cocktail containing Eterneon-Red 645 Azide, which detects EdU, was prepared as per the instructions provided by the manufacturer, and the cells were then incubated for 30 min at RT while being protected from light. Followed by washing twice, cell nuclei were stained with 8 µM Hoechst 33342 solution. Imaging was carried out using the INCell Analyzer 2000 (GE Healthcare Life Sciences), using the filters Cy5 (red) and DAPI (blue) to identify proliferating and total cells. In total 20 pictures of each well was taken at the 20x magnification. The examination of taken pictures was performed using IN Cell Developer Toolbox software by using installed protocol and calculation analysis of obtained results was conducted in OriginLab Pro software.

3.9 Analysis of cellular morphology

Cells were seeded in 8-well Lab-Tek chamber slides at a density of $1x10^4$ cells/well and incubated for 24 hours to allow attachment. After removing the medium, the cells were washed with DPBS and fixed with 4% formaldehyde in DPBS by incubation for 15 min. Next, 0.1% Triton X-100 solution in DPBS was added and incubated for 3 min, followed by the addition of 1% BSA and 20 min of incubation. The cytoskeleton was stained with Alexa Flour 488 phalloidin dye using the stock and dilutions prepared according to the manufacturer's instructions,150 µL of staining mixture was added to each well, incubating for 20 min in the dark. Nuclei were then stained with Hoechst 33342 dye (final concentration of 16 µM), and 150 µL of this solution was added to the cells for 10 min in the dark. After each step of this procedure, the cells were gently washed with DPBS, and all incubations were performed at RT. Once the staining was completed, the cells were washed twice with DPBS, and the chambers were filled with DPBS.

Table 11. Reagents used for morphology staining.

Reagent	**Supplier**
DPBS	Gibco, Thermo Fisher
Formaldehyde 16% (w/v), methanol-free	Pierce, Thermo Fisher
Triton-X	Sigma Aldrich, Merck
BSA	Sigma Aldrich, Merck
Phalloidin-488	Abcam
Hoechst 33348	Invitrogen, Thermo Fisher

The morphology of cell were studied with FV1000 confocal laser scanning microscope (Olympus). The drop of silicone-immersed oil was put on the 1.4 oil immersion lens. Images were observed with x60 magnification lens. For imaging, Phalloidin-488 was excited at a 488 nm and detected with emission filters 560-590 nm. Hoechst 33348 was excited using a 405 nm wavelength and detected with emission filters set from 425 to 475 nm.

3.10 Analysis of cell size

Cells were seeded in T25 bottles and induced as previously described. After the DOX treatment, cells were trypsinized and gathered in 1.5 ml test tube. Centrifugation for 5 min at 1200 rpm allowed to discard supernatant, and cells were resuspended in 100 µL PBS. The cell solution was analyzed using a FlowSight flow cytometer (Amnis, Luminex), where cells were measured in a bright field at the slowest flow rate setting. This allowed for the measurement and comparison of the size of unattached individual cells between treated and untreated samples. Data and pictures of 1000 events were collected and analyzed in IDEAS® 6.3 software. A template for gating was used across all data sets, and histograms were created based on the area in μm^2.

3.11 Preparation of liposomes

For liposome preparation, 1,2-dioleoyl-sn-glycero-3-phosphocholine (DOPC), 1,2-distearoyl-sn-glycero-3-phosphoethanolamine (DSPE) and cholesterol, which chemical structure is presented in Figure 6, were dissolved in chloroform, while fisetin was dissolved in absolute ethanol to achieve the desired concentrations (Table X). The table content changed depending on the weighed ingredients to obtain final concentrations. All components were thoroughly vortexed to ensure complete dissolution, then combined according to the formulation details in Table 4). After mixing, chloroform and ethanol were evaporated under a gentle argon flow , leaving the mixture spread along the bottle walls to prevent “jelly-like” clumps. Next, HEPES buffer (0.06M, pH 7.4) was added to reach the final concentration, and the sample was vortexed, to ensure no residue remained on the walls. The mixture was then placed at 4 °C for 24 hours to allow liposomes to encapsulate fisetin inside their structure. The liposomes were passed through the extruder 11 times to standardize their size to around 100 nm. For this purpose, membranes with the size of 0.8 µm, 0.4 µm, 0.2 µm and 0.1 µm in diameter were used. The extruder, filter membranes and Hamilton syringes were first rinsed with HEPES buffer. One of the syringes was designated as “dirty” to introduce the solution into the extruder, while the other, labeled "clean," collected the final product. Finally, the extruded liposomes were transferred to new, clean containers.

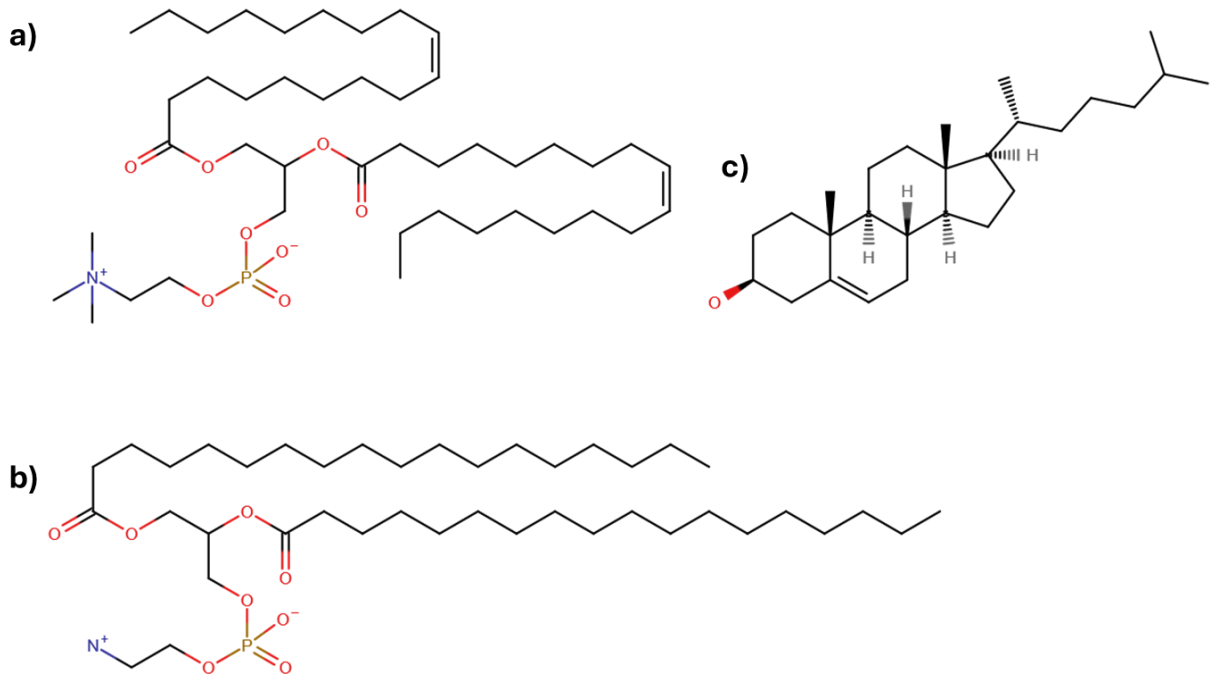

Figure 6. Chemical structures of a) DOPC, b) DSPE and c) cholesterol, components used to formulate liposomes.

Table 12. List or components and reagents used for liposomes formulation.

Reagents	**Supplier**
DOPC	Avanti Lipids
DSPE	Avanti Lipids
Cholesterol	Sigma Aldrich, Merck
Chloroform	Sigma Aldrich, Merck
Fisetin	AmBeed
Absolute ethanol (99.9%)	Sigma Alrdich, Merck
Hepes buffer	Sigma Aldrich, Merck
Sephadex G-25 column	Cytiva
Nile Red	Sigma Aldrich, Merck

Table 13. Concentration of compounds used for formulation of liposomes

Name	Concentration (mg/mL)	mL	mg
DOPC	20.66	3872	80
DSPE (18:0/18:0 PE)	10	1400	14
Cholesterol	10	700	7
Fisetin	1.70	2.58	4.38

Table 14. Formulation of liposome nanoparticles

Liposomes with fisetin (8 mg/mL)			
Name	%	mg	µL
DOPC	78	40	1936.11
DSPE	13	6.66	666
Cholesterol	6	3.08	308
Fisetin	3	1.54	907.12
Total		51.28	3817.23
Add Hepes		6.41	

Liposomes (8 mg/mL)			
Name	%	mg	µL
DOPC	80.4	40	1936
DSPE	13.4	6.66	666
Cholesterol	6.2	3.08	308
Total		49.74	2910
Add Hepes		6.22	

The liposomes solution was filtered through a Sephadex G-25 column to purify the liposomes and separate the free fisetin. Prior to filtration, the Sephadex column was first equilibrated with 25 ml of HEPES buffer. Following equilibration, 2.5 ml of liposome-fisetin solution was added to the column and 3.5 ml of Hepes was applied to facilitate elution into a clean collection bottle. The solution passed through the column by gravitational force. Finally, the fisetin concentration in the purified liposome solution was calculated.

3.12 Analysis of the fisetin loading into liposomes

A calibration curve was prepared to evaluate the concentration of fisetin and its entrapment efficiency (EE%) within liposomes. The measurements were performed on fluoroSENS spectrofluorometer (Gilden photonics). The excitation spectrum of fisetin exhibited maximum at $\lambda_{exc.}$ 418 nm, while the highest emission maximum was recorded at λ_{em} 486 nm. Square equation $(\mathrm{y} = 237.35\mathrm{x} + 5347.8,\ \mathrm{R}^2 = 0.9996)$ was prepared for further calculations.

Liposomes with and without fisetin were diluted in methanol at a ratio 1:50, and the fluorescence was measured on a fluoroSENS spectrofluorometer at λ_{em} 486 nm. The concentration of fisetin in µg/mL was calculated based on square equation and the entrapment efficiency was calculated with the equation presented below.

$$\mathrm{EE\%} = \frac{\text{Mass of drug in liposomes}}{\text{Mass of drug in formulation}} * 100\%$$

Equation 2. Entrapment Efficiency

3.13 Examination of liposomes size and charge

Size distribution, polydispersity, and ζ potential of prepared liposomes were analyzed by Dynamic Light Scattering (DLS). This technique analyzes the intensity fluctuations of light scattered from nanoparticles undergoing Brownian motion to define the nanoparticle population's size distribution. For each sample, 10 µL of liposome solution was added to 990 µL of distilled water and put into a folded capillary cell. All measurements were performed simultaneously for

liposomes with and without fisetin by Zetasizer Nano (Malvern) and results were expressed as mean values with standard deviations (mean ± SD, n=3).

3.14 Analysis of liposomes morphology

CryoSEM images were prepared with the help of dr hab. Olena Ivashchenko. Briefly, around 20 µL of prepared liposomes were placed onto the metal holder. The sample was promptly frozen by immersing it in slushed nitrogen to achieve faster cooling than with liquid nitrogen at its boiling point (-196 °C). Next, the sample was transferred to the preparation chamber using a cryo transfer device and preserved under vacuum conditions to prevent contamination and moisture. Finally, the sample was moved from the preparation chamber to the SEM chamber for further examination and imaging.

3.15 Analysis of liposomes uptake

To analyze the uptake of liposomes by cells, the stock of Nile Red dye suspended in ethanol at 1mg/mL concentration was added at a concentration of 1 µL per 500 µL of the final sample volume. The dye was incorporated during the synthesis step into the chloroform mixture containing lipids and fisetin, as per the formulation table in Chapter 3.11, to determine if fisetin affects liposome internalization. Liposomes were then added to attached cells in LabTek, achieving a final fisetin concentration of 160 µM, and incubated for 4 hours to allow for liposome internalization. The cells were then fixed and stained as described in Chapter 3.9.

The prepared cells were analyzed using an FV1000 confocal laser scanning microscope at 60x magnification, as described in Chapter 3.9. Nile Red was excited with excitation wavelength at 638 nm and collected with 650-670 nm. 3D images were captured and then further analyzed using IMARIS software in XYZ mode to visualise the liposomes that were internalised within the cells. This approach allowed the differentiation between the signal from inside the cell and the signal from the cell surface.

3.16 Cytotoxicity of fisetin loaded liposomes and its effect on SASP

To assess the cytotoxicity of free fisetin, empty liposomes and liposomes containing encapsulated fisetin, on senescent and non-senescent cells, the Live/Dead assay was conducted. After seeding approximately $2x10^3$ cells into 96-well plates in triplicates and allowing them to

attach for 24 hours, the liposomes were diluted to obtain the fisetin concentrations at a range of 12.5 µM – 160 µM in two-fold dilutions. The concentration of the empty liposomes was also diluted to match the stock concentration of the liposomes with fisetin, and these empty liposomes were further diluted to the same final concentration as the liposomes with fisetin and their final concentration were calculated accordingly. The cells were then incubated with both types of liposomes and free drug for 48 hours. Following this incubation, the Live/Dead staining was performed using a staining mixture containing 2 µM EthD-2, 2 µM Calcein and 8 µM Hoechst 33342 in DPBS. After discarding the medium, the wells were immediately filled with 100 µL of staining mixture, and the cells were incubated at 37 °C for 30 min. The plates with cells were subsequently placed into the INCell Analyzer 2000 (GE Healthcare Life Sciences) for imaging. All nuclei were counted as total cells, while the red nuclei were identified as dead cells. The counting process was conducted using Toolbox software, and subsequent calculations were carried out in MS Excel, using formula presented below. Cell viability percentage was calculated to determine both mean value and standard deviation.

$$\text{Cell viability } \% = \frac{(\text{number of blue nuclei} - \text{number of red nuclei})}{\text{number of blue nuclei}} * 100\%$$

Equation 3. Percentage of cell viability based on Live/Dead assay

Next, senescent cells were prepared in the same manner as previously described in triplicate 96-well plates and incubated with liposomes with fisetin. The ELISA was performed, as described in Chapter 3.6. The results were calculated based on freshly prepared standard curves and presented as a graph.

Chapter 4 – results and discussion

4.1 Senescence induction and viability studies

Senescence plays an important role in cancer recurrence as the cell cycle arrest is reversible for therapy-induced senescent cells and can affect the tumor microenvironment with SASP, leading to metastasis, as explained in Chapter 1.4.2. To analyze the possible effects of drug delivery systems prepared from liposomes with encapsulated fisetin, a cellular senescence induction protocol becomes necessary to ensure a high number of senescent cells for further analysis. This chapter contains the work performed on the senenscence induction process, the analysis of the viability of the cells after treatment with topoisomerase II inhibitor known as DOX, as well as the evaluation of various hallmarks of senescence.

Lung cancer is the most common type of cancer and the leading cause of cancer-related deaths, as reported by the World Health Organization (WHO). Considering this, experiments were conducted using two cell lines originating from lung tissue. A549 is an epithelial carcinoma cell line isolated from the lung tissue of a 58-year-old Caucasian male with lung cancer [102]. WI38 is a fibroblast cell line isolated from the lung tissue of a 3-month-old female fetus [1].

4.1.1 Cellular senescence induction

Cellular senescence of the A549 cell line was induced with DOX according to the protocol outlined by Żuryń et al. [100], explained in Chapter 3.2 and illustrated in Figure 7a. A range of DOX's concentrations based on Żuryń et al. work, were expanded, and the concentrations 0.05, 0.1, 0.2, 0.4, and 0.8 µM were tested. The final concentration was selected based on the results of a viability assay and a senescence-associated beta-galactosidase (SA-β-gal) assay. These assays were used to determine the optimal concentration of the senescence-inducing treatment with DOX that would maximize the percentage of senescent cells while minimizing cell death.

Protocols available in the literature were applied for senescence induction on WI38 cell line. The concentrations of DOX suggested by Casella et al. [101] resulted in of very low number of viable cells. On the other hand, the protocol provided by Baar et al. [5] suggested lower concentrations, which resulted in a small percentage of senescent cells. This high disproportion

of non-senescent cells could potentially disturb the samples or interfere with the analysis of the senescent cells in further experiments, making it difficult to draw reliable conclusions from the data. This suggested that a middle ground between the two protocols was needed to obtain an optimal balance of senescent and non-senescent cells for subsequent analysis. Concentrations 0.75, 1, 1.5, 2 and 3 µM were chosen for further examination due to fact that this range is between the two protocols mentioned earlier. The incubation conditions were kept the same as those used for the A549 cell line to simplify the experimental procedure while maintaining and comparing two different cell lines simultaneously. In the result, two ranges of DOX concentrations were used to treat the A549 cancer cell line and the healthy WI38 fibroblast cell line with the same incubation conditions.

During the month-long maintenance of senescent cultures, small "islands" of proliferating cells began to form within the A549 cell line, showed in Figure 7b, indicating a renewal of cell division and escape from the senescent state. In contrast, no such changes were observed in the senescent WI38 cell line, which remained in a stable non-proliferative state over the same period of time, suggesting that the A549 cell line was more prone to senescence escape compared to the WI38 cell line. As the cells formed a multilayer colony, analysis by SA-β-gal staining to confirm the loss of senescence status is very challenging due to the discolouration.

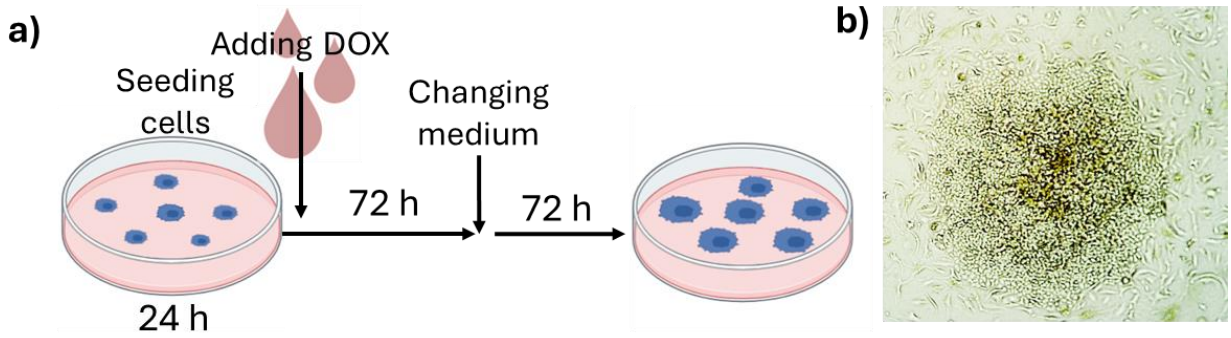

Figure 7. a) Graphical illustration of the senescence induction procedure. b) Representative picture of a cellular “island” created by proliferating cells after 1 month of senescent culture maintenance.

4.1.2 Viability

Initially, a 2-(4-Iodophenyl)-3-(4-nitrophenyl)-5-(2,4-disulfophenyl)-2H-tetrazolium (WST-1) assay was performed to investigate the viability of cells treated with chosen concentrations of the chemotherapeutic agent DOX, as the same assay had been successfully used by Yang et al. on the K-562 cell line in their previous work [103] and by Chang-Chien et al. on the A549 cell line [65]. After conducting the experiment, the results indicated that the viability of cells treated with DOX was surprisingly high, above 100%, as shown in Figure 8a-b, suggesting that the chemotherapeutic agent appeared to enhance their viability. However, upon closer inspection of the culture under an inverted light microscope, it became apparent that the actual number of viable cells present was significantly lower than expected, based on WST-1 results, indicating a potential discrepancy between the WST-1 assay results and the actual cell numbers. The WST-1 assay is commonly used as a viability test, as it analyzes the metabolic activity of cells. Our findings indicate a higher metabolic activity in senescent cells, which led us to perform an experiment to analyze this parameter.

Therefore we decided to conduct a Live/Dead assay instead of the WST-1 assay to determine cell viability. This method relied on flow cytometry measurements and determination of the number of cells stained with EthD-2, a fluorescent dye that binds to DNA only when the cell membrane is compromised, as showed in Figure 8e-f. This method allows for more accurate quantification of live and dead cells in the sample compared to the indirect measurement of metabolic activity provided by the WST-1 assay. This experiment aimed to find the concentration of DOX that maintained approximately 80% cell viability, which would allow for the investigation of cellular responses without the high level of cell death. Although the lowest investigated concentration for A549 cells resulted in 100% viability, as presented in Figure 8c-d, this data point was further removed from the analysis due to the assumption that the DOX concentration was too low to influence the cells significantly.

The 0.4, 0.8, 2 and 3 µM concentrations were excluded from further trials, as they exhibited viability below 80%. High concentrations of DOX for each cell line appeared to be too toxic, leading to a significant reduction in the number of viable cells compared to the other tested

concentrations, indicating that such high doses may not be suitable for inducing senescence without causing excessive cell death.

After determining a safe dosage of DOX to induce senescence, a comprehensive set of well-established and widely accepted senescent biomarkers was employed to evaluate and confirm the induction of cellular senescence thoroughly.

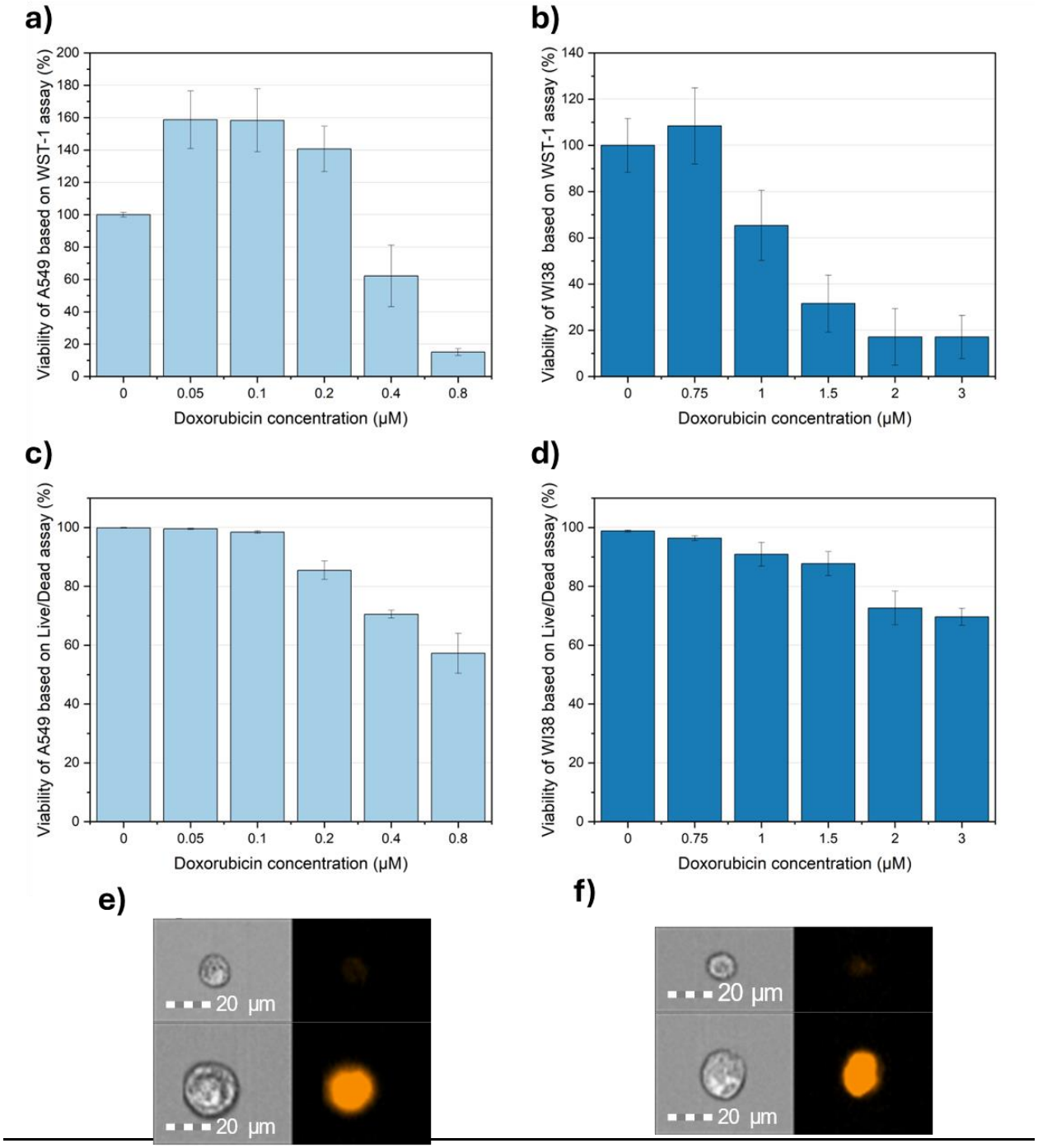

Figure 8. The WST-1 assay shows metabolic activity exceeding 100% in a) A549 and b) WI38 cells treated with low concentrations of DOX, leading to the use of the Live/Dead assay. This assay detects fluorescent dye bound to the DNA of cells without membrane integrity, indicating apoptosis. The percentage of viable cells for c) A549 and d) WI38 is based on flow cytometry imaging, which also demonstrates the contrast in intensity of fluorescent signal between live and dead cells for e) A549 and f) WI38 cell lines.

4.1.3 Analysis of senescence biomarkers

In this study, multiple senescence biomarkers were investigated to provide a more comprehensive assessment of cellular senescence. Currently available markers lack specificity to distinguish senescent from non-senescent cells. Therefore, it is very important to combine them for a complete characterization of senescence, which was noted as significant by Wiley et al. in their studies [104]. Biomarkers used in these studies included detection of SA-βgal, changes in morphology (cell size, formation of SAHF, depletion of LMN), production of SASP and lack of proliferation.

4.1.3.1 SA-β-gal

Both, A549 and WI38 cells incubated with selected concentration of DOX determined by the cell viability assays for each cell line were treated with SA-β-gal histochemical staining kit, that measures activity of SA-β-gal in cell cultures by hydrolysis of X-gal. This staining results in the accumulation of distinctive blue color in senescent cells. Hoechst 33342 fluorescent dye that binds to DNA was used to count the total number of cells on the slide accurately. For each of chosen concentrations for both cell lines based on viability, 30 microscopy images of were taken to calculate the number of senescent cells. Since the blue signal was unevenly distributed in the cells, it could not be automatically counted by ImageJ Software. Instead, the multipoint tool was used for analysis after merging the channels of fluorescently stained nuclei and SA-β-gal stained cells in dark-field mode, as depicted in Figure 9b. It allowed us to manually count all cells affected by the SA-β-gal staining and calculate the percentage of SA-β-gal positive and negative cells as showed in Figure 9c. Although staining of cell nuclei in WI38 cell samples did not produce satisfactory visual results, it was sufficient for cell counting. It is important to note that the WI38 cells exhibit replicative senescence after undergoing multiple passages in a culture much faster than it was noticed in A549 culture. Therefore, it is crucial to carefully track the passage numbers when comparing the non-senescent WI38 cells with the senescent counterparts in order to ensure an accurate interpretation of the results. Hence, WI38 cells were used up to the 9th passage, as further passages noticeably slowed down cell division. The senescent cells displayed a more vibrant and visible blue staining, exhibiting increased SA-β-gal activity compared to the non-senescent cells (Figure 9a). The most intense staining for A549 cells was observed at 0.1 and 0.2

µM DOX concentrations. At the 0.05 µM DOX concentration, the number of cells displaying negative SA-β-gal signals was noticeably higher. Similar situation was observed for WI38 cells, where blue signals of SA-β-gal was more visible for 1 µM DOX concentration, while 0,75 and 1,5 µM DOX concentration were at similar, lower count. This suggests that the non-senescent cells may over time outgrow the senescent cells and dominate the culture.

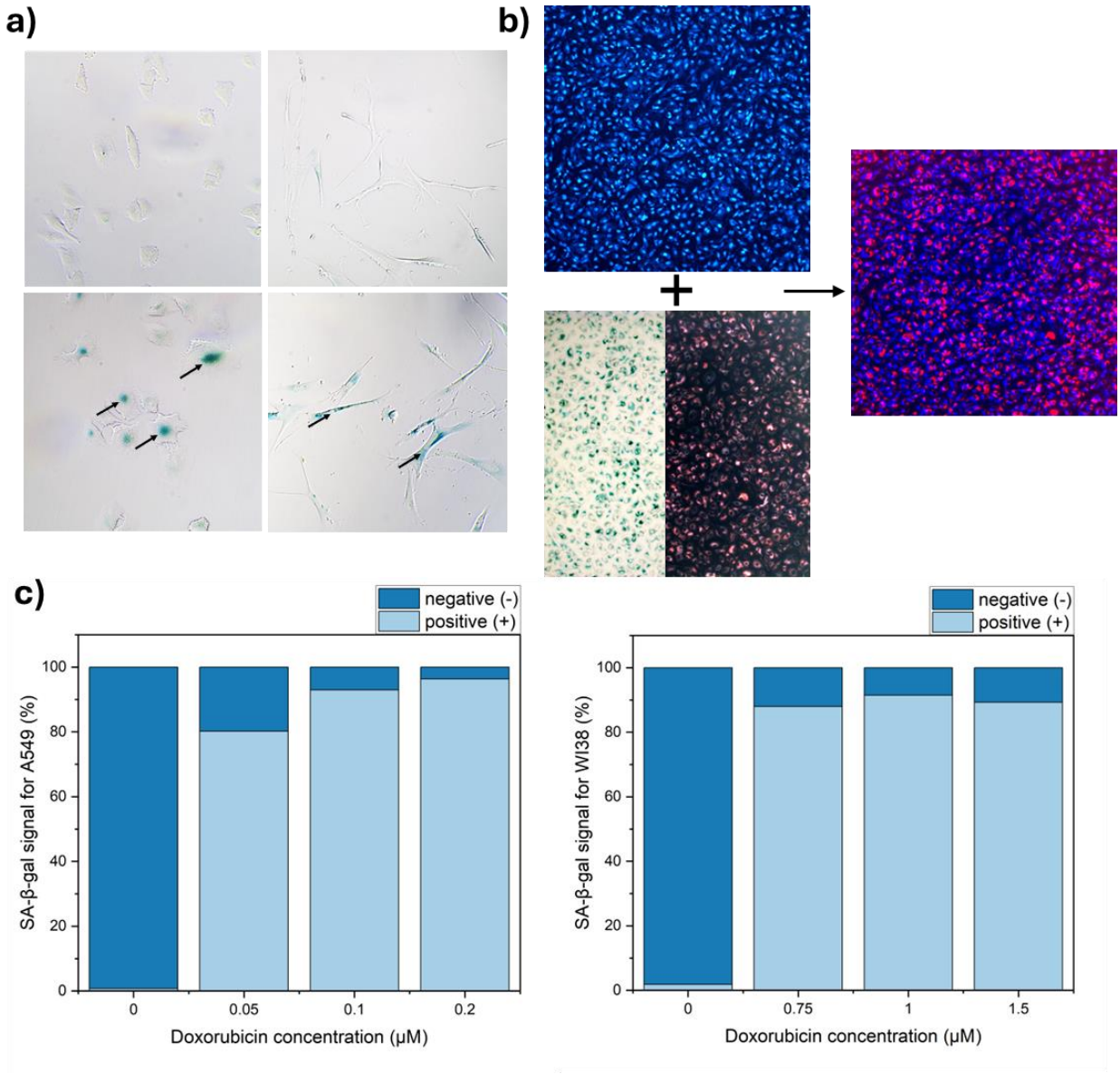

Figure 9. SA-β-gal assay results. a) Representative images of SA-βgal histochemical staining of A549 cells (left side) and WI38 (right side) without (top) and with (bottom) DOX treatment. b) Step-by-step method used for cell counting in ImageJ software. Images of SA-β-gal stained cells were taken in dark field mode. Images of Hoechst 33342 stained cells were taken in fluorescence mode. The images form fluorescence and dark field modes were merged and a multiselection tool was used to count all nuclei with SA-β-gal positive cells and the remaining nuclei without SA-β-gal signal. c) Established percentages of SA-β-gal positively and negatively stained cells.

Based on a comprehensive analysis yielding the highest percentage of SA-βgal positive cells, while also maintaining a high level of cell viability, DOX concentrations of 0,1and 0,2 µM for A549 cells and 0,75 and 1 µM for WI38 cells were selected for further experiments.

4.1.3.2 Morphology analysis

Differences in the morphology of senescent and non-senescent cells is another senescence hallmark analyzed in this research. After fluorescence staining of the nuclei and cytoskeleton, significant differences in size and morphology were observed between senescent and non-senescent A549 cells (Figure 10a). Non-senescet A549 cells were small and round. On the other hand, senescent A549 cells exhibited a larger appearance in both the cytoskeleton and the nuclei. In the case of the WI38 cell line, no noticeable changes were observed in the overall structure and organization of the cytoskeleton. However, the nuclei of these senescent cells exhibited a distinct "spotty" appearance, pointed in Figure 10b by white arrows, which was attributed to the formation of senescent associated heterochromatin foci (SAHF). The presence of these SAHF is a characteristic feature of cellular senescence. Our findings align with the conclusion that SAHF formation exhibits cell type-specific characteristics, as it is visible only for the WI38 cell line and not for the A549 cell line. However, since we examined only one stress stimulus, we cannot make definitive statements regarding the impact of other stress stimuli, such as oxidative stress or DNA damage, on SAHF induction.

The difference in cell size was further confirmed using flow cytometry. The area of detached cells in μm^2 was measured, and senescent cells were compared to their non-senescent counterparts. The visible shift in the flow cytometry histograms shown in Figure 11 clearly demonstrates that the increase in cell size observed in the confocal images was indeed due to an actual increase in the size of the senescent cells rather than just a flattening of the cytoskeleton. This finding suggests that the senescent cells undergo significant structural changes, resulting in a distinct enlargement of their size compared to the non-senescent cells. The flow cytometry data provides quantitative evidence to support the visual observations from the confocal microscopy, strengthening the conclusion that an increase in overall cell size accompanies senescence. Analysis of the WI38 cell line indicates that the range of cell sizes in senescent cells is much broader than in non-senescent cells, suggesting that they can exhibit a wider variation in their size compared to their non-senescent counterparts. This increased size variation observed in the senescent WI38 cells likely reflects the heterogeneity of the senescent state, where individual cells may undergo varying degrees of enlargement as part of the senescence process. However,

increased size variation is not a reliable or consistent marker for identifying senescent cells in the WI38 cell line, as it is for the A549 cell line, where a clear and consistent increase in overall cell size is observed as a characteristic and defining feature of the senescent phenotype in that cell line.

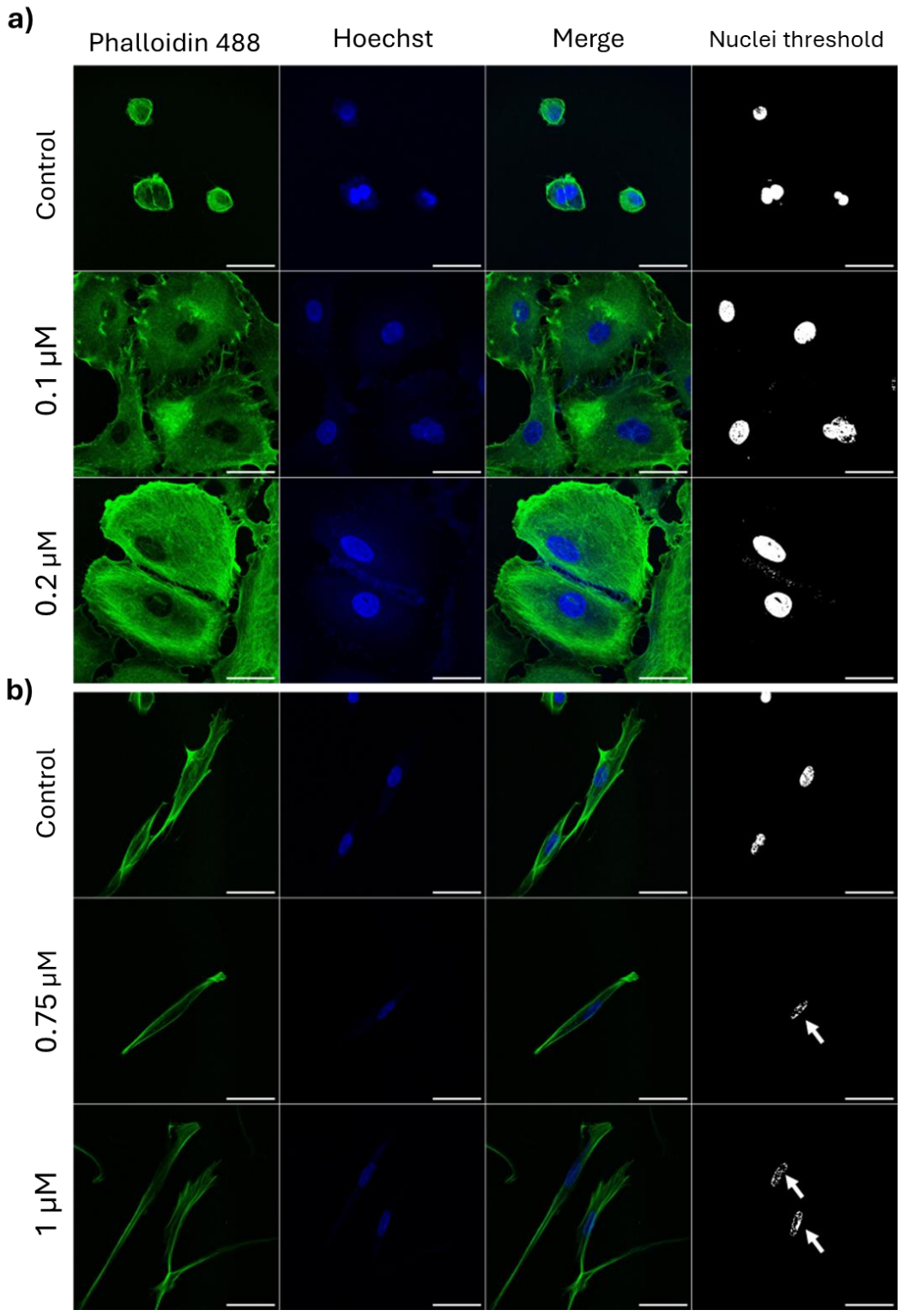

Figure 10. Confocal images of cells before and after undergoing cellular senescence with two chosen DOX concentrations for further analysis for a) A549 and b) WI38 cell lines with untreated cells used as a control. Scale bar = 50 µm. Images show each color channel separately, merged

channels, and edited picture of nuclei in ImageJ Software to make SAHF more visible by applying threshold in adjustment option (white arrows).

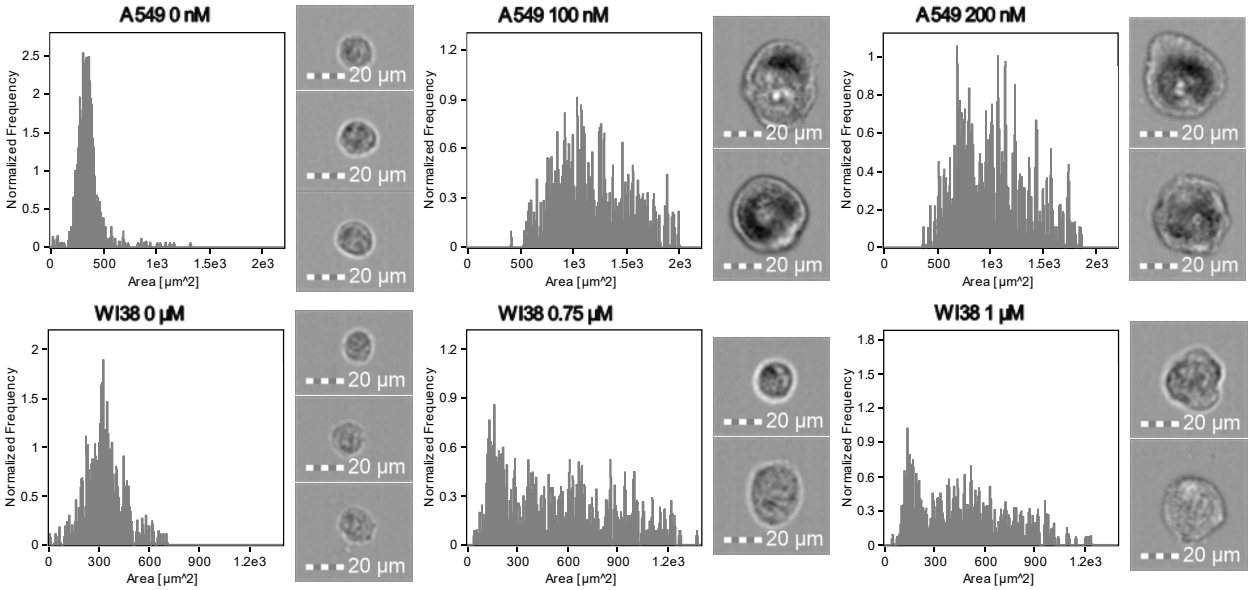

Figure 11. Cell size determination using imaging flow cytometry. Shifts in histograms represent changes in size of cells, which are described as visible area of the cell's surface in μm^2, with examples of images taken during the measurements.

4.1.3.3 Proliferation study

One of the most characteristic hallmarks of senescent cells is their cell cycle arrest and, therefore, their lack of proliferation ability. Cells treated with DOX showed a decrease in EdU (a thymidine analogue) incorporation, indicating a reduction in DNA synthesis and cell division. This reduction in DNA replication is evidenced by the absence of the characteristic red fluorescent signal in the microscopy images, visible in Figure 12a-b, which would normally indicate the presence of actively proliferating cells. The loss of proliferative capacity is a key feature that distinguishes senescent cells from their actively dividing counterparts. Comparing these results with the percentage of SA-β-gal positive cells, we can assume that some cells, even with higher expression of β-galactosidase, can remain proliferative and continue to divide despite these senescence-associated changes. This suggests that the presence of SA-β-gal activity, a commonly

used marker of cellular senescence, does not always correlate with a complete exit from the cell cycle in all senescent cells.

According to the American Type Culture Collection (ATCC) data sheets, the population doubling time for the WI38 cell line is reported to be approximately 24 hours, while the A549 cell line has a slightly faster doubling time of around 22 hours. These values represent the typical growth rates observed for these cell lines under standard culture conditions. For A549 cell line, the EdU positive was at 52% for non-senescent cells, while after treatment with DOX, this value lowered to 6% for 0.1 µM DOX concentration and 1% for 0.2 µM DOX concentration (Figure 12c). However, our observations showed that the non-senescent WI38 cell line required 48 hours to show 49% positive EdU cells, while senescent WI38 cells exhibit 10% EdU-positive cells at a concentration of 0.75 µM DOX and 2% EdU-positive cells at a concentration of 1 µM DOX (Figure 12d). Moreover, the doubling time for non-senescent cells increased with each successive passage, indicating a gradual slowdown in the proliferation rate of the WI38 cells over time. This suggests that the WI38 cell line exhibited signs of replicative senescence, with the cells dividing at a slower rate as they aged in culture.

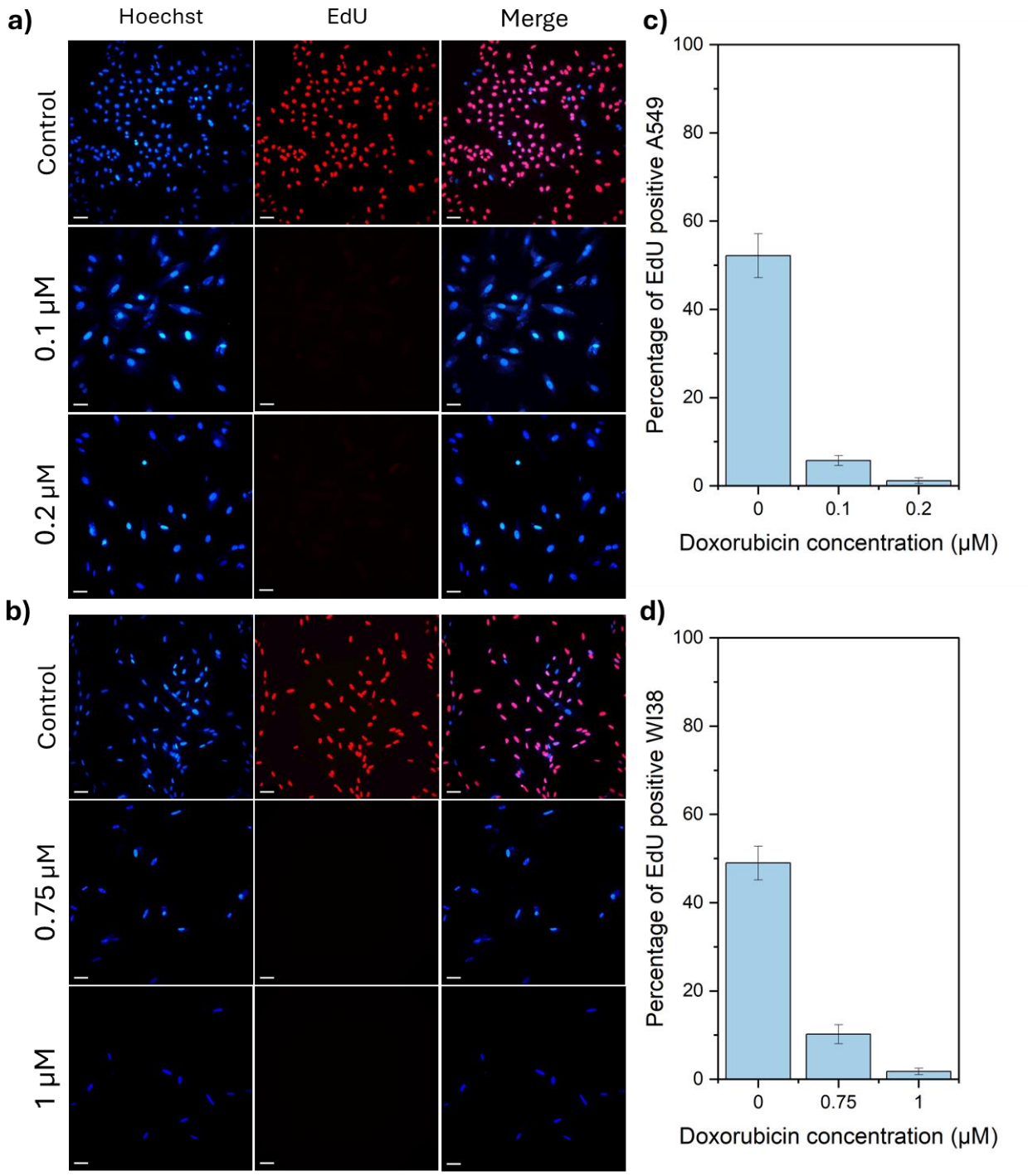

Figure 12. Fluorescence microscope images representing the results of EdU assay for a) A549 and b) WI38 with the percentage of proliferative cells in population of c) A549 and d) WI38 after treatment with DOX. Scale bar = 50 µm

The DOX concentrations of 0.2 µM for A549 and 1 µM for WI38 were selected, as those concentrations demonstrated the lowest percentage of proliferative cells, which is a desirable outcome for further experiments.

4.1.3.4 Metabolic activity

To assess the metabolic activity of senescent cells compared to non-senescent cells, we used WST-1 assay, which was also first used to determine the viability of cells after DOX treatment, which gave us contradictory results. Based on our findings and the available literature, we can assume that metabolic activity in senescent cells varies depending on the specific cell type and/or the senescence-inducing factors employed. Viability assays that rely solely on the metabolic activity of cells may prove misleading if used without considering the specific cell type or the type of senescence-inducing factors used. The metabolic profile of senescent cells can vary significantly depending on these aspects mentioned above, highlighting the importance of carefully selecting appropriate assays that take into account the complex and dynamic nature of cellular senescence across different experimental conditions.

Our studies first determined the appropriate DOX concentrations needed to reliably induce a state of cellular senescence in both of the cell lines examined. We conducted a comparative analysis of the metabolic activity levels between the senescent and non-senescent cells. Both cell lines demonstrated a marked increase in metabolic activity in the senescent cells compared to their non-senescent counterparts, as showed in Figure 13. Specifically, the A549 senescent cells exhibited more than 6 times the metabolic activity of the untreated control group, while the WI38 senescent cells showed over 4 times higher metabolic activity than the non-senescent controls. This suggests that senescent cells may undergo distinct metabolic changes that contribute to their altered phenotype and function. This finding also demonstrates that assays relying on metabolic activity are not suitable for investigating viability when studying the influence of senescent stimuli, as elevated metabolic activity can provide misleading results.

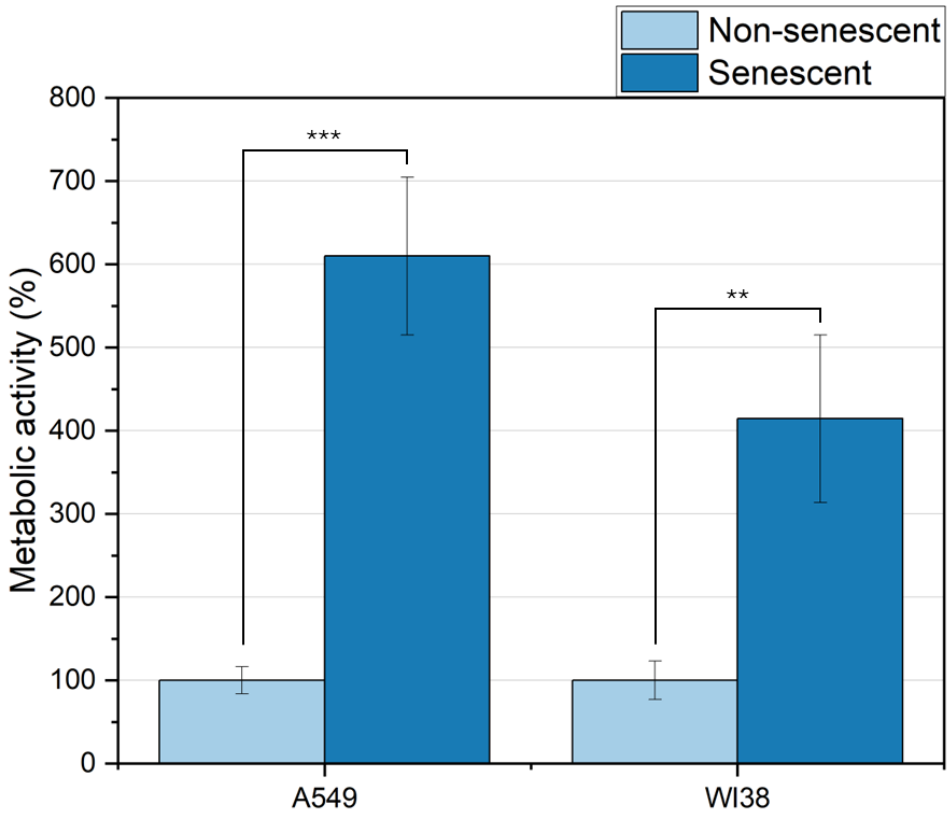

Figure 13. The results of WST-1 assay. Percentage of metabolic activity of senescent cells, compared to non-senescent cells used as control (at 100%). ** $p \leq 0.01$, *** $p \leq 0.0001$

4.1.3.5 Presence of lamins

The nuclear lamina is a complex structure composed of various protein components, including the lamins A, B1, B2, and C. Decreased level of lamin B1 is a biomarker of cellular senescence, as demonstrated and established by the work of Freund et al [39]. In this work, nuclear lamin A (LMNA) and nuclear lamin B2 (LMNB2) expressions was measured by qPCR. Analysis showed differences in expression of both proteins between senescent and non-senescent cells.

The changes in expression levels of the LMNA gene across both cell types analyzed was determined to be statistically insignificant, as presented in Figure 14. Conversely, the expression

of the LMNB2 gene, which is present in Figure 14 for both cell types, exhibits a significant reduction in senescent cells compared to non-senescent counterpart.

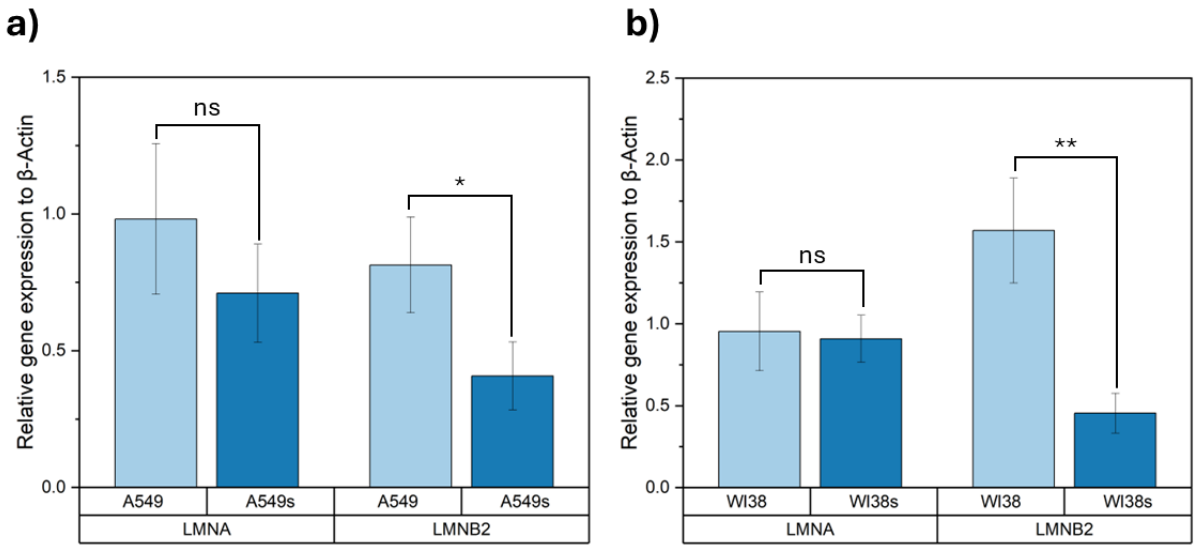

Figure 14. Expression of LMNA and LMNB2 for a) A549 and b) WI38 cells (gene expression relative to β-Actin). s – senescent. ns $p > 0.05$, * $p \leq 0.05$, ** $p \leq 0.01$

The results of this study provide compelling evidence that, in the context of A549 and WI38 cell lines, LMNB2 emerges as a potential biomarker for the cellular senescence process. In contrast, LMNA does not appear to serve as an effective indicator of this phenomenon.

4.1.3.6 Evaluation of SASP components

Interleukins 6 and 8 (IL6 and IL8) are among the most common components of SASP found in various publications analyzing different cell lines and senescence inducers [105], [106], [107], [108], [109]. In this thesis we used enzyme-linked immunosorbent assay (ELISA) to measure the concentrations of these interleukins released into the medium by senescent cells and non-senescent cells based on calibration curves, depicted in Figure 15. The results provide insights into the altered secretory profile of senescent cells and help characterize the SASP associated with cellular senescence. The results demonstrated significant differences in the A549 cell line, with senescent A549 cells exhibiting a marked increase in inflammatory cytokine production compared

to their non-senescent counterparts. Specifically, the senescent A549 cells displayed nearly a two-fold higher level of IL-6 compared to the non-senescent A549 cells. Moreover, an astonishing 10-fold increase in IL-8 levels was observed in the senescent A549 cells in comparison to the non-senescent A549 cells. The results for A549 cell line are presented in Figure 16a. The interleukin concentrations within the WI38 cell line were approximately 10 pg/mL higher in senescent cells than their non-senescent counterparts as shown in Figure 16b. While the increases were not as substantial as those observed in the A549 cell line, the data still demonstrates a notable difference in the inflammatory profile between senescent and non-senescent WI38 cells.

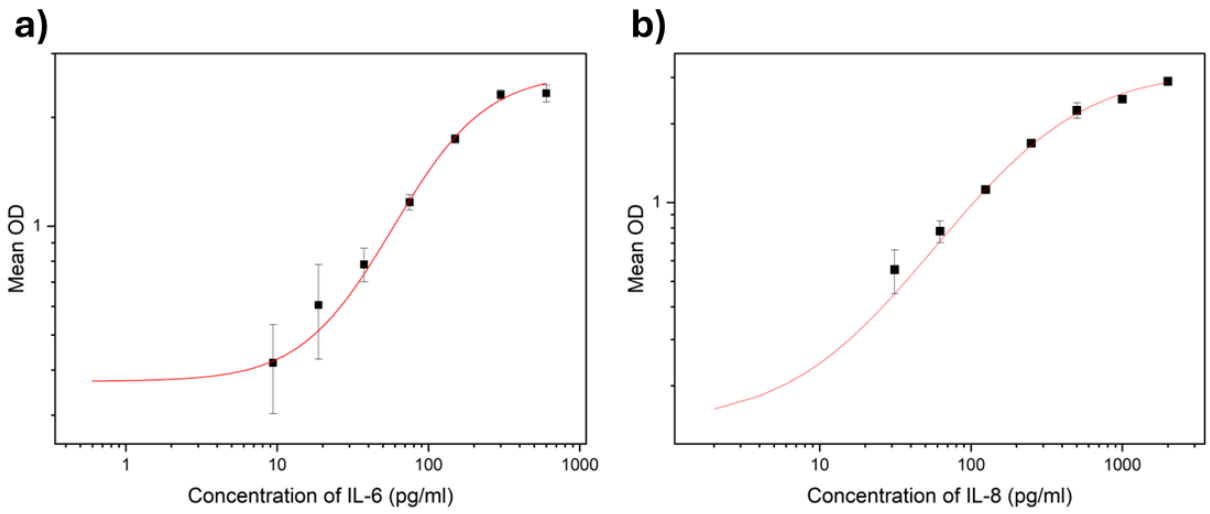

Figure 15. Standard curves of a) IL-6 and b) IL-8

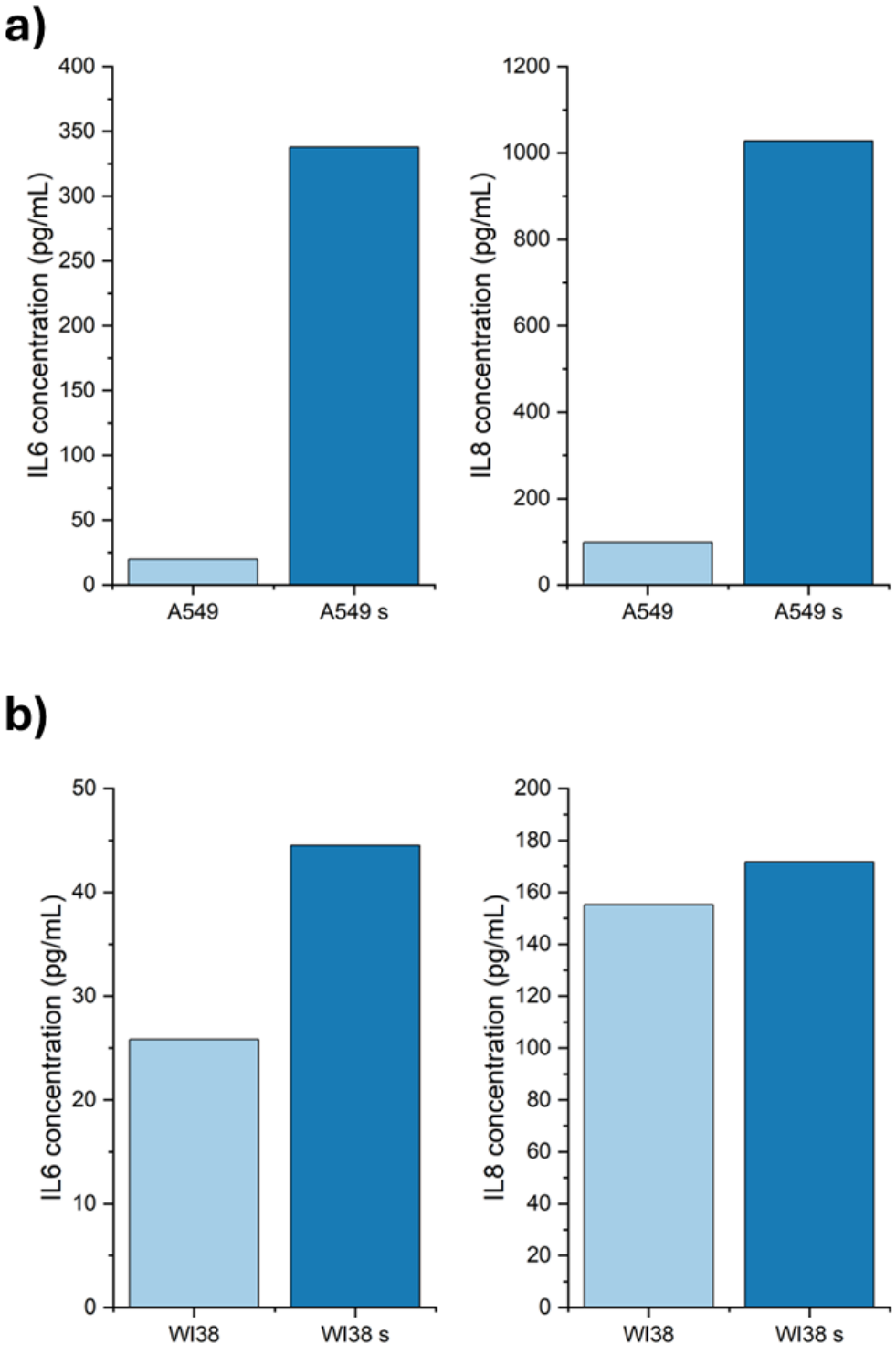

Figure 16. Representation of a) IL6 and b) IL8 expression in pg/ml for A549 and WI38 based on standard curves for each interleukin. s – senescent.

4.1.4 Discussion on senescence induction and identification

The sensitivity of different cell lines to senescence inducers, including chemotherapeutics, can vary significantly. This can be attributed to the inherent heterogeneity among cell lines, their genetic backgrounds, and their distinct molecular profiles. For instance, Valenzuela et al. successfully induced senescence in the gastric cancer cell lines using 0.5 μM of the CDK4/6 inhibitor palbociclib [55], while Karabicici et al. were studying hepatocellular carcinoma Huh7 cell lines and inducing senescence with 0.1 μM concentration of DOX [72]. Both research groups proved the efficiency of their studies with various senescence markers such as SA-βgal, level of SASP components or the proliferation profile. This shows that an important step in senescence research is to experimentally find the correct method of senescence induction procedure. In the work of Demaria et al., DOX was successfully used as senescence inducer at a concentration of 250 nM on mouse dermal fibroblasts (MDFs). However, their supplementary data reveals that the same concentration of DOX used on the human colon carcinoma cell line (HCA2) did not yield outstanding results for SA-βgal staining or EdU assay, in contrast to their findings for MDFs [56]. Hernandez-Segura et al. conducted extensive studies exploring various methods of inducing senescence on BJ fibroblasts, including the use of DOX, ionizing radiation, UV-radiation, and oxidative stress. In their work, they claimed the procedures they outlined would effectively induce senescence in different types of fibroblasts, including WI38. However, their method involving a 250 nM concentration of DOX would not be effective in our case [110]. Establishing the optimal conditions for inducing senescence in cells is crucial, as the specific techniques and parameters may need to be adjusted based on the cell type, tissue source, or laboratory setting. Moreover, an established method by one research team may not work for another laboratory for various reasons, such as differences in cell culture conditions, reagents, or experimental protocols, as noticed in our studies. Careful optimization and validation of senescence induction methods are essential for consistent and reliable results in this field of research.

When designing senescence induction methods, it is crucial to monitor cell viability, as senescence inducers can be cytotoxic. Numerous assays are available to assess cell viability, including methods that can analyze the metabolic activity of cells or the integrity of the cell membrane. Chang-Chien et al. used the WST-1 assay on the A549 cell line, which showed around

160% viability in our case. While their research did not find significant changes, further investigation confirmed that the studied cells were indeed senescent [65]. Brandl et al. employed a Live/Dead assay to determine the doses of H_2O_2 that affected mesenchymal stem cell lines derived from patient samples. They identified a lethal dose that induced apoptosis in the cells and range of H_2O_2 concentrations that triggered cellular senescence, which was further confirmed through SA-βgal staining [111]. Also, Rovira et al. used Live/Dead assay for flow cytometry analysis to remove dead SK-MEL-103 cells from their calculations after treatment with DOX and pabociclib. This allowed them to focus their analysis on the viable cells. The authors mentioned that they used only two repetitions for one variation instead of the standard three, justifying this by a lack of available cells. This could have been caused by low cell viability and instant lack of proliferation at the used concentrations of the DOX and palbociclib treatments, indicating that the treatments may have significantly impacted the survival and proliferation of the SK-MEL-103 cells. However, the researchers did not provide specific data on cell viability, which would have been important to evaluate the experimental methods and results [112].

In summary, spontaneous escape from cellular senescence can occur through a variety of mechanisms, but the underlying causes have not been fully explained in detail. It remains unclear whether some cases may involve multiple escape mechanisms occurring simultaneously or if each documented instance of senescence escape is connected to a distinct and specific escape mechanism. Further research is needed to fully understand the complex and diverse pathways that can lead to the bypass of cellular senescence programs in different cell types and contexts.

Identification of senescent cells relies heavily on SA-β-gal as an important first marker to assess the success of induction methods. Interestingly, the intensity of SA-β-gal staining has been found to depend on the specific stress stimuli experienced by the cells, as reported in the research conducted by Was et al [113]. This suggests that the degree of β-galactosidase expression can vary based on the type and severity of the cellular stressors present. Similarly to our approach of counting SA-β-gal positive cells, Hernandez-Segura et al. merged images of SA-β-gal and DAPI stained cells, which enabled them to calculate the percentage of SA-β-gal positive cells in culture [110]. This method provides a quantitative measure of senescence induction, allowing researchers to evaluate the efficacy of different senescence-inducing treatments. Recently, scientists

developed a macro for the Fiji program to count SA-β-gal and DAPI-stained cells automatically. While the differences between manual counting and using the macro are remarkable, during our experiments, we encountered an issue where the β-gal signal was divided into two halves due to its localization on each side of the nuclei, creating two "half-moons" of blue staining. This was often counted as two cells by the ImageJ software. However, this specific scenario is not addressed in the research, raising questions about the influence of overall cellular shape on the accuracy of such senescence assay analyses using macro script [114].

Our findings indicate that senescent cells may undergo changes in size and shape, but these alterations are not always apparent, raising questions about whether such changes depend on the specific cell line and/or the type of stress stimulus applied. Bojko et al. analyzed the morphological changes across various cancer cell lines, including A549 cells. Their study revealed that the visible changes in the size and structure of the cytoskeleton and nuclei differed depending on the specific chemotherapeutic agents used as stress stimuli to induce cellular senescence [2]. Meanwhile, Moujaber et al. found that microtubules exhibited substantial disorganization in senescent cells relative to their non-senescent counterparts [115]. These studies demonstrate that senescent cells undergo significant changes in cellular morphology and nuclear architecture, as well as remodelling of the cytoskeleton, during the senescence process. Kosar et al. conducted a comprehensive investigation to study the formation of SAHF across various cell lines subjected to different senescence-inducing stimuli. While SAHF was consistently observed in all the tested cell lines in response to one specific stress stimulus, interestingly, no such SAHF formation was evident when the cells were exposed to a different stress stimulus. This finding suggests that the formation of SAHF is a highly context-dependent process, with its occurrence being dependent on the specific senescence inducer applied on specific cell lines [38].

Cellular senescence is a state of cell cycle arrest, where the cell loses the ability to continue dividing. This non-proliferative condition can be reliably identified and quantified using the EdU assay, as used in our study and the work by Karabicici et al. Moreover, this assay enables an in-depth investigation of cell proliferation dynamics that follow the induction of senescence [72]. Interestingly, the use of BrdU, another nucleoside analogue-based assay similar to EdU, has been reported to potentially induce cellular senescence in some experimental settings. This is an

important consideration, as the choice of assay can have significant impacts on the assessment of cellular senescence and the interpretation of experimental results [116]. Furthermore, cell proliferation after senescence-inducing treatments can also be assessed through simple manual cell counting methods, which provide a cost-effective and accessible alternative to relying solely on manufactured assay kits. This approach, as demonstrated in the study by Valenzuela et al., allows researchers to directly quantify changes in cell numbers following senescence induction without requiring specialized equipment or reagents [55].

Similar to the approach taken in our own experiments, Shin and colleagues employed the 3-(4,5-dimethylthiazol-2-yl)-2,5-diphenyltetrazolium bromide (MTT) assay to specifically evaluate the mitochondrial function and metabolic activity of the cells that had been subjected to treatment, rather than simply assessing their overall viability [117]. The MTT test is analogous to the WST-1 assay, as both of these colorimetric tests measure the metabolic activity of cells and are commonly utilized as viability assays in biological research. These assays work by detecting the reduction of tetrazolium salts, which occurs due to the activity of cellular dehydrogenase enzymes, and thus provide an indirect measure of the number of viable, metabolically active cells present in a sample. Their investigation revealed that the cells subjected to treatment with H_2O_2 exhibited significantly higher metabolic activity and mitochondrial function compared to the untreated control cells. In contrast, Yang et al. utilized the WST-1 assay as a proliferation assay, and their results on the K-562 cell line showed that after 2 days of DOX treatment, the cells maintained the same absorbance level, indicating a state of proliferation arrest [103]. These results led us to assume the suitability of this assay for our studies. On the other hand, Hou et al. examined the effects of D-galactose on human astrocyte cells and determined the dose required to induce senescence using the WST-1 assay [118]. Their study revealed that increasing concentrations of D-galactose led to a dose-dependent reduction in the viability of the treated astrocyte cells.

Lamins were analyzed in detail by Freund et al. as potential senescent biomarkers and their study established lamin B1 as senescence biomarker. They thoroughly examined the expression levels of all the lamins present in the nuclear envelope using Western blot techniques. Their findings revealed no significant differences in the expression of the LMNA and LMNB2 lamin

proteins during the process of cellular senescence. In contrast, LMNB1 showed a significant decrease, suggesting that the selective downregulation of lamin B1 is a key molecular event associated with cellular senescence [39]. The discrepancy between our results and those of Freund et al. may be due to the different experimental approaches and cell lines employed. While Freund et al. utilized the HCA2 cell line and treated the cells with 10-Gy ionizing radiation, our analysis was conducted on different cell lines with different stress stimuli, which could account for the observed variations in lamin expression patterns during cellular senescence. Another study investigating the influence of UV radiation on keratinocytes, conducted by Wang et al., also showed a significant difference in the level of LMNB1 expression before and after treatment and slight changes in LMNA expression after exposure to stress stimuli [119]. These findings collectively suggest that the selective downregulation of lamin B1 is a critical event in the process of cellular senescence, and that the specific experimental conditions and cell types used can influence the observed lamin expression patterns.

The components of the SASP can differ based on the cell type and the triggers that induce cellular senescence. However, the inflammatory cytokines IL-6 and IL-8 are frequently observed as part of the SASP, and these were the focus of examination in our research. In the study of Kim et al., the levels of IL-6 and IL-8 were found to differ depending on the method of senescence induction in the human dermal fibroblast (HDF) cell line. While DOX-induced senescent cells showed a significant increase in the levels of both interleukins, replicative senescent cells exhibited different results for IL-6. Specifically, the level of IL-6 was found to decrease in replicative senescent cells compared to their non-senescent counterparts. This suggests that the mechanism of senescence induction can profoundly impact the inflammatory profile of senescent cells [120]. The level of IL6 was significantly elevated in senescent A549 cells, as observed in our study. Additionally, the MRC-5 cell line exhibited considerably higher levels of IL6 than non-senescent cells. Furthermore, the researchers measured the levels of the inflammatory cytokines IL1β and IL6 in MRC-5 cells after treatment with a combination of Dasatinib with other senolytic drugs such as quercetin, resveratrol and ellagic acid. Interestingly, the levels of these interleukins were even higher in the treated senescent cells compared to the non-treated, senescent cells, suggesting that senescent cells may have an increased secretion of these inflammatory mediators upon

treatment with senolytic agents [121]. In a different study, Chen et al. investigated the anti-aging gene Klotho by examining the levels of various interleukins in the human embryonic lung fibroblast (HELF) cell line after inducing cellular senescence through two treatment methods, one with the Bleomycin and second with hydrogen peroxide. In both cases, the levels of interleukins, such as IL-6 and IL-8 were significantly elevated in senescent cells. However, when Klotho, an anti-aging gene, was overexpressed, the expression of these key inflammatory cytokines was markedly reduced, suggesting Klotho may play a role in modulating the SASP in these cells [122].

4.2 Liposome nanoparticles

Liposomes are a highly promising drug delivery system currently being used and have the potential for future applications in delivering senotherapeutic drugs, especially water-insoluble like fisetin. The methodology used in this study was based on established methods found in literature, with concentrations and techniques selected from research conducted by Mignet et al. [123] with further improvements necessary to adapt the approach for use in our laboratory. Further analysis of the prepared liposomes involved carefully measuring their size and surface charge characteristics, as well as thoroughly evaluating the encapsulation efficiency of the fisetin and its subsequent cellular uptake and internalization by target cells. This comprehensive evaluation provided insights into liposomal formulation's physical properties and drug delivery capabilities, which are crucial factors in developing an effective therapeutic system.

4.2.1 Preparation and characterization of liposomes and fisetin loaded liposomes

The liposomes were prepared using the conventional thin-film hydration method, also known as the Bangham method, after its discovery by Bangham in 1965 [124]. The simplified preparation protocol of liposomes is presented in Figure 17a, with their final composition shown in Figure 17b. DSPE, DOPC, cholesterol were dissolved in chloroform. Liposomes that were encapsulating the fisetin, beside lipids, had also added dissolved fisetin in ethanol, which was then mixed with lipid solution. The solution was then evaporated, leaving a thin lipid film on the inside of the container. This lipid layer was then rehydrated with an aqueous HEPES buffer solution and thoroughly agitated to form the liposomes. Extrusion method was used to regulate the size of liposomes. The process of extrusion through 0.1 µm porous membranes proved to be extremely challenging and often resultied in filter breakage due to the high pressure required. To address this issue, a range of filters with various pore sizes (Ø 800, 400, 200, 100 nm) was used to facilitate a smoother and more efficient extrusion process. However, this process resulted in some residual material being retained on the filters, which posed a challenge in determining the precise concentration of the final liposome solution. We observed that the duration of lipid hydration was a crucial factor in the experiment. We found that the batches, that were extruded immediately after adding HEPES, without the 24 h hydratation step, exhibited a remarkably low fisetin concentration in consecutive

measurements. This suggested that the timing of the lipid hydration process significantly impacted the final fisetin concentration in the samples.

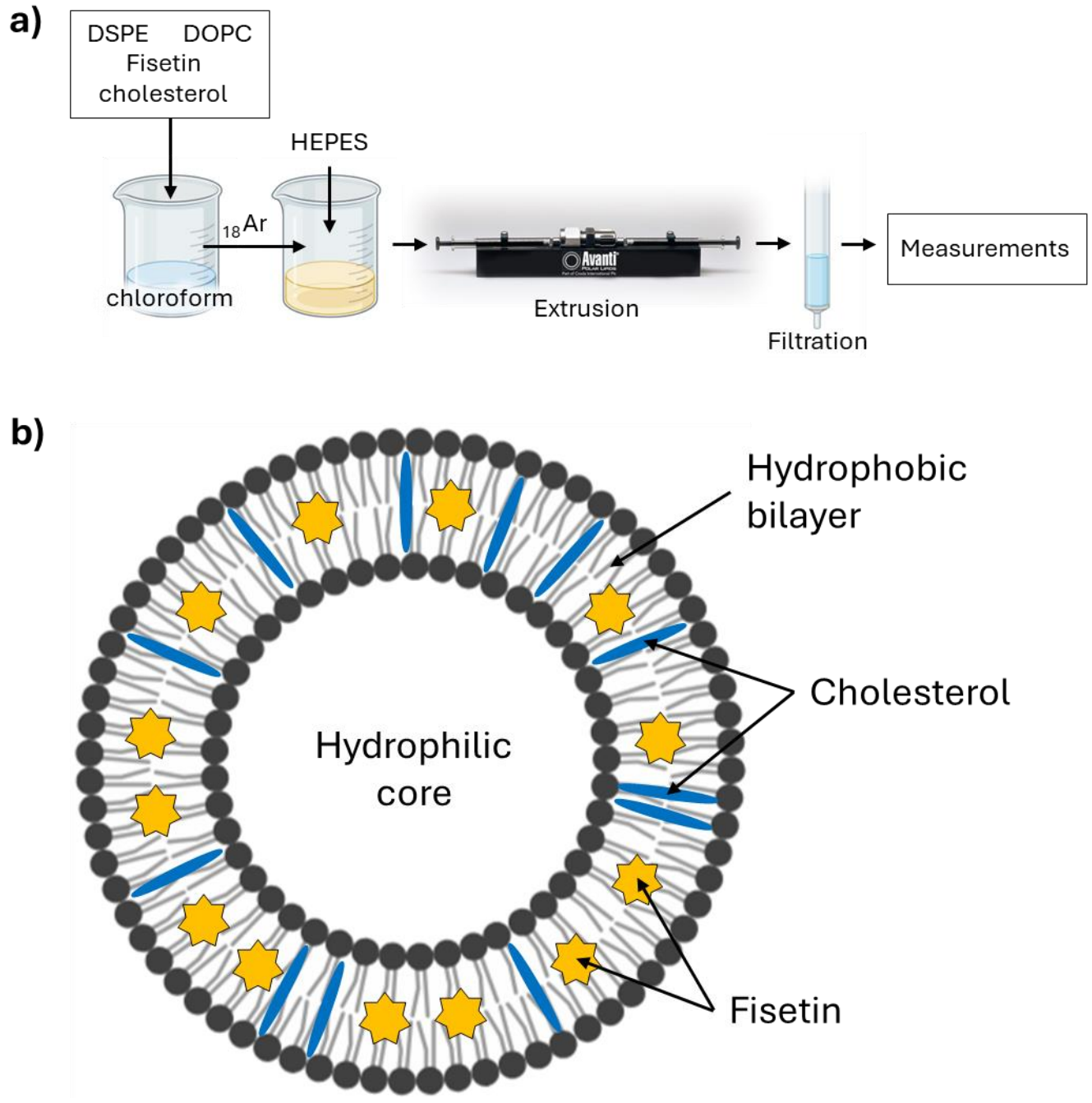

Figure 17. Graphical representation of a) liposomes synthesis' procedure with measurements and b) liposome composition.

4.2.1.1 Dynamic Light Scattering (DLS)

The size and their ζ-potential of analyzed iposomes were determined immediately after preparation using the DLS method. This technique measures the intensity of the scattered light caused by the particles in aqueous solution and provides information on the size distribution and surface charge of liposome nanoparticles. The stability of the liposomes was then analyzed by measuring their size and ζ-potential again after 30 days of storage in HEPES buffor at 4 °C. This provided insight into how the liposome properties changed over time under refrigerated storage conditions. Additionally, measurements were conducted to assess the impact of the extrusion step when the filters size was changed to a smaller size during the preparation process. This allowed us to observe any changes in the liposome characteristics caused by the extrusion through the different pore sizes. All DLS measurements were performed at room temperature to ensure consistency and eliminate potential temperature effects on the liposome properties. The DLS measurements showed that:

1) The size of empty liposomes was approximately 115.9 nm ± 0.9 with a polydispersity of 0.155 ± 0.004 and a ζ-potential of -20.3 mV ± 0.6, while the size of liposomes containing fisetin was about 95.1 nm ± 1.0 with a polydispersity at 0.178 ± 0.008 and ζ-potential is at -11.6 ± 1.2.
2) Size of empty liposomes after 30 days was around 116.5 nm ± 0.2 with polydispersity at 0.181 ± 0.017 and ζ-potential was at -8.25 mV ± 0.54, while size of liposomes with encapsulated fisetin was around 92.5 nm ± 0.3 with polydispersity at 0.184 ± 0.017 and ζ-potential is at -7.0 ± 0.3.
3) Mean size of liposomes was about 879.6 nm ± 0.8 after extrusion through Ø 800 nm filter membrane, 433.6 nm ± 0.6 after extrusion through Ø 400 nm filter membrane, 186.5 nm ± 0.2 after extrusion through Ø 200 nm filter membrane. The ζ-potential was not measured.

Extrusion of the liposomes through each successively smaller membrane size significantly reduced their overall size, making the final liposomes similar in size to the filter pores they had to pass through during the extrusion process. This significant size reduction was a crucial step in the preparation of the liposomes for further experimentation. There is small difference in size

between empty liposomes and fisetin loaded liposomes, however, this size difference is still within an acceptable range, making the liposomes suitable for further work. The ζ-potential, which indicates the surface charge of the liposomes, is higher in the case of fisetin-loaded liposomes compared to the unloaded vesicles. This suggests that the incorporation of the fisetin drug may have altered the initially highly negative charge of the liposomes. Furthermore, after 30 days of storage, there were no significant changes in the size of the liposomes, which is visible in Figure 18a-b, but both the fisetin-loaded and empty samples showed a notable increase in ζ-potential, displaying similar final values. The rise in ζ-potential approaching 0 may suggest the potential formation of aggregates, however, the size does not confirm their creation.

The polydispersity index (PDI) indicates the variability in the size distribution of particles within a given sample. The PDI value close to 0.0 indicates a monodisperse sample with uniform particle size, while a value closer to 1.0 suggests a more heterogeneous distribution of particle size distribution. The desired PDI for nanoparticles is value < 0.2, which indicates low polydispersity [125]. Here, the PDI for all liposomes was below 0.2, which indicates low polydispersity for all measured liposomes. Within this range, it was noticed that PDI increased after a month, which could be caused by aggregates creation, although, as previously mentioned, the size does not provide confirmation of their formation.

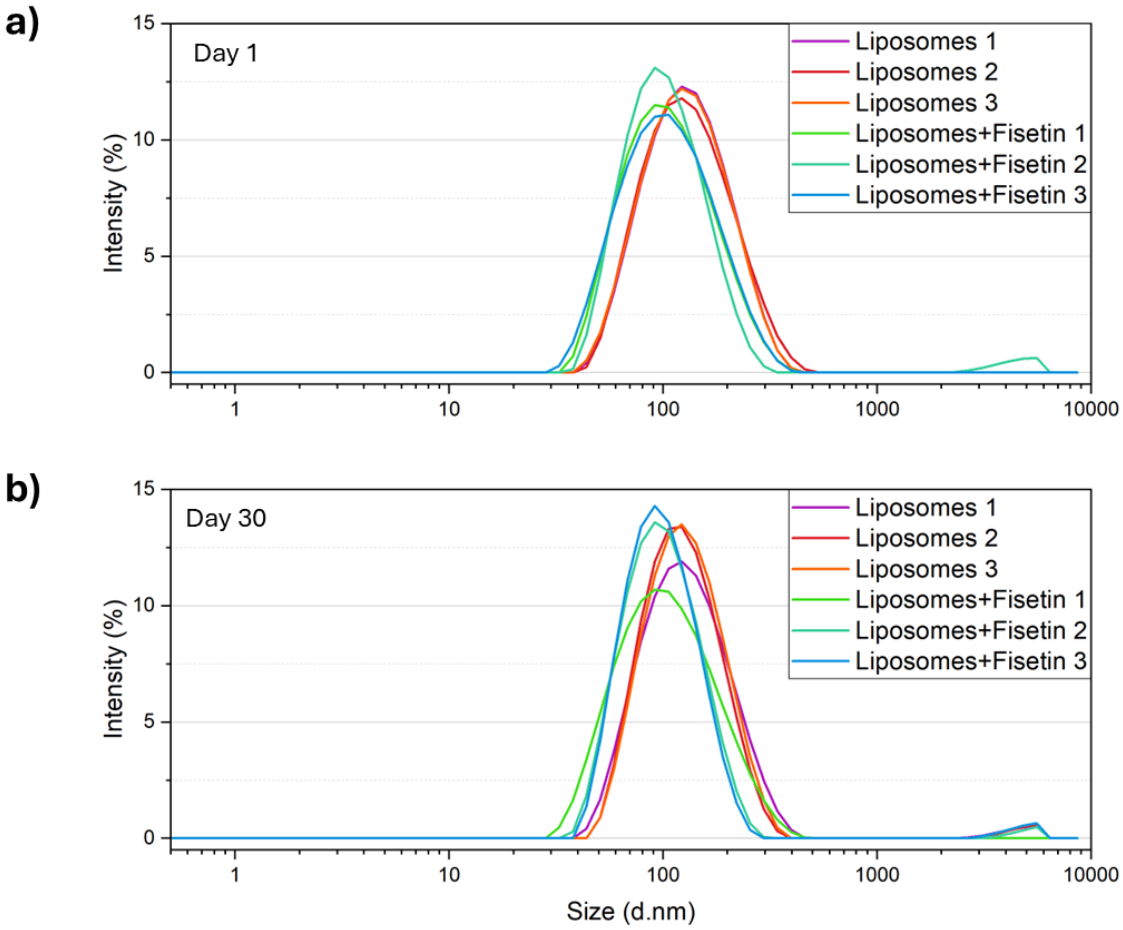

Figure 18. Size distribution by intensity at a) day 1 and b) after 30 days of storage at 4 °C

Table 15. Size, PDI and ζ-potential were determined by DLS on day 1 and on day 30 to analyze the stability of liposomes; data represented mean ± SD, n=3

	Day 1			Day 30		
	d. nm	PDI	ζ-potential mV	d. nm	PDI	ζ-potential mV
Liposomes	115.9 ± 0.9	0.155 ± 0.004	-20.3 ± 0.6	116.5 ± 1.0	0.181 ± 0.017	-8.3 ± 0.5
Liposomes + Fisetin	95.1 ± 0.9	0.178 ± 0.008	-11.6 ± 1.2	92.5 ±0.3	0.184 ± 0.017	-7.0 ± 0.3

Table 16. Size and PDI of empty liposomes after extrusion through Ø 800, 400, 200 and 100 nm membranes

Size of filter	d. nm	PDI
800 nm	879.6 ±108.6	0.758 ± 0.116
400 nm	433.6 ± 27.53	0.625 ± 0.121
200 nm	186.5 ± 2.8	0.204 ± 0.006
100 nm	115.9 ± 0.9	0.155 ± 0.004

4.2.1.2 Liposome morphology evaluation

The cryogenic scanning electron microscopy (CryoSEM) images were obtained with the help of prof. AMU dr. hab. Olena Ivashchenko. These images were used to analyze the morphology and structure organization of both types of liposomes. Additionally, the CryoSEM results were compared with the DLS measurements to gain a comprehensive understanding of the size characteristics of the liposomes. The measurement was performed shortly after the preparation

of liposomes was completed. The images showed that liposomes were round and regular in shape with a smooth surface, which is presented in Figure 19a. The addition of fisetin did not appear to interfere with or alter their overall morphology. Liposomes containing fisetin tend to attach to each other and form elongated chain-like structures, visible in Figure 19b, while empty liposomes do not exhibit this behavior. The formation of these liposome chains is a notable effect of incorporating fisetin into the liposomal structure. It was observed that during the image capture process, the liposomes were easily melting under the laser of the microscope, making it difficult to obtain clear and stable images, as the objects of interest were drifting away from the focal point. This phenomenon posed a challenge in obtaining high-quality micrographs of the liposomal structures.

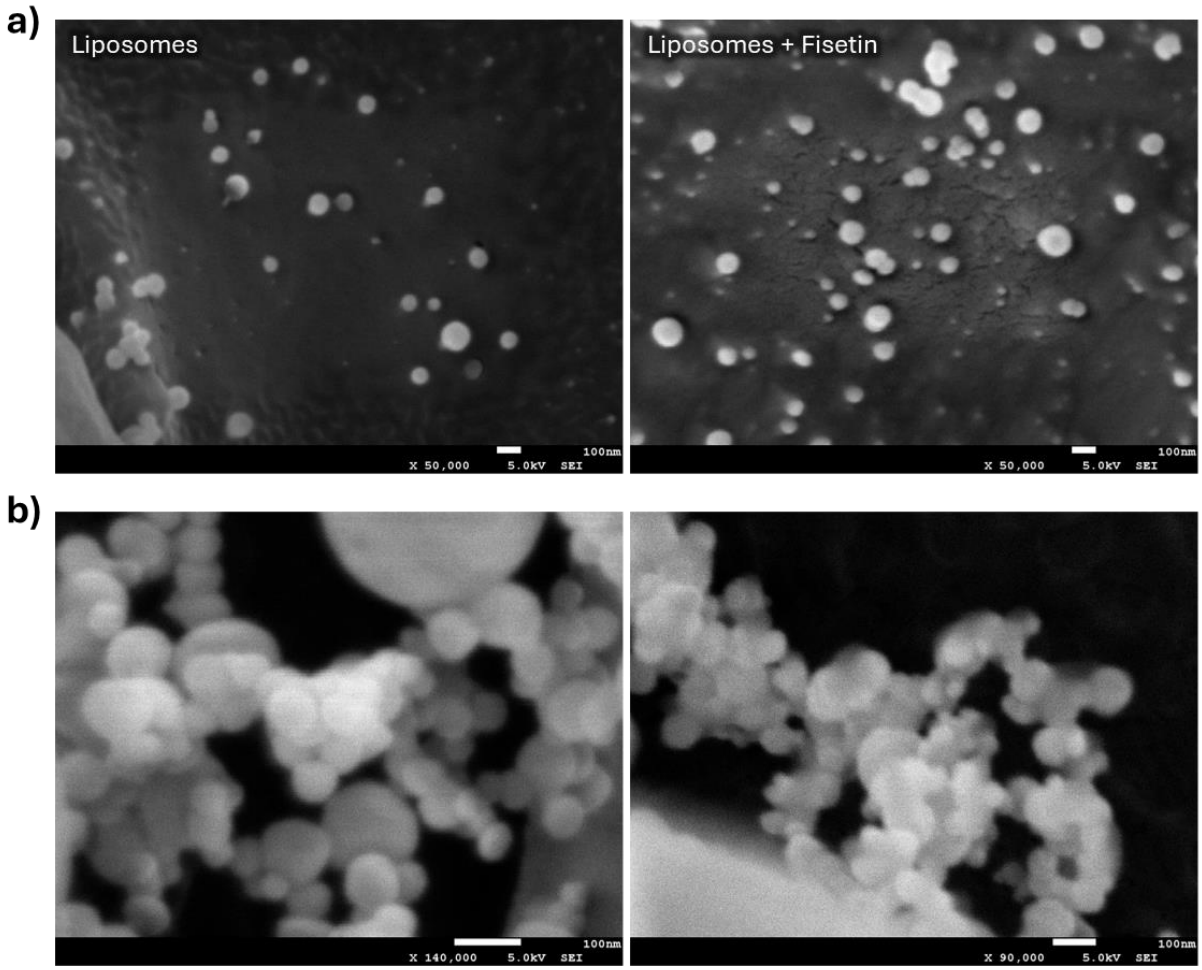

Figure 19. CryoSEM images of a) empty liposomes (left) and liposomes loaded with fisetin (right) at the same scale and b) closeup picture of the chain-like structure formed by liposomes with fisetin. Scale bars = 100 nm

4.2.1.3 Concentration evaluation

The DLS and Cryo-SEM data suggest that liposomes are successfully formed, but these methods alone do not provide any direct information about whether the drug of interest is actually encapsulated within the interior of the liposomes, and additional analyses were needed to determine the drug encapsulation efficiency and confirm the drug incorporation within the liposomal structure. The concentration of fisetin enclosed within the liposomes was determined following the purification process, which eliminated any unbound drug from the solution as a result of the size-exclusion properties of the Sephadex gel filtration column. During this purification step, free fisetin molecules were trapped within the porous Sephadex matrix due to

their smaller size, while the liposomes containing encapsulated fisetin were able to pass through the column thanks to the gravitational force, allowing for the measurement of the final fisetin concentration within the liposomal formulation. To evaluate the concentration of fisetin and its entrapment efficiency, we prepared a calibration curve of fisetin, as shown in Figure 20a. Fisetin's fluorescence was measured using a spectrofluorometer. The excitation spectrum showed fisetin's maximum emission was obtained at an excitation wavelength (λ) at 418 nm, which is the value used for further measurements.

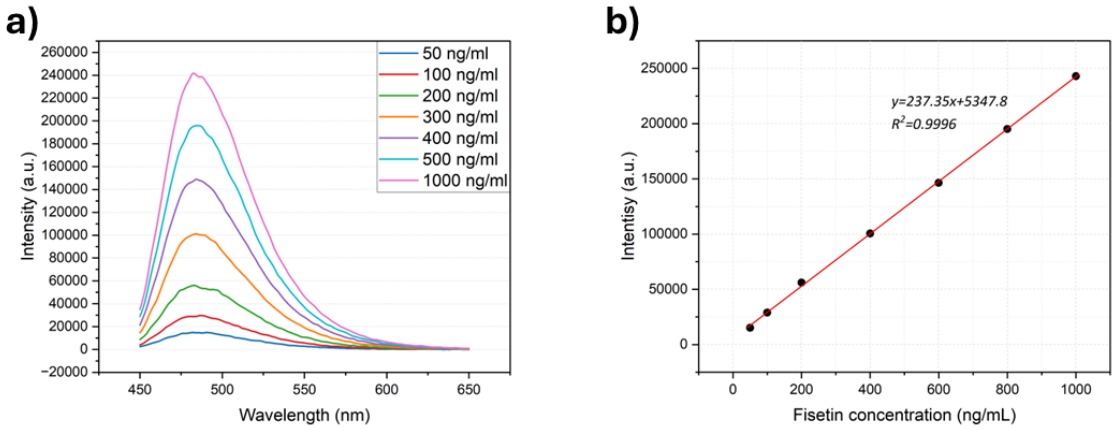

Figure 20. Fisetin was measured at different concentration with excitation at 418 nm to create a) calibration curve and b) standard curve which was prepared based on calibration curve.

Next, we measured the fluorescence of fisetin by dissolving 100 µL of vesicles in 5 mL of methanol, obtaining a 1:50 dilution ratio. Methanol was used to disrupt the liposome structure, which allowed for the measurement and quantification of the encapsulated fisetin drug within the liposomes. Separately, the measurements were performed for blank methanol and for empty liposomes dissolved in methanol, and these values were then subtracted to obtain the fluorescence measurement for fisetin alone, isolating its signal from any background effects coming from the scattering of the vesicles. Further calculations were based on a standard calibration curve, with the highest emission at λ 482 nm. The obtained numbers were then substituted into the linear function formula and calculated in µg/mL, which was further converted into µM concentrations to provide a more unified unit for this research.

The encapsulation efficiency (EE%) was determined by measuring the obtained concentration of fisetin after purification through Sephadex column and divided by the initial concentration of the drug, according to the formula (Equation 1, Chapter 3.14). After calculations, the value of EE% was determined to be approximately 13.68%. It was observed that the time period between dissolving the liposomal film in HEPES buffer and the extrusion step is a crucial factor in the liposomal formulation, as it impacts the ability of the drug to be effectively incorporated into the liposomal structure, as mentioned in the previous section (Chapter 4.2.1). Initially, an extrusion step was performed immediately after dissolving liposomes in HEPES, which showed EE% at 3.77%. This change was critical for further experiments as the concentration was too low for the planned *in vitro* cytotoxicity assay.

4.2.2 Cellular uptake

Cellular uptake refers to the process by which cells bring molecules and nanoparticles into their interior across the cell membrane. This is crucial for many biological functions, including drug delivery. Cellular uptake can happen through several pathways, like phagocytosis, endocytosis, or macropinocytosis [126], [127]. Understanding these mechanisms is vital for increasing efficiency of drug delivery systems and developing effective therapies.

To analyze the cellular uptake of the liposomes, Nile Red fluorescent dye was added to the liposome mixture during preparation, as described in Jagielski et al. [128], with slight modifications described in Chapter 2.4.15. The labelled liposomes were then added to the cells and incubated for 4 hours, allowing them to potentially enter the cells. The time of incubation was chosen based on the literature [129]. After the incubation period, high-resolution, three-dimensional confocal fluorescence microscopy images of the cells were captured. This imaging technique provided detailed, 3D visualizations of the intracellular localization of the fluorescently labelled liposomes within the cells. Based on these 3D images, most of the stained liposomes appear to be attached or adsorbed on the cell surface, with only a few liposomes inside the cells, which are pointed at with white arrow in Figure 21. Since the cells were attached to the surface before administering the liposomes, those could not have been trapped below the cell surface. Only a few liposomes were located inside the cells according to the red fluorescence signal observed within the intracellular compartments. This indicates that the liposomes were able to cross the cell membrane and accumulate inside the cell. The limited internalization observed could be due to various factors, such as the liposomes' size, composition, or surface properties (surface charge), which may affect their ability to be efficiently taken up by the cells. The low uptake of cells may primarily be attributed to the negative surface charge of the liposomes, which does not facilitate attraction between the negatively charged cell membranes and the liposomes.

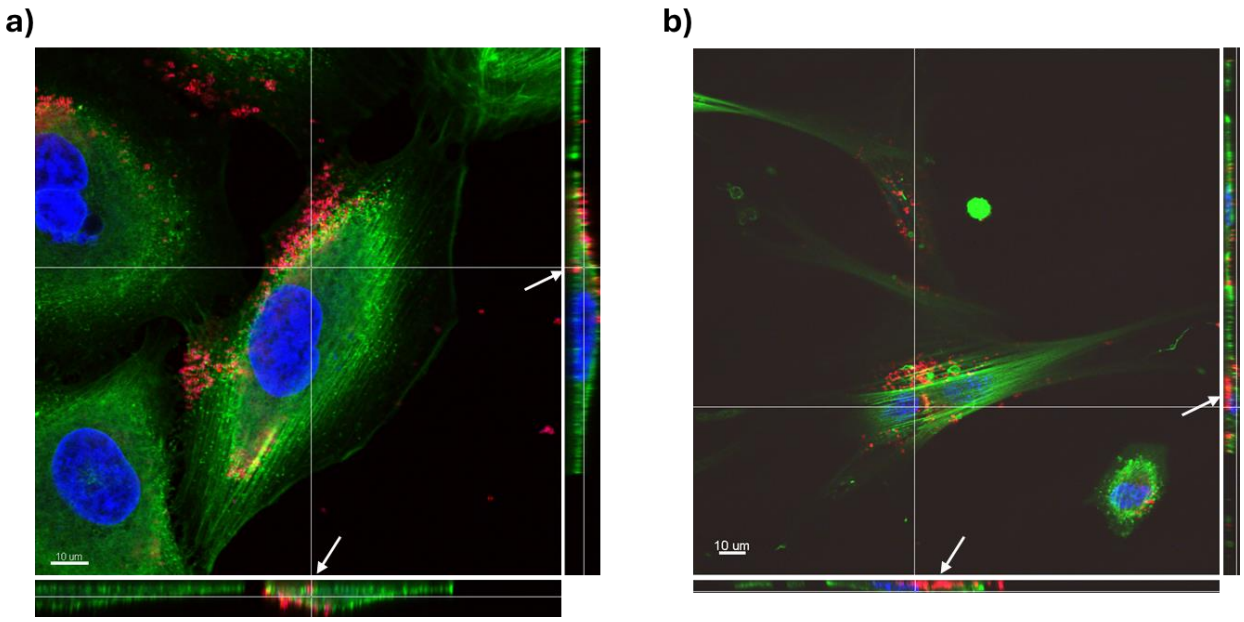

Figure 21. 3D Images of a) A549 and b) WI38 after incubation with liposomes. Pictures show the cell in three positions (front, side, top), which helps identify if liposomes are inside the cell (white arrows) or on the surface. Scale bar = 10 µm.

4.2.3 Cytotoxicity of liposomes

To ensure the safety of the nanocarriers for cells, a Live/Dead assay was performed. The live/dead assay is a common method used to evaluate the biocompatibility and safety of nanocarriers, as it can provide a quantitative measure of the percentage of viable and non-viable cells after exposure to the nanoparticles. The concentration of liposomes was determined based on the desired concentration of the encapsulated fisetin compound. A wide range of liposome concentrations were tested (0-300 µg/ml, prepared in two-fold dilution series), and no cytotoxic or negative effects on cell viability were observed in this experiment.

The cells did not exhibit any significant cytotoxic effects after an incubation period of 48 hours with empty liposomes. This observation suggests that the empty liposomes are biocompatible and do not induce harmful responses within the cellular environment. Furthermore, the lack of cytotoxicity indicates that these liposomes can be safely utilized in various applications without affecting cell viability as seen in Figure 22. Overall, the results demonstrate that empty liposomes can ensure minimal toxicity to the cells over an extended incubation period.

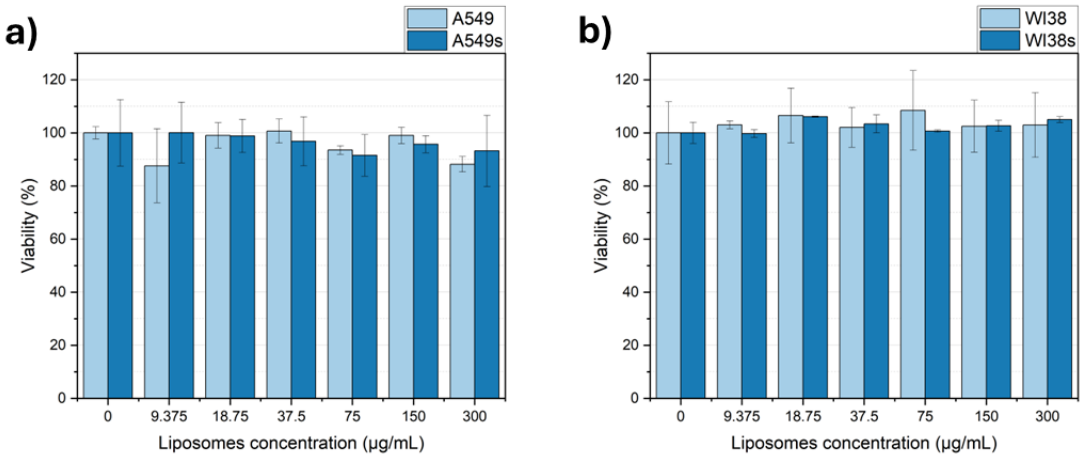

Figure 22. Results of Live/Dead assay after 48 hours of incubation with empty liposomes for a) A59 cells and b) WI38 cells, where viability is shown as a function of concentration.

4.2.4 Discussion on preparation and characterization of liposomes

The process of liposome preparation involves several techniques that can greatly influence their properties, including the size or encapsulation efficiency of drugs. Selecting the appropriate preparation method is essential and is determined by various factors, such as the physicochemical characteristics of the drug being encapsulated. Liposomes were prepared based on the study by Mignet et al. They explored various formulations and preparation methods, including sonication, homogenization, lipid cake formulation, and thin-film hydration. In our study, we used the last method, as it produced the smallest particles with the highest encapsulation efficiency (EE%) of 62% compared to the other techniques [123]. However, in our case the EE% obtained by Mignet et al. was not achieved in our case, which could be due to the use of different methods of evaporation of organic solvent. In their research, they utilized a Buchi evaporator, a specialized piece of chemical equipment, to thoroughly remove the organic solvent and carefully deposit a lipid film coating the interior walls of the flask [123]. We applied a stream of argon to evaporate the chloroform while moving the flask, ensuring that a lipid film could stay on the glass walls.

The size of nanoparticles plays a crucial role in their efficacy as drug delivery systems. Liposomes are categorized by their size as small unilamellar vesicles (SUV) <100 nm, large unilamellar vesicles (LUV) >100 nm and giant unilamellar vesicles (GUV) >1000 nm. In the study

of Cazzolla et al., the authors examined the significant role of the extrusion step that follows the thin-film hydration method used in the synthesis of liposomes. They observed that increasing the number of extrusions resulted in smaller liposome sizes. Interestingly, while the PDI remained constant throughout their experiments, indicating a uniform distribution of liposome sizes, the authors noted a noteworthy trend regarding zeta potential. They found that as the nanoparticles became smaller, their zeta potential values decreased correspondingly [130]. Extrusion presents a significant drawback due to material loss on the membranes. In their study, Pereira et al. utilized a similar method to create docetaxel-loaded liposomes, assessing lipid loss by collecting samples prior to the extrusion step, which could provide valuable insights for our research. However, their publication lacks comprehensive details regarding the methodology used for this specific aspect of their work [131]. Scanning electron eicroscopy (SEM) and transmission electron microscopy (TEM) techniques are essential to validate the size and morphology of the prepared nanoparticles. While liposomes and lipid nanoparticles are traditionally spherical in shape, several studies have reported the existence of uniquely shaped lipid nanoparticles. For instance, in the research conducted by Jagielski et al., which explored the development of lipid liquid crystalline nanoparticles, Cryo-TEM images showcased their distinctive cubic shape [128]. Another study by Cao et al. also realed star-shaped lipid nanoparticles, as demonstrated through TEM imaging [132].

The cell membrane is inherently negatively charged, which significantly influences the uptake of nanoparticles, particularly liposomes. The surface charge of nanoparticles is critical in determining their interaction with cell membranes and their subsequent internalization. Positively charged nanoparticles have been shown to have increased uptake in both phagocytic and non-phagocytic cell lines. This enhanced uptake is primarily due to attractions between the positively charged nanoparticles and the negatively charged components of the cell membrane. For example, cationic nanoparticles demonstrate enhanced internalization in various cell types due to electrostatic interactions with negatively charged components on the cell surface. This enhanced uptake of cationic nanoparticles compared to anionic nanoparticles has been observed in studies of Jeon et al. [133]. The negative surface charge of nanoparticles, including liposomes, can be effectively modified through the formation of a corona on their surface. This approach, as

demonstrated in the research conducted by Wolfram et al., highlights the potential for enhancing the properties and functionalities of these nanoparticles [134]. Kang et al. conducted a comprehensive study that revealed the dynamics of liposome uptake by cells, highlighting the influence of charge on this process. They found that liposomes with cationic, anionic, and neutral charges are internalized by cells in a time-dependent manner, suggesting that the duration of exposure plays a significant role in their uptake efficiency. Additionally, the researchers identified specific endocytic pathways responsible for this uptake, which vary depending on the charge of the liposomes, as they observed that both anionic and cationic liposomes are mostly taken up through a micropinocytosis [127].

Encapsulation efficiency is a critical factor in preparation of liposomal drug delivery systems, as it influences both the therapeutic efficacy and safety of the formulation. This metric refers to the proportion of a drug that is successfully encapsulated within the liposomes, relative to the total amount of drug used during the preparation process. Mignet et al. established a protocol for the production of liposomes encapsulating fisetin, achieving an impressive encapsulation efficiency of 62% [123]. In contrast, our findings revealed a significantly lower encapsulation efficiency of approximately 13%. This discrepancy may be caused by several factors previously discussed, including lipid composition variations and preparation methods. Additionally, Javani et al. reported on the encapsulation of quercetin, a senotherapeutic drug similar to fisetin, into niosomes. Their results indicated an encapsulation efficiency of 78% with one surfactant combination and 48% with another, highlighting the influence of formulation variables on efficiency [135]. Furthermore, Saddiqi et al. documented an encapsulation efficiency of around 50% for Tylosin using a similar preparation method [136].

Studying how nanoparticles are uptaken by cells is essential in the field of nanomedicine because it affects both the effectiveness of treatments and the risk of toxicity. Several factors influence this interaction, such as the particles' size, shape, surface charge, and coating materials, all of which play a role in cellular uptake. The uptake experiments conducted by Alekseeva et al. utilized multiple cell lines, revealing that each line exhibited different capabilities for nanoparticle uptake within a 2-hour incubation period. This variability underscores the importance of cellular context in determining how effectively nanoparticles can be internalized by different cell types

[129]. In the research conducted by Åberg et al., various nanoparticles, including liposomes, were investigated. They emphasized that cell size is a crucial characteristic that correlates with nanoparticle uptake. Larger cells generally exhibit a greater capacity for internalizing nanoparticles compared to smaller cells. Additionally, Åberg et al. noted that other important factors influencing uptake include the presence of specific receptors and various molecules involved in the mechanisms of cellular internalization [137]. These findings illustrate the complexity of nanoparticle-cell interactions and suggest that cell physical and biological characteristics play significant roles in determining uptake efficiency. Moreover, the work of Vtyurina et al. demonstrated that altering the size of nanoparticles significantly influences both the kinetics of uptake and the quantity of nanoparticles being internalized. The size of nanoparticles affects several critical factors, including their interactions with cell membranes, the pathways through which they are trafficked within cells, and their ultimate subcellular localization [126]. This finding is consistent with previous research indicating that smaller nanoparticles tend to have higher cellular uptake rates due to their enhanced ability to diffuse across cellular barriers [137]. Furthermore, liposomes utilize both endocytic pathways and direct membrane fusion for cellular entry. The choice of mechanism can depend on various factors such as liposome composition, surface modifications, and the specific cellular environment. Overall, these studies highlight the multifaceted nature of nanoparticle uptake, where size, cell type, and surface characteristics converge to influence how effectively nanoparticles are internalized by cells.

The interaction of liposomes with biological systems can result in different levels of cytotoxicity, which is affected by various factors such as the composition of the liposomes, their surface charge, and the characteristics of the encapsulated substances. Saddiqi et al. also used the thin-film hydration method to prepare liposomes composed of egg phosphatidylcholine and cholesterol. Cytotoxicity experiments were conducted, and the results demonstrated that their liposomes did not exhibit any signs of cytotoxicity, even at high doses. However, the viability of treated cells started decreasing only when the drug was encapsulated within the liposomes, which ultimately proved the safety of the liposomal formulation [136]. The study by Trang Phan et al. found a similar effect, where the viability of cells was maintained at over 80% when using empty liposomes. In contrast, drug-loaded liposomes decreased cell viability to below 30%, suggesting

that the presence of drugs within the liposomes had a harmful impact on cells [138]. Researchers often exclude experiments with empty liposomes and are instead investigating the difference in viability between free drugs and drugs encapsulated in liposomes. This is because liposomes are known for their safety and biocompatibility properties [139] however, it is crucial to always carefully check the safe dosage of both the drug and the carrier, as the well-known principle, "The dose makes the poison," applies in this context as well. As demonstrated by Cui et al., the dosage as well as the specific lipids employed in creating liposomes are crucial factors that can impact the efficacy and safety of liposomal formulations. Their study examined the use of peptide lipids and quaternary ammonium lipids. The drastic decline in cell viability with increasing dosage of these lipid formulations indicated their cytotoxicity, which is an important consideration when developing liposomal therapeutics [140].

4.3 Senotherapeutic effect of fisetin

Fisetin is commonly known as one of the best senolytics, selectively inducing apoptosis in senescent cells. However, studies have shown that not all senescent cells are sensitive to this drug [76], [141]. Here, we analyzed its cytotoxicity to senescent cells in comparison to non-senescent cells to ensure that it would act selectively. Additionally, ELISA was performed to study the senescent cells' secretion of two common SASP compounds, IL6 and IL8, to analyze their potential senomorphic properties.

4.3.1 Senolysis

Senolytics work by targeting on the senescent cell anti-apoptotic pathways (SCAPs) that allow senescent cells to evade apoptosis. By disrupting these pathways, senolytics induce apoptosis in senescent cells, effectively reducing their numbers and minimazing their harmful effects on surrounding tissues.

The Live/Dead assay enabled us to investigate the potential senolytic properties of fisetin, a flavonoid recognized for its various health benefits. This assay allowed us to assess cell viability while also providing insights into cellular morphology by staining the cytoskeleton. Red-stained nuclei indicated dead cells, while the blue-stained nuclei represented all cells, regardless of viability. To quantify cell viability, we compared the number of red-stained nuclei to the total

number of blue-stained nuclei. This comparison enabled us to calculate the percentage of viable cells across different concentrations of fisetin to better understand its effects. For fisetin to be classified as a senolytic agent, it was essential to demonstrate significant cytotoxicity towards senescent cells while exhibiting minimal toxicity towards non-senescent, healthy cells. However, our experimental data revealed a decline in viability at an 80 µM concentration of fisetin, which affected both senescent and non-senescent cell populations equally as shown in Figure 23a-b. These findings suggest that fisetin did not exhibit the senolytic properties for the A549 and WI38 cell lines, as it lacked the necessary selectivity between the two cell types. Fluorescent images obtained from the INCell Analyzer 2000 demonstrated that senescent cells exhibited morphological changes, becoming irregular in shape and shrinking when adhered to the surface (Figure 23d). Furthermore, these changes became more visible as the concentration of fisetin increases. Additionally, an EdU assay was performed to determine whether senescent cells were able to escape their cell cycle arrest following fisetin treatment. Result showed no significant changes in cell proliferation across the tested of fisetin concentrations, suggesting that the treatment did not induce any notable re-entry into the cell cycle for the senescent cells, as presented in Figure 23c.

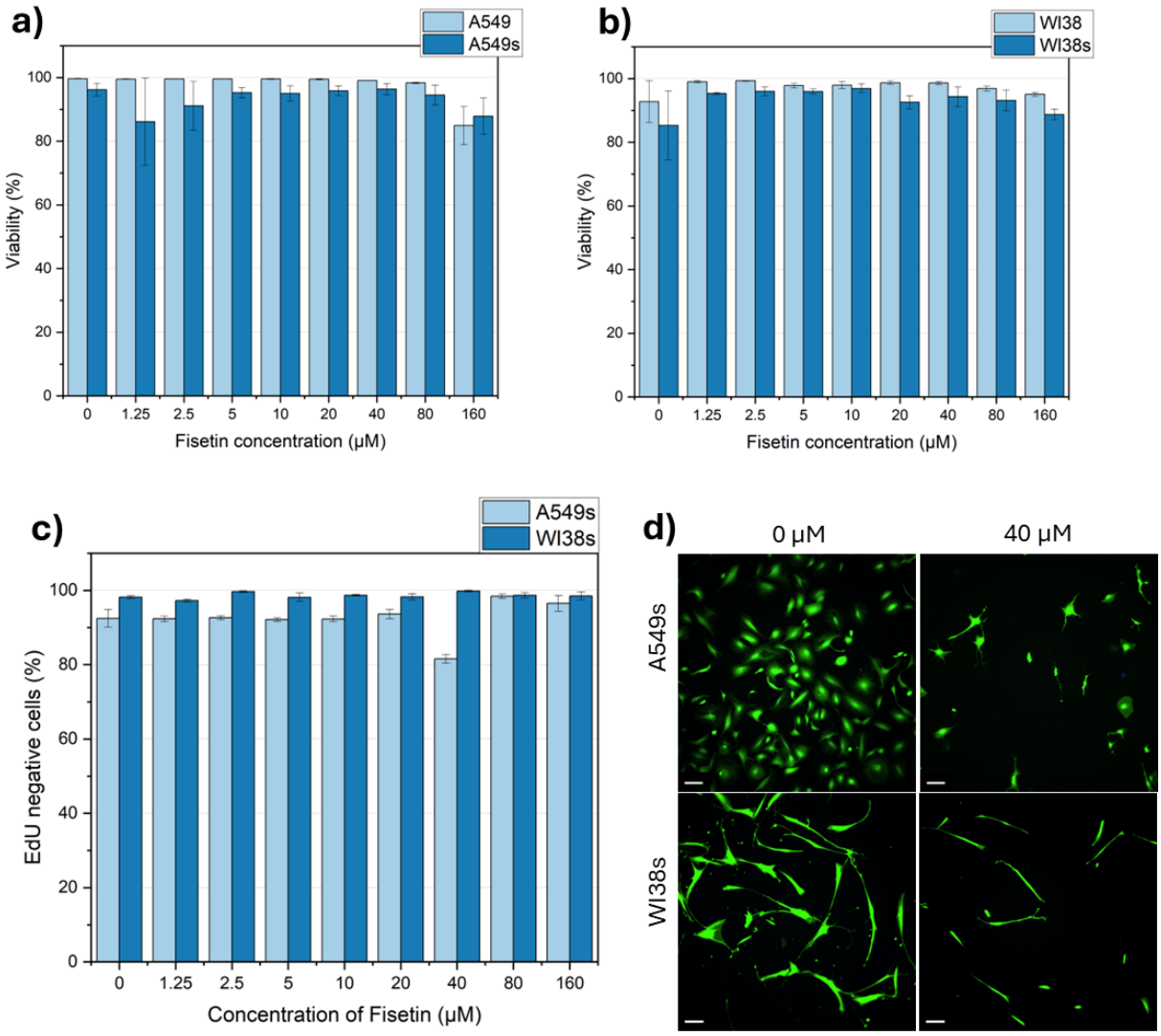

Figure 23. Viability of a) A549 and b) WI38 after 48 hours treatment with free Fisetin. c) Results of the EdU assay with d) representative pictures of senescent cells with and without Fisetin treatment. Scale bar = 50 μm

In the next step of our study, we conducted a Live/Dead assay on senescent cells treated with liposomes containing encapsulated fisetin. The primary aim of this experiment was to determine whether encapsulating fisetin within liposomes would have a greater effect on senescent cells than administering fisetin in its free form. The results presented in Figure 24 showed no significant differences in cell viability between treatments with liposomal fisetin and the free drug. This

finding suggests that the encapsulation of fisetin in liposomes did not enhance its effectiveness in reducing the viability of senescent cells.

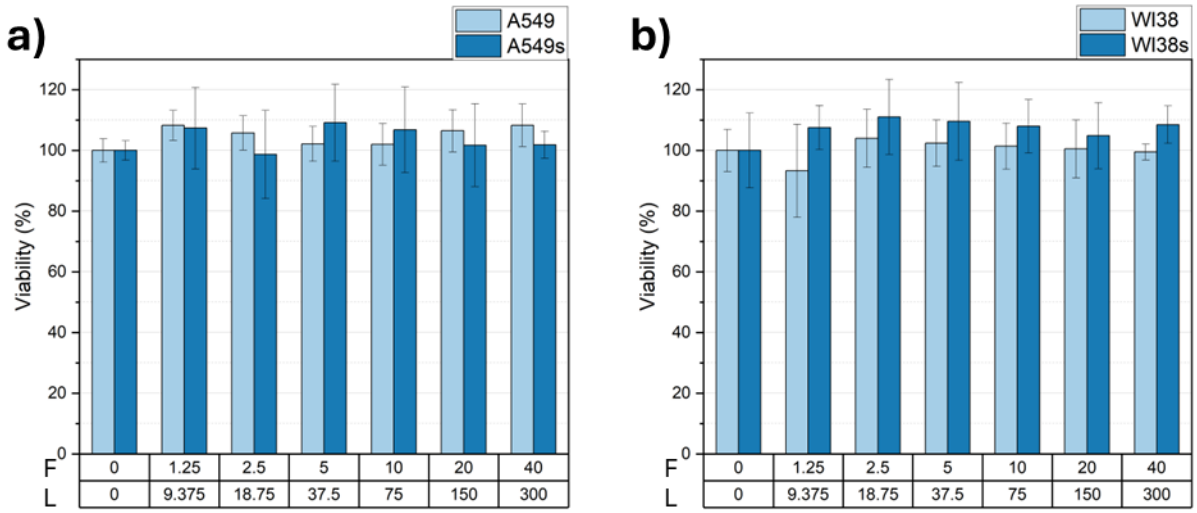

Figure 24. Viability of a) A549 cells and b) WI38 cells after 48 hours treatment with fisetin encapsulated in liposomes. Horizontal axis shows concentration of fisetin (F) in µM (top) and corresponding concentration of liposomes (L) in µg/mL (bottom)

4.3.2 Senomorphism

While senolytics selectively eliminate senescent cells, senomorphics focus on mitigating the harmful effects of the SASP without destroying these cells, which is primarly for chronic inflammation and tissue degradation.

To investigate the differences in SASP secretion, we seeded equal amounts of senescent and non-senescent cells, treated them with fisetin for 48 hours, and then incubated them in a drug-free medium for an additional 24 hours. This experimental design enabled us to evaluate SASP secretion over the 24-hour period. Additionally, we prepared untreated senescent and non-senescent cells to conduct a comparative analysis of SASP secretion between the two cell states. The cells showed significant differences in interleukin concentrations between senescent and non-senescent cells, as previously discussed in Chapter 4.1.3.6 (Figure 15). The results of this

experiment are presented separately in Figure 25 for A549 cell line and Figure 26 for WI38 cell line.

For the A549 cell line, the results indicated that even at the lowest tested concentration, liposomes containing fisetin reduced IL-6 and IL-8 levels by more than half. Across all fisetin concentrations IL-6 and IL-8 levels were similar between liposomal treatments but remained elevated compared to levels in non-senescent cells. While fisetin encapsulated in liposomes maintained interleukin levels at comparable rates, higher concentrations of fisetin (80 µM and 160 µM) as a free drug led to significantly lower interleukin levels compared to those liposomes-encapsulated form.

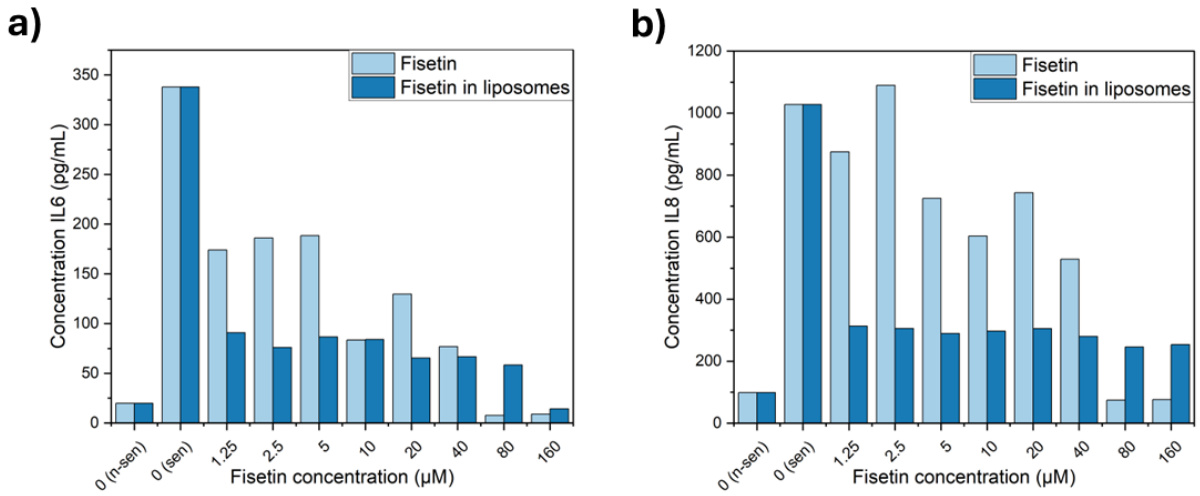

Figure 25. Results of ELISA assay for A549 cells include a) IL6 concentration and b) IL8 concentration after using fisetin encapsulated in liposomes and free drug.

The differences in IL-6 concentrations were less visible in the WI38 cell line compared to the A549 cell line. However, each concentration of fisetin encapsulated in liposomes reduced interleukin levels, bringing them to the same level or below those secreted by non-senescent cells. Notably, the reduction in IL-8 concentrations was more significant with fisetin encapsulated in liposomes than the reduction observed for IL-6. For IL-6, the levels remained largely similar between the encapsulated fisetin and the free drug.

Overall, these findings suggest that fisetin, when encapsulated in liposomes, demonstrates a significantly greater impact on SASP secretion than its free form.

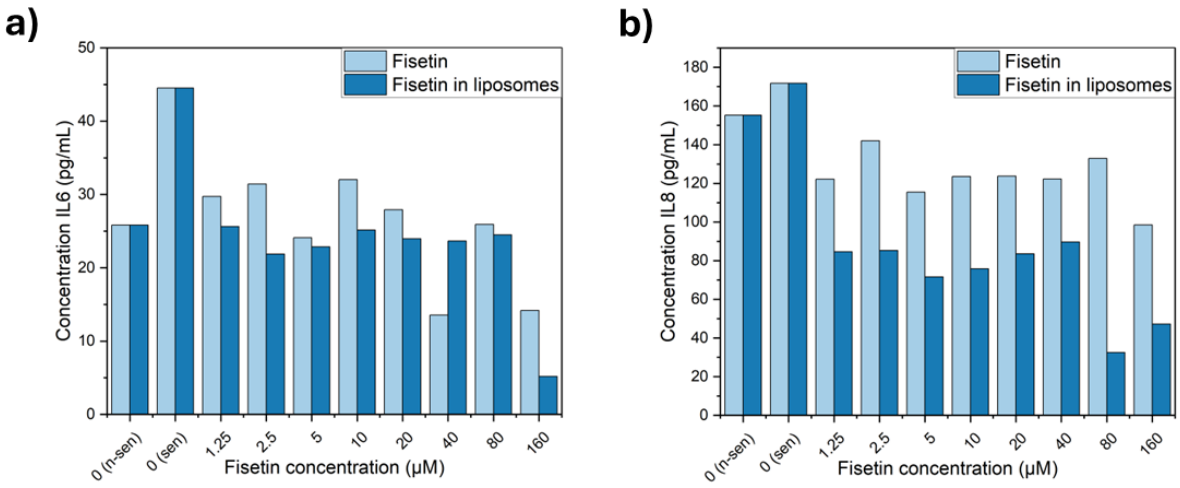

Figure 26. Results of ELISA assay for WI38 cells include a) IL6 concentration and b) IL8 concentration after using fisetin encapsulated in liposomes and free drug.

4.3.3 Discussion on senotherapeutic effects of fisetin

Current senotherapeutic strategies encompass a range of approaches, including conventional senolytics, prodrugs, proteins, and the use of nanocarriers for delivering senolytics. Nanocarriers offer an effective method for transporting otherwise insoluble drugs and can be specifically designed to target senescent cell populations by modifying their surface properties.

During their investigation into the effects of fisetin, Zhu et al. found that it exhibited senolytic properties in the HUVEC cell line. However, it did not induce apoptosis in senescent IMR90 cells [76]. Contrary, Yousefzadeh et al. reported that fisetin effectively promoted senolysis in the IMR90 cell line in a dose-dependent manner. They also discovered that quercetin, another well-known senolytic, was ineffective at a concentration of 5 μM in the MEF cell line, while fisetin at the same concentration led to a significant decrease in cell numbers [141]. *In vivo* experiments by Xu et al. with dasatinib and quercetin reduced naturally occurring senescent cells and pro-inflammatory cytokine secretion, enhancing overall health and extending lifespan [142]. Cai et al. introduced an innovative strategy by developing the β-galactosidase-targeted prodrug SSK1,

which activates in the presence of β-galactosidase. Their impressive viability results across various cell lines and the induction of cellular senescence by multiple agents suggest that this approach holds significant potential for eliminating senescent cells [143]. Similarly, González-Gualda et al. utilized galacto-conjugation of navitoclax, also activated by β-galactosidase. Their research on several cell lines subjected to different senescence inducers consistently showed that viability assays indicated apoptosis in senescent cells while preserving the viability of non-senescent cells [144]. Additionally, Guerrero et al. modified the prodrug duocarmycin with galactose to create a mechanism similar to that of González-Gualda et al., which is also activated by β-galactosidase. These findings were validated both *in vitro* and *in vivo* [145].

Unlike senolytics, which have been extensively researched for their ability to eliminate senescent cells, senomorphics have received less attention. This is primarily because senomorphics do not focus on removing these cells, which is the primary objective of many studies. However, while senolytics can be challenging to apply due to their dependence on specific cell lines, senomorphics do not seem to share this limitation. Moreover, senomorphics provide a complementary approach that aims to alleviate the negative effects of senescent cells without removing them.

In their research, Wang et al. focused on rapamycin, a well-known inhibitor of the SASP, due to its effects on the mTOR signalling pathway. They found that treating mice with rapamycin resulted in decreased β-gal staining and lower levels of pro-inflammatory cytokines [146]. Meanwhile, Lim et al. investigated avenanthramide C, which they identified as a modulator of the SASP. Their analysis of key SASP components, including TGF-β1, IL-6, and IL-8, confirmed a significant reduction in their concentrations after treatment. Furthermore, they observed changes in the morphology of senescent cells following the application of avenanthramide C and a decrease in the number of β-gal positive cells [147]. Rutin, another senomorphic agent, demonstrated a reduction in the secretion of various SASP components in the study conducted by Liu et al. They examined the conditioned medium from senescent cells on prostate cancer cells and found that these cancer cells adopted a malignant phenotype. However, prostate cancer cells treated additionally with rutin exhibited downregulation of all malignant functions [148]. In study on adipocyte differentiation and its connection to cellular senescence, Ali et al. found that resveratrol exhibits senomorphic activity at low concentrations in bone marrow stromal stem cells, significantly

reducing the gene expression of SASP components and inflammation markers [149]. However, resveratrol can induce cellular senescence or apoptosis at higher concentrations, as other researchers reported[150], [151].

Chapter 5 – Conclusions

This thesis aimed to establish a protocol for inducing cellular senescence induction using a chemotherapeutic drug, develop a nanocarrier for a senotherapeutic drug, and analyze its effects on senescent cells. The research presented here offers valuable insights into the induction and characterization of cellular senescence, as well as the development of liposomal nanocarriers for potential senotherapeutic applications. The key conclusions drawn from this study are as follows:

1. Induction of senescent cells using DOX was successful, as confirmed by senescence markers:
    - Senescence was effectively induced in A549 and WI38 cell lines using DOX at concentrations of 0.2 µM and 1 µM, respectively. This induction process maintained cell viability at approximately 80%, demonstrating minimal cytotoxicity while successfully triggering the senescent state.
    - The SA-β-gal was at the highest level in case of 0.2 µM of DOX concentration for A549 cell line. In case of WI38 cell line, SA-β-gal was at similar level at DOX concentrations 0.75 and 1.5 µM, however 0.75 µM concentration showed the lowest cytotoxic effect on cells.
    - The induction of senescence triggered a cascade of morphological alterations in both A549 and WI38 cell lines. Some of the morphological shifts were observed across both cell lines, and others manifested in a cell line-specific manner. In the A549 cell line, changes in size are more visible compared to the WI38 cell line. While non-senescent A549 cells showed maximum of about 500 μm^2, it was minimal size for senescent A549. For WI38, the size range of senescent cells expanded, but it also overlapped with the size range of non-senescent WI38 cells. Nuclear alterations are only visible in WI38 cells, which display a dotted pattern, whereas A549 senescent cells do not show a similar pattern.

- Senescent cells not only sustained metabolic function but also significantly enhanced overall metabolic activity compared to their non-senescent counterparts, showing over 4x higher metabolic activity percentage for senescent WI38 and more than 6x higher metabolic activity for senescent A549.
- Senescent cells no longer divide, but the A549 cell line showed the ability to re-enter the cell cycle after approximately one month of culture maintenance, while WI38 did not exhibit similar properties.
- Elevated levels of IL6 and IL8 in senescent cells confirmed these interleukins as components of the SASP in these cell lines. However, the interleukins concentrations between non-senescent and senescent WI38 cell line were not that differing as for A549 cell line.

2. Successful preparation of liposomes with encapsulated fisetin:
    - Liposomes were successfully prepared using the thin-film hydration method according to DLS and CryoSEM techniques. CryoSEM images demonstrated that liposomes are round and smooth.
    - The liposomes demonstrated suitable size (95-116 nm) and stability over a 30-day period. Both version of liposomes had PDI below 0.2, which indicates low polydispersity with insignificant increase after 30 days. The electric charge of liposomes was negative, which highly decreased in empty liposomes after 30 days, however no aggregates were formed.
    - Fisetin was successfully encapsulated within liposomes with an encapsulation efficiency of approximately 13.68%, which is applicable for experiments on cells.
    - Cellular uptake studies using Nile Red to label liposomes showed successful internalization of the nanocarriers by both A549 and WI38 cells, however due to the negative charge of liposomes, the uptake was not very high.
3. Evaluation of fisetin's senotherapeutic properties:
    - Fisetin did not demonstrate senolytic effects, failing to eliminate senescent cells in either cell line selectively in concentrations 1.25 – 160 μM.

- Fisetin exhibited senomorphic properties in both A549 and WI38 cell lines at concentrations ranging from 1.25 to 160 µM. In the A549 cell line, the levels of interleukins did not decrease to the same extent as observed in the non-senescent control for both interleukins. Conversely, in the WI38 cell line, the concentration of IL-6 was comparable to that of the non-senescent control. However, for IL-8, the concentration was reduced to below that seen in the non-senescent control.
- Fisetin encapsulated in liposomes showed enhanced effectiveness compared to free drug. Fisetin in free form was more effective compared to encapsulated fisetin in higher concentrations (80 – 160 µM) when treated senescent A549.

The studies presented in this thesis lay a solid foundation for future experiments. One promising direction involves the development of senescence-induction protocols prepared for various cell lines, allowing for a comprehensive analysis of the effects of fisetin on these different models. Additionally, enhancing the liposome formulation protocol could significantly improve encapsulation efficiency and facilitate better internalization by target cells. These advancements will not only deepen our understanding of cellular senescence but also optimize therapeutic delivery systems.

Bibliography

[1] Hayflick L, “The Limited *in vitro* Lifetime of Human Diploid Cell Strains,” Exp Cell Res, vol. 37, no. 3, pp. 614–639, 1965, doi: https://doi.org/10.1016/0014-4827(65)90211-9.

[2] A. Bojko, J. Czarnecka-Herok, A. Charzynska, M. Dabrowski, and E. Sikora, “Diversity of the senescence phenotype of cancer cells treated with chemotherapeutic agents,” Cells, vol. 8, no. 12, Dec. 2019, doi: 10.3390/cells8121501.

[3] Y. Luo et al., “Exploring the impacts of senescence on implantation and early embryonic development using totipotent cell-derived blastoids,” J Adv Res, 2024, doi: 10.1016/j.jare.2024.02.011.

[4] S. Da Silva-Álvarez et al., “Cell senescence contributes to tissue regeneration in zebrafish,” Aging Cell, vol. 19, no. 1, Jan. 2020, doi: 10.1111/acel.13052.

[5] N. Peng, H. H. Kang, Y. Feng, A. M. Minikes, and X. Jiang, “Autophagy inhibition signals through senescence to promote tumor suppression,” Autophagy, vol. 19, no. 6, pp. 1764–1780, 2023, doi: 10.1080/15548627.2022.2155794.

[6] C. Franceschi and J. Campisi, “Chronic inflammation (Inflammaging) and its potential contribution to age-associated diseases,” Jun. 01, 2014, Oxford University Press. doi: 10.1093/gerona/glu057.

[7] M. K. Ruhland et al., “Stromal senescence establishes an immunosuppressive microenvironment that drives tumorigenesis,” Nat Commun, vol. 7, Jun. 2016, doi: 10.1038/ncomms11762.

[8] D. Muñoz-Espín et al., “Programmed cell senescence during mammalian embryonic development,” Cell, vol. 155, no. 5, p. 1104, Nov. 2013, doi: 10.1016/j.cell.2013.10.019.

[9] M. H. Yun, H. Davaapil, and J. P. Brockes, “Recurrent turnover of senescent cells during regeneration of a complex structure,” Elife, vol. 4, no. e05505, 2015, doi: 10.7554/eLife.05505.001.

[10] H. Gal et al., “Molecular pathways of senescence regulate placental structure and function,” EMBO J, vol. 38, no. 18, Sep. 2019, doi: 10.15252/embj.2018100849.

[11] N. Gomez-Lopez et al., “Preterm labor in the absence of acute histologic chorioamnionitis is characterized by cellular senescence of the chorioamniotic membranes,” Am J Obstet Gynecol, vol. 217, no. 5, pp. 592.e1-592.e17, Nov. 2017, doi: 10.1016/j.ajog.2017.08.008.

[12] E. S. Lucas et al., “Recurrent pregnancy loss is associated with a pro-senescent decidual response during the peri-implantation window,” Commun Biol, vol. 3, no. 1, Dec. 2020, doi: 10.1038/s42003-020-0763-1.

[13] L. S. Cox and C. Redman, “The role of cellular senescence in ageing of the placenta,” Placenta, vol. 52, pp. 139–145, Apr. 2017, doi: 10.1016/j.placenta.2017.01.116.

[14] T. Guan, J. Li, C. Chen, and Y. Liu, “Self-Assembling Peptide-Based Hydrogels for Wound Tissue Repair,” Apr. 01, 2022, John Wiley and Sons Inc. doi: 10.1002/advs.202104165.

[15] H. E. Walters, K. E. Troyanovskiy, A. M. Graf, and M. H. Yun, “Senescent cells enhance newt limb regeneration by promoting muscle dedifferentiation,” Aging Cell, vol. 22, no. 6, Jun. 2023, doi: 10.1111/acel.13826.

[16] K. Meyer, B. Hodwin, D. Ramanujam, S. Engelhardt, and A. Sarikas, “Essential Role for Premature Senescence of Myofibroblasts in Myocardial Fibrosis,” 2016.

[17] B. Faz-López, J. Morales-Montor, and L. I. Terrazas, “Role of Macrophages in the Repair Process during the Tissue Migrating and Resident Helminth Infections,” 2016, Hindawi Limited. doi: 10.1155/2016/8634603.

[18] A. Kouli et al., “T lymphocyte senescence is attenuated in Parkinson’s disease,” J Neuroinflammation, vol. 18, no. 1, Dec. 2021, doi: 10.1186/s12974-021-02287-9.

[19] J. R. Herdy et al., “Increased post-mitotic senescence in aged human neurons is a pathological feature of Alzheimer’s disease,” Cell Stem Cell, vol. 29, no. 12, pp. 1637-1652.e6, Dec. 2022, doi: 10.1016/j.stem.2022.11.010.

[20] N. Campbell and J. Reece, “The Key Roles of Cell Division,” in Biology, 9th ed., Boston: Benjamin Cummings, 2011.

[21] J. C. M. Mombach, C. A. Bugs, and C. Chaouiya, “Modelling the onset of senescence at the G1/S cell cycle checkpoint,” BMC Genomics, vol. 15, no. 7, Oct. 2014, doi: 10.1186/1471-2164-15-S7-S7.

[22] K. Engeland, “Cell cycle regulation: p53-p21-RB signaling,” May 01, 2022, Springer Nature. doi: 10.1038/s41418-022-00988-z.

[23] R. Kumari and P. Jat, “Mechanisms of Cellular Senescence: Cell Cycle Arrest and Senescence Associated Secretory Phenotype,” Mar. 29, 2021, Frontiers Media S.A. doi: 10.3389/fcell.2021.645593.

[24] F. Baus, V. Gire, D. Fisher, J. Piette, and V. Dulić, “Permanent cell cycle exit in G2 phase after DNA damage in normal human fibroblasts,” EMBO J, vol. 22, no. 15, pp. 3992–4002, 2003, doi: https://doi.org/10.1093/emboj/cdg387.

[25] Y. Johmura et al., “Necessary and sufficient role for a mitosis skip in senescence induction,” Mol Cell, vol. 55, no. 1, pp. 73–84, Jul. 2014, doi: 10.1016/j.molcel.2014.05.003.

[26] C. Ye et al., “Radiation-induced cellular senescence results from a slippage of long-term G2 arrested cells into G1 phase,” Cell Cycle, vol. 12, no. 9, pp. 1424–1432, May 2013, doi: 10.4161/cc.24528.

[27] Y. Mitsui and E. L. Schneider, “Relationship between cell replication and volume in senescent human diploid fibroblasts,” Mech Ageing Dev, vol. 5, pp. 45–56, 1976.

[28] G. E. Neurohr et al., “Excessive Cell Growth Causes Cytoplasm Dilution And Contributes to Senescence,” Cell, vol. 176, no. 5, pp. 1083-1097.e18, Feb. 2019, doi: 10.1016/j.cell.2019.01.018.

[29] J. Lengefeld et al., “Cell size is a determinant of stem cell potential during aging,” 2021.

[30] Mammoto Tadanori et al., “Effects of age-dependent changes in cell size on endothelial cell proliferation and senescence through YAP1,” Aging, vol. 11, no. 17, pp. 7051–7069, 2019, doi: https://doi.org/10.18632%2Faging.102236.

[31] S. Xie and J. M. Skotheim, “A G1 Sizer Coordinates Growth and Division in the Mouse Epidermis,” Current Biology, vol. 30, no. 5, pp. 916-924.e2, Mar. 2020, doi: 10.1016/j.cub.2019.12.062.

[32] H. H. Wang, Y. J. Wu, Y. M. Tseng, C. H. Su, C. L. Hsieh, and H. I. Yeh, “Mitochondrial fission protein 1 up-regulation ameliorates senescence-related endothelial dysfunction of human endothelial progenitor cells,” Angiogenesis, vol. 22, no. 4, pp. 569–582, Nov. 2019, doi: 10.1007/s10456-019-09680-2.

[33] S. Rizza et al., “S-nitrosylation drives cell senescence and aging in mammals by controlling mitochondrial dynamics and mitophagy,” Proc Natl Acad Sci U S A, vol. 115, no. 15, pp. E3388–E3397, 2018, doi: 10.1073/pnas.1722452115.

[34] C. Morsczeck, A. Reck, and T. E. Reichert, “Changes in AMPK activity induces cellular senescence in human dental follicle cells,” Exp Gerontol, vol. 172, Feb. 2023, doi: 10.1016/j.exger.2022.112071.

[35] S. Mai, N. Brehm, G. Auburger, J. Bereiter-Hahn, and M. Jendrach, “Age-related dysfunction of the autophago-lysosomal pathway in human endothelial cells,” Pflugers Arch, vol. 471, no. 8, pp. 1065–1078, Aug. 2019, doi: 10.1007/s00424-019-02288-x.

[36] G. P. Dimri et al., “A biomarker that identifies senescent human cells in culture and in aging skin *in vivo* (replicative senescence/tumor suppression/18-galactosidase) Communicated by Arthur,” 1995.

[37] K. M. Aird and R. Zhang, “Detection of senescence-associated heterochromatin foci (SAHF),” Methods in Molecular Biology, vol. 965, pp. 185–196, 2013, doi: 10.1007/978-1-62703-239-1_12.

[38] M. Kosar, J. Bartkova, S. Hubackova, Z. Hodny, J. Lukas, and J. Bartek, “Senescence-associated heterochromatin foci are dispensable for cellular senescence, occur in a cell type- And insult-dependent manner, and follow expression of p16ink4a,” Cell Cycle, vol. 10, no. 3, pp. 457–468, Feb. 2011, doi: 10.4161/cc.10.3.14707.

[39] A. Freund, R. M. Laberge, M. Demaria, and J. Campisi, “Lamin B1 loss is a senescence-associated biomarker,” Mol Biol Cell, vol. 23, no. 11, pp. 2066–2075, Jun. 2012, doi: 10.1091/mbc.E11-10-0884.

[40] M. Sadaie et al., “Redistribution of the Lamin B1 genomic binding profile affects rearrangement of heterochromatic domains and SAHF formation during senescence,” Genes Dev, vol. 27, no. 16, pp. 1800–1808, Aug. 2013, doi: 10.1101/gad.217281.113.

[41] J. P. Coppé et al., “Senescence-associated secretory phenotypes reveal cell-nonautonomous functions of oncogenic RAS and the p53 tumor suppressor.,” PLoS Biol, vol. 6, no. 12, 2008, doi: 10.1371/journal.pbio.0060301.

[42] Y. H. Kim, Y. W. Choi, J. Lee, E. Y. Soh, J. H. Kim, and T. J. Park, “Senescent tumor cells lead the collective invasion in thyroid cancer,” Nat Commun, vol. 8, 2017, doi: 10.1038/ncomms15208.

[43] N. Igarashi et al., “Hepatocyte growth factor derived from senescent cells attenuates cell competition-induced apical elimination of oncogenic cells,” Nat Commun, vol. 13, no. 1, Dec. 2022, doi: 10.1038/s41467-022-31642-4.

[44] D. Shang et al., “Activation of epidermal growth factor receptor signaling mediates cellular senescence induced by certain pro-inflammatory cytokines,” Aging Cell, vol. 19, no. 5, May 2020, doi: 10.1111/acel.13145.

[45] X. Xing et al., “Local Elimination of Senescent Cells Promotes Bone Defect Repair during Aging,” ACS Appl Mater Interfaces, vol. 14, no. 3, pp. 3885–3899, Jan. 2022, doi: 10.1021/acsami.1c22138.

[46] J. Guillon et al., “Regulation of senescence escape by TSP1 and CD47 following chemotherapy treatment,” Cell Death Dis, vol. 10, no. 3, Mar. 2019, doi: 10.1038/s41419-019-1406-7.

[47] Y. Chien et al., “Control of the senescence-associated secretory phenotype by NF-κB promotes senescence and enhances chemosensitivity,” Genes Dev, vol. 25, no. 20, pp. 2125–2136, Oct. 2011, doi: 10.1101/gad.17276711.

[48] R. M. Laberge et al., “MTOR regulates the pro-tumorigenic senescence-associated secretory phenotype by promoting IL1A translation,” Nat Cell Biol, vol. 17, no. 8, pp. 1049–1061, Aug. 2015, doi: 10.1038/ncb3195.

[49] N. Herranz et al., “mTOR regulates MAPKAPK2 translation to control the senescence-associated secretory phenotype,” Nat Cell Biol, vol. 17, no. 9, pp. 1205–1217, Sep. 2015, doi: 10.1038/ncb3225.

[50] A. Freund, C. K. Patil, and J. Campisi, “P38MAPK is a novel DNA damage response-independent regulator of the senescence-associated secretory phenotype,” EMBO Journal, vol. 30, no. 8, pp. 1536–1548, Apr. 2011, doi: 10.1038/emboj.2011.69.

[51] S. Özcan et al., “Unbiased analysis of senescence associated secretory phenotype (SASP) to identify common components following different genotoxic stresses,” Aging, vol. 8, no. 7, pp. 1316–1327, 2016, doi: https://doi.org/10.18632%2Faging.100971.

[52] V. Gorgoulis et al., “Cellular Senescence: Defining a Path Forward,” Oct. 31, 2019, Cell Press. doi: 10.1016/j.cell.2019.10.005.

[53] N. Basisty et al., “A proteomic atlas of senescence-associated secretomes for aging biomarker development,” PLoS Biol, vol. 18, no. 1, Jan. 2020, doi: 10.1371/journal.pbio.3000599.

[54] J. P. Coppé, P. Y. Desprez, A. Krtolica, and J. Campisi, “The senescence-associated secretory phenotype: The dark side of tumor suppression,” Feb. 02, 2010. doi: 10.1146/annurev-pathol-121808-102144.

[55] C. A. Valenzuela, L. Vargas, V. Martinez, S. Bravo, and N. E. Brown, “Palbociclib-induced autophagy and senescence in gastric cancer cells,” Exp Cell Res, vol. 360, no. 2, pp. 390–396, Nov. 2017, doi: 10.1016/j.yexcr.2017.09.031.

[56] M. Demaria et al., “Cellular senescence promotes adverse effects of chemotherapy and cancer relapse,” Cancer Discov, vol. 7, no. 2, pp. 165–176, Feb. 2017, doi: 10.1158/2159-8290.CD-16-0241.

[57] F. Arcamone et al., “Adriamycin, 14-Hydroxydaunomycin, a New Antitumor Antibiotic from S. peucetius var. caesius,” 1969.

[58] B. Jawad, L. Poudel, R. Podgornik, N. F. Steinmetz, and W. Y. Ching, “Molecular mechanism and binding free energy of doxorubicin intercalation in DNA,” Physical Chemistry Chemical Physics, vol. 21, no. 7, pp. 3877–3893, 2019, doi: 10.1039/c8cp06776g.

[59] O. Tacar, P. Sriamornsak, and C. R. Dass, “Doxorubicin: An update on anticancer molecular action, toxicity and novel drug delivery systems,” Feb. 2013. doi: 10.1111/j.2042-7158.2012.01567.x.

[60] R. E. Nicoletto and C. M. Ofner, “Cytotoxic mechanisms of doxorubicin at clinically relevant concentrations in breast cancer cells,” Mar. 01, 2022, Springer Science and Business Media Deutschland GmbH. doi: 10.1007/s00280-022-04400-y.

[61] M. Fumagalli, F. Rossiello, C. Mondello, and F. d’Adda di Fagagna, “Stable cellular senescence is associated with persistent DDR activation,” PLoS One, vol. 9, no. 10, Oct. 2014, doi: 10.1371/journal.pone.0110969.

[62] X. Wu, X. Zhou, S. Wang, and G. Mao, “DNA damage response(DDR): a link between cellular senescence and human cytomegalovirus,” Dec. 01, 2023, BioMed Central Ltd. doi: 10.1186/s12985-023-02203-y.

[63] A. Celeste et al., “Genomic instability in mice lacking histone H2AX,” Science (1979), vol. 296, no. 5569, pp. 922–927, May 2002, doi: 10.1126/science.1069398.

[64] “KEGG PATHWAY Database.” Accessed: Aug. 18, 2024. [Online]. Available: https://www.kegg.jp/kegg/pathway.html

[65] J. Chang-Chien, J. L. Huang, H. J. Tsai, S. L. Wang, M. L. Kuo, and T. C. Yao, “Particulate matter causes telomere shortening and increase in cellular senescence markers in human lung epithelial cells,” Ecotoxicol Environ Saf, vol. 222, Oct. 2021, doi: 10.1016/j.ecoenv.2021.112484.

[66] T. J. Mead and V. Lefebvre, “Proliferation assays (BrdU and EdU) on skeletal tissue sections,” Methods in Molecular Biology, vol. 1130, pp. 233–243, 2014, doi: 10.1007/978-1-62703-989-5_17.

[67] R. Sager, “Senescence As a Mode of Tumor Suppression,” 1991.

[68] M. Ruscetti et al., “NK cell-mediated cytotoxicity contributes to tumor control by a cytostatic drug combination,” Science (1979), vol. 362, pp. 1416–1422, 2018, [Online]. Available: https://www.science.org

[69] T. Yasuda, H. Baba, and T. Ishimoto, “Cellular senescence in the tumor microenvironment and context-specific cancer treatment strategies,” Mar. 01, 2023, John Wiley and Sons Inc. doi: 10.1111/febs.16231.

[70] J. Tato-Costa et al., “Therapy-induced cellular senescence induces epithelial-to-mesenchymal transition and increases invasiveness in rectal cancer,” Clin Colorectal Cancer, vol. 15, no. 2, pp. 170-178.e3, Jun. 2016, doi: 10.1016/j.clcc.2015.09.003.

[71] A. Okuma, A. Hanyu, S. Watanabe, and E. Hara, “P16Ink4a and p21Cip1/Waf1 promote tumour growth by enhancing myeloid-derived suppressor cells chemotaxis,” Nat Commun, vol. 8, no. 1, Dec. 2017, doi: 10.1038/s41467-017-02281-x.

[72] M. Karabicici, S. Alptekin, Z. Fırtına Karagonlar, and E. Erdal, “Doxorubicin-induced senescence promotes stemness and tumorigenicity in EpCAM−/CD133− nonstem cell population in hepatocellular carcinoma cell line, HuH-7,” Mol Oncol, vol. 15, no. 8, pp. 2185–2202, Aug. 2021, doi: 10.1002/1878-0261.12916.

[73] L. Yang, J. Fang, and J. Chen, “Tumor cell senescence response produces aggressive variants,” Cell Death Discov, vol. 3, no. 1, Dec. 2017, doi: 10.1038/cddiscovery.2017.49.

[74] E. Brenner et al., “Cancer immune control needs senescence induction by interferon-dependent cell cycle regulator pathways in tumours,” Nat Commun, vol. 11, no. 1, Dec. 2020, doi: 10.1038/s41467-020-14987-6.

[75] R. S. Roberson, S. J. Kussick, E. Vallieres, S.-Y. J. Chen, and D. Y. Wu, “Escape from Therapy-Induced Accelerated Cellular Senescence in p53-Null Lung Cancer Cells and in Human Lung Cancers,” AACR Journals, vol. 65, no. 7, pp. 2795–2803, 2005, [Online]. Available: http://www.physics.csbsju.edu/stats/t-test.html

[76] Y. Zhu et al., “New agents that target senescent cells: the flavone, fisetin, and the BCL-XL inhibitors, A1331852 and A1155463,” Aging, vol. 9, no. 3, pp. 955–963, 2017, doi: https://doi.org/10.18632%2Faging.101202.

[77] J. C. Chamcheu et al., “Fisetin, a 3,7,3’,4’-tetrahydroxyflavone inhibits the PI3K/Akt/mTOR and MAPK pathways and ameliorates psoriasis pathology in 2D and 3D organotypic human inflammatory skin models,” Cells, vol. 8, no. 9, Sep. 2019, doi: 10.3390/cells8091089.

[78] T. Ersahin, N. Tuncbag, and R. Cetin-Atalay, “The PI3K/AKT/mTOR interactive pathway,” Mol Biosyst, vol. 11, no. 7, pp. 1946–1954, Jul. 2015, doi: 10.1039/c5mb00101c.

[79] Josef Herzig, “Studien fiber Quercetin und seine Derivate,” Monatsh Chem, vol. 12, pp. 177–190, 1891, doi: https://doi.org/10.1007/BF01538594.

[80] N. Khan, D. N. Syed, N. Ahmad, and H. Mukhtar, “Fisetin: A dietary antioxidant for health promotion,” Jul. 10, 2013. doi: 10.1089/ars.2012.4901.

[81] M. J. Yousefzadeh et al., “Fisetin is a senotherapeutic that extends health and lifespan,” EBioMedicine, vol. 36, pp. 18–28, Oct. 2018, doi: 10.1016/j.ebiom.2018.09.015.

[82] L. Zhang, L. E. Pitcher, V. Prahalad, L. J. Niedernhofer, and P. D. Robbins, “Recent advances in the discovery of senolytics,” Mech Ageing Dev, vol. 200, Dec. 2021, doi: 10.1016/j.mad.2021.111587.

[83] S. Adepu and S. Ramakrishna, “Controlled drug delivery systems: Current status and future directions,” Oct. 01, 2021, MDPI. doi: 10.3390/molecules26195905.

[84] H. Nsairat, D. Khater, U. Sayed, F. Odeh, A. Al Bawab, and W. Alshaer, “Liposomes: structure, composition, types, and clinical applications,” May 01, 2022, Elsevier Ltd. doi: 10.1016/j.heliyon.2022.e09394.

[85] G. Sanità, B. Carrese, and A. Lamberti, “Nanoparticle Surface Functionalization: How to Improve Biocompatibility and Cellular Internalization,” Nov. 26, 2020, Frontiers Media S.A. doi: 10.3389/fmolb.2020.587012.

[86] G. M. T. de Oliveira, E. M. N. de Oliveira, T. C. B. Pereira, R. M. Papaléo, and M. R. Bogo, “Implications of exposure to dextran-coated and uncoated iron oxide nanoparticles to developmental toxicity in zebrafish,” Journal of Nanoparticle Research, vol. 19, no. 12, Dec. 2017, doi: 10.1007/s11051-017-4074-5.

[87] S. Shukla, A. Jadaun, V. Arora, R. K. Sinha, N. Biyani, and V. K. Jain, “*In vitro* toxicity assessment of chitosan oligosaccharide coated iron oxide nanoparticles,” Toxicol Rep, vol. 2, pp. 27–39, Jan. 2015, doi: 10.1016/j.toxrep.2014.11.002.

[88] H. Ren et al., “Role of Liposome Size, Surface Charge, and PEGylation on Rheumatoid Arthritis Targeting Therapy,” ACS Appl Mater Interfaces, vol. 11, no. 22, pp. 20304–20315, Jun. 2019, doi: 10.1021/acsami.8b22693.

[89] N. Joudeh and D. Linke, “Nanoparticle classification, physicochemical properties, characterization, and applications: a comprehensive review for biologists,” Dec. 01, 2022, BioMed Central Ltd. doi: 10.1186/s12951-022-01477-8.

[90] D. Muñoz-Espín et al., “A versatile drug delivery system targeting senescent cells,” EMBO Mol Med, vol. 10, no. 9, Sep. 2018, doi: 10.15252/emmm.201809355.

[91] A. E. Ekpenyong-Akiba et al., “Detecting and targeting senescent cells using molecularly imprinted nanoparticles,” Nanoscale Horiz, vol. 4, no. 3, pp. 757–768, 2019.

[92] L. Chibaya et al., “Nanoparticle delivery of innate immune agonists combines with senescence-inducing agents to mediate T cell control of pancreatic cancer (preprint),” bioRxiv, 2023, doi: 10.1101/2023.09.18.558307.

[93] H. Orlikowska-Rzeznik et al., “Dehydration of Lipid Membranes Drives Redistribution of Cholesterol Between Lateral Domains,” Journal of Physical Chemistry Letters, vol. 15, no. 16, pp. 4515–4522, Apr. 2024, doi: 10.1021/acs.jpclett.4c00332.

[94] M. C. Sánchez-Cerviño, C. P. Fuioaga, L. I. Atanase, G. A. Abraham, and G. Rivero, “Electrohydrodynamic Techniques for the Manufacture and/or Immobilization of Vesicles,” Feb. 01, 2023, MDPI. doi: 10.3390/polym15040795.

[95] G. Pauli, W. L. Tang, and S. D. Li, “Development and characterization of the solvent-assisted active loading technology (SALT) for liposomal loading of poorly water-soluble compounds,” Sep. 01, 2019, MDPI AG. doi: 10.3390/pharmaceutics11090465.

[96] M. J. Mitchell, M. M. Billingsley, R. M. Haley, M. E. Wechsler, N. A. Peppas, and R. Langer, “Engineering precision nanoparticles for drug delivery,” Feb. 01, 2021, Nature Research. doi: 10.1038/s41573-020-0090-8.

[97] D. Guimarães, A. Cavaco-Paulo, and E. Nogueira, “Design of liposomes as drug delivery system for therapeutic applications,” May 15, 2021, Elsevier B.V. doi: 10.1016/j.ijpharm.2021.120571.

[98] L. Maja, K. Željko, and P. Mateja, “Sustainable technologies for liposome preparation,” Nov. 01, 2020, Elsevier B.V. doi: 10.1016/j.supflu.2020.104984.

[99] M. P. Baar et al., “Targeted Apoptosis of Senescent Cells Restores Tissue Homeostasis in Response to Chemotoxicity and Aging,” Cell, vol. 169, no. 1, pp. 132-147.e16, Mar. 2017, doi: 10.1016/j.cell.2017.02.031.

[100] A. Zuryń, M. Gagat, A. A. Grzanka, L. Gackowska, and A. Grzanka, “Expression of cyclin B1 after induction of senescence and cell death in non-small cell lung carcinoma A549 cells,” Folia Histochem Cytobiol, vol. 50, no. 1, pp. 58–67, 2012, doi: 10.5603/FHC.2012.0008.

[101] G. Casella et al., “Transcriptome signature of cellular senescence,” Nucleic Acids Res, vol. 47, no. 14, pp. 7294–7305, Aug. 2019, doi: 10.1093/nar/gkz555.

[102] D. J. Giard et al., “*In Vitro* Cultivation of Human Tumors: Establishment of Cell Lines Derived From a Series of Solid Tumors,” J Natl Cancer Inst, vol. 51, no. 5, pp. 1417–1423, 1973, [Online]. Available: https://academic.oup.com/jnci/article/51/5/1417/962555

[103] M. Y. Yang et al., “Induction of cellular senescence by doxorubicin is associated with upregulated miR-375 and induction of autophagy in K562 cells,” PLoS One, vol. 7, no. 5, May 2012, doi: 10.1371/journal.pone.0037205.

[104] C. D. Wiley et al., “Analysis of individual cells identifies cell-to-cell variability following induction of cellular senescence,” Aging Cell, vol. 16, no. 5, pp. 1043–1050, Oct. 2017, doi: 10.1111/acel.12632.

[105] M. J. Schafer et al., “The senescence-associated secretome as an indicator of age and medical risk,” JCI Insight, vol. 5, no. 12, Jun. 2020, doi: 10.1172/jci.insight.133668.

[106] H. Kim et al., “Metformin inhibits chronic kidney disease-induced DNA damage and senescence of mesenchymal stem cells,” Aging Cell, vol. 20, no. 2, Feb. 2021, doi: 10.1111/acel.13317.

[107] S. Gonçalves et al., “COX2 regulates senescence secretome composition and senescence surveillance through PGE2,” Cell Rep, vol. 34, no. 11, Mar. 2021, doi: 10.1016/j.celrep.2021.108860.

[108] N. Igarashi et al., “Hepatocyte growth factor derived from senescent cells attenuates cell competition-induced apical elimination of oncogenic cells,” Nat Commun, vol. 13, no. 1, Dec. 2022, doi: 10.1038/s41467-022-31642-4.

[109] J. Guillon et al., “Regulation of senescence escape by TSP1 and CD47 following chemotherapy treatment,” Cell Death Dis, vol. 10, no. 3, Mar. 2019, doi: 10.1038/s41419-019-1406-7.

[110] A. Hernandez-Segura, S. Brandenburg, and M. Demaria, “Induction and validation of cellular senescence in primary human cells,” Journal of Visualized Experiments, vol. 2018, no. 136, Jun. 2018, doi: 10.3791/57782.

[111] A. Brandl, M. Meyer, V. Bechmann, M. Nerlich, and P. Angele, “Oxidative stress induces senescence in human mesenchymal stem cells,” Exp Cell Res, vol. 317, no. 11, pp. 1541–1547, 2011, doi: 10.1016/j.yexcr.2011.02.015.

[112] M. Rovira et al., “The lysosomal proteome of senescent cells contributes to the senescence secretome,” Aging Cell, vol. 21, no. 10, Oct. 2022, doi: 10.1111/acel.13707.

[113] H. Was et al., “Some chemotherapeutics-treated colon cancer cells display a specific phenotype being a combination of stem-like and senescent cell features,” Cancer Biol Ther, vol. 19, no. 1, pp. 63–75, Jan. 2018, doi: 10.1080/15384047.2017.1385675.

[114] A. Krzystyniak, A. Gluchowska, G. Mosieniak, and E. Sikora, “Fiji-Based Tool for Rapid and Unbiased Analysis of SA-β-Gal Activity in Cultured Cells,” Feb. 01, 2023, MDPI. doi: 10.3390/biom13020362.

[115] O. Moujaber et al., “Cellular senescence is associated with reorganization of the microtubule cytoskeleton,” Cellular and Molecular Life Sciences, vol. 76, no. 6, pp. 1169–1183, Mar. 2019, doi: 10.1007/s00018-018-2999-1.

[116] F. Tóth, Z. Moftakhar, F. Sotgia, and M. P. Lisanti, “*In Vitro* Investigation of Therapy-Induced Senescence and Senescence Escape in Breast Cancer Cells Using Novel Flow Cytometry-Based Methods,” Cells, vol. 13, no. 10, May 2024, doi: 10.3390/cells13100841.

[117] J. S. Shin et al., “Senescent tumor cells in colorectal cancer are characterized by elevated enzymatic activity of complexes 1 and 2 in oxidative phosphorylation,” J Pathol Transl Med, vol. 57, no. 6, pp. 305–314, Nov. 2023, doi: 10.4132/jptm.2023.10.09.

[118] J. Hou, Y. Yun, J. Xue, M. Sun, and S. Kim, “D-galactose induces astrocytic aging and contributes to astrocytoma progression and chemoresistance via cellular senescence,” Mol Med Rep, vol. 20, no. 5, pp. 4111–4118, 2019, doi: 10.3892/mmr.2019.10677.

[119] A. S. Wang, P. F. Ong, A. Chojnowski, C. Clavel, and O. Dreesen, “Loss of lamin B1 is a biomarker to quantify cellular senescence in photoaged skin,” Sci Rep, vol. 7, no. 1, Dec. 2017, doi: 10.1038/s41598-017-15901-9.

[120] S. J. Kim, M. Chun, J. Wan, C. Lee, K. Yen, and P. Cohen, “GRSF1 is an age-related regulator of senescence,” Sci Rep, vol. 9, no. 1, Dec. 2019, doi: 10.1038/s41598-019-42064-6.

[121] M. C. X. de Godoy, J. A. Macedo, and A. Gambero, “Researching New Drug Combinations with Senolytic Activity Using Senescent Human Lung Fibroblasts MRC-5 Cell Line,” Pharmaceuticals, vol. 17, no. 1, Jan. 2024, doi: 10.3390/ph17010070.

[122] B. Chen et al., “Overexpression of klotho inhibits HELF fibroblasts SASP-related protumoral effects on non-small cell lung cancer cells,” J Cancer, vol. 9, no. 7, pp. 1248–1258, 2018, doi: 10.7150/jca.23967.

[123] N. Mignet et al., “Development of a liposomal formulation of the natural flavonoid fisetin,” in International Journal of Pharmaceutics, Feb. 2012, pp. 69–76. doi: 10.1016/j.ijpharm.2011.04.066.

[124] A. D. Bangham, M. M. Standish, and J. C. Watkins, “Diffusion of univalent ions across the lamellae of swollen phospholipids,” J Mol Biol, vol. 13, no. 1, pp. 238–252, 1965, doi: 10.1016/S0022-2836(65)80093-6.

[125] S. Khadke, C. B. Roces, R. Donaghey, V. Giacobbo, Y. Su, and Y. Perrie, “Scalable solvent-free production of liposomes,” Journal of Pharmacy and Pharmacology, vol. 72, no. 10, pp. 1328–1340, Oct. 2020, doi: 10.1111/jphp.13329.

[126] N. Vtyurina, C. Åberg, and A. Salvati, “Imaging of nanoparticle uptake and kinetics of intracellular trafficking in individual cells,” Nanoscale, vol. 13, no. 23, pp. 10436–10446, Jun. 2021, doi: 10.1039/d1nr00901j.

[127] J. H. Kang, W. Y. Jang, and Y. T. Ko, “The Effect of Surface Charges on the Cellular Uptake of Liposomes Investigated by Live Cell Imaging,” Pharm Res, vol. 34, no. 4, pp. 704–717, Apr. 2017, doi: 10.1007/s11095-017-2097-3.

[128] J. Jagielski et al., “Comprehensive and comparative studies on nanocytotoxicity of glyceryl monooleate- and phytantriol-based lipid liquid crystalline nanoparticles,” J Nanobiotechnology, vol. 19, no. 1, Dec. 2021, doi: 10.1186/s12951-021-00913-5.

[129] A. A. Alekseeva et al., “Liposomal formulation of a methotrexate lipophilic prodrug: Assessment in tumor cells and mouse T-cell leukemic lymphoma,” Int J Nanomedicine, vol. 12, pp. 3735–3749, May 2017, doi: 10.2147/IJN.S133034.

[130] A. Cazzolla et al., “Synthesis of cationic liposome nanoparticles using a thin film dispersed hydration and extrusion method,” PLoS One, vol. 19, no. 4 April, Apr. 2024, doi: 10.1371/journal.pone.0300467.

[131] S. Pereira, R. Egbu, G. Jannati, and T. Al-Jamal, “Docetaxel-loaded liposomes: the effect of lipid composition and 1 purification on drug encapsulation and *in vitro* toxicity,” Int J Pharm, vol. 514, no. 1, pp. 150–159, Nov. 2016, doi: https://doi.org/10.1016/j.ijpharm.2016.06.057.

[132] S. Cao et al., “Shape Matters: Comprehensive Analysis of Star-Shaped Lipid Nanoparticles,” Front Pharmacol, vol. 11, Apr. 2020, doi: 10.3389/fphar.2020.00539.

[133] S. Jeon, J. Clavadetscher, D. K. Lee, S. V. Chankeshwara, M. Bradley, and W. S. Cho, “Surface charge-dependent cellular uptake of polystyrene nanoparticles,” Nanomaterials, vol. 8, no. 12, Dec. 2018, doi: 10.3390/NANO8121028.

[134] J. Wolfram et al., “Shrinkage of pegylated and non-pegylated liposomes in serum,” Colloids Surf B Biointerfaces, vol. 114, pp. 294–300, Feb. 2014, doi: 10.1016/j.colsurfb.2013.10.009.

[135] R. Javani, F. S. Hashemi, B. Ghanbarzadeh, and H. Hamishehkar, “Quercetin-loaded niosomal nanoparticles prepared by the thin-layer hydration method: Formulation development, colloidal stability, and structural properties,” LWT, vol. 141, Apr. 2021, doi: 10.1016/j.lwt.2021.110865.

[136] M. E. Saddiqi, A. Abdul Kadir, F. F. J. Abdullah, M. Z. Abu Bakar Zakaria, and I. S. Banke, “Preparation, characterization and *in vitro* cytotoxicity evaluation of free and liposome-encapsulated tylosin,” OpenNano, vol. 8, Nov. 2022, doi: 10.1016/j.onano.2022.100108.

[137] C. Åberg, V. Piattelli, D. Montizaan, and A. Salvati, “Sources of variability in nanoparticle uptake by cells,” Nanoscale, vol. 13, no. 41, pp. 17530–17546, Nov. 2021, doi: 10.1039/d1nr04690j.

[138] D. Thuy Nguyen Pham, D. Thanh Nguyen, T. Kieu Trang Phan, and T. Quoc Tran, “Characterization, Release Pattern, and Cytotoxicity of Liposomes Loaded With α-Mangostin Isolated From Pericarp of Mangosteen (Garcinia mangostana L.),” Nat Prod Commun, vol. 15, no. 11, pp. 1–8, 2020.

[139] I. P. Gomes, J. de O. Silva, G. D. Cassali, A. L. B. De Barros, and E. A. Leite, “Cisplatin-Loaded Thermosensitive Liposomes Functionalized with Hyaluronic Acid: Cytotoxicity and *In Vivo* Acute Toxicity Evaluation,” Pharmaceutics, vol. 15, no. 2, Feb. 2023, doi: 10.3390/pharmaceutics15020583.

[140] S. Cui et al., “Correlation of the cytotoxic effects of cationic lipids with their headgroups,” Toxicol Res (Camb), vol. 7, no. 3, pp. 473–479, 2018, doi: 10.1039/c8tx00005k.

[141] M. J. Yousefzadeh et al., “Fisetin is a senotherapeutic that extends health and lifespan,” EBioMedicine, vol. 36, pp. 18–28, Oct. 2018, doi: 10.1016/j.ebiom.2018.09.015.

[142] M. Xu et al., “Senolytics improve physical function and increase lifespan in old age,” Nat Med, vol. 24, no. 8, pp. 1246–1256, Aug. 2018, doi: 10.1038/s41591-018-0092-9.

[143] Y. Cai et al., “Elimination of senescent cells by β-galactosidase-targeted prodrug attenuates inflammation and restores physical function in aged mice,” Cell Res, vol. 30, no. 7, pp. 574–589, Jul. 2020, doi: 10.1038/s41422-020-0314-9.

[144] E. González-Gualda et al., “Galacto-conjugation of Navitoclax as an efficient strategy to increase senolytic specificity and reduce platelet toxicity,” Aging Cell, vol. 19, no. 4, Apr. 2020, doi: 10.1111/acel.13142.

[145] A. Guerrero et al., “Galactose-modified duocarmycin prodrugs as senolytics,” Aging Cell, vol. 19, no. 4, Apr. 2020, doi: 10.1111/acel.13133.

[146] R. Wang et al., “Rapamycin inhibits the secretory phenotype of senescent cells by a Nrf2-independent mechanism,” Aging Cell, vol. 16, no. 3, pp. 564–574, Jun. 2017, doi: 10.1111/acel.12587.

[147] J. S. Lim et al., “Identification of a novel senomorphic agent, avenanthramide C, via the suppression of the senescence-associated secretory phenotype,” Mech Ageing Dev, vol. 192, Dec. 2020, doi: 10.1016/j.mad.2020.111355.

[148] H. Liu et al., “Rutin is a potent senomorphic agent to target senescent cells and can improve chemotherapeutic efficacy,” Aging Cell, vol. 23, no. 1, Jan. 2024, doi: 10.1111/acel.13921.

[149] D. Ali et al., “Resveratrol inhibits adipocyte differentiation and cellular senescence of human bone marrow stromal stem cells,” Bone, vol. 133, Apr. 2020, doi: 10.1016/j.bone.2020.115252.

[150] S. Ji et al., “Resveratrol promotes oxidative stress to drive DLC1 mediated cellular senescence in cancer cells,” Exp Cell Res, vol. 370, no. 2, pp. 292–302, Sep. 2018, doi: 10.1016/j.yexcr.2018.06.031.

[151] B. Li et al., “Resveratrol sequentially induces replication and oxidative stresses to drive p53-CXCR2 mediated cellular senescence in cancer cells,” Sci Rep, vol. 7, no. 1, 2017, doi: 10.1038/s41598-017-00315-4.

Table of figures

Table of tables

Table of equations